# Molecular and optical characterization of dissolved organic matter in the Central Arctic Ocean

Dissertation

to obtain an academic doctorate in natural sciences

-Dr. rer. nat.-

at the University of Bremen

in the Department of Biology/Chemistry

Xianyu Kong,

November 30th, 2022

Supervisors:

1. Prof. Dr. Boris Koch
2. Prof. Dr. Tilmann Harder

## Public dissertation colloquium:

On November 30th, 2022, in UFT, Room 1790

## Members of the examination committee:

Prof. Dr. Jan-Hendrik Hehemann

Prof. Dr. Boris Koch

Prof. Dr. Tilmann Harder

Dr. Urban Wünsch

Fabian Moye

Tom-Niklas Hollwedel

Universität Bremen

# Versicherung an Eides Statt

Ich, Xianyu Kong,

versichere an Eides Statt durch meine Unterschrift, dass ich die vorstehende Arbeit selbständig und ohne fremde Hilfe angefertigt und alle Stellen, die ich wörtlich dem Sinne nach aus Veröffentlichungen entnommen habe, als solche kenntlich gemacht habe, mich auch keiner anderen als der angegebenen Literatur oder sonstiger Hilfsmittel bedient habe.
Ich versichere an Eides Statt, dass ich die vorgenannten Angaben nach bestem Wissen und Gewissen gemacht habe und dass die Angaben der Wahrheit entsprechen und ich nichts verschwiegen habe.
Die Strafbarkeit einer falschen eidesstattlichen Versicherung ist mir bekannt, namentlich die Strafandrohung gemäß § 156 StGB bis zu drei Jahren Freiheitsstrafe oder Geldstrafe bei vorsätzlicher Begehung der Tat bzw. gemäß § 161 Abs. 1 StGB bis zu einem Jahr Freiheitsstrafe oder Geldstrafe bei fahrlässiger Begehung.

Ort, Datum / Unterschrift

## Acknowledgement

I would like to thank my doctoral advisors Prof. Dr. Boris Koch and Prof. Dr. Tilmann Harder for giving me the opportunity to work on my PhD project at the Alfred-Wegener-Institute, mentoring me as a PhD student at the University of Bremen, and providing me valuable guidance over the last years. I would like to thank the members of my thesis advisory committee Prof. Dr. Boris Koch, Prof. Dr. Tilmann Harder, Dr. Ulf Bickmeyer, and Dr. Urban Wünsch for suggestions on improving my PhD project.

I wish to thank to my colleagues from the "Marine Chemistry" working group at the Alfred-Wegener-Institute, namely Boris Koch, Martin Graeve, Kai-Uwe Ludwichowski, Claudia Burau, Valeria Adrian, Jana Geuer, Erik Stein, Sinah Müller, Kerstin Ksionzek, Matthias De Albuquerque Woll, Tim Leefmann, Heiner Baumgarten, Dieter Janssen, Kristin Kampen, Jan Tebben, Martin Prinzler, Marlo Bareth, Yvonne Jenniges and Fabian Moye for their support in the lab and life.

I am grateful to Dr. Oliver Lechtenfeld and Jan Kaesler for their help with the LC-FTMS measurements and Prof. Colin Stedmon and Dr. Mats Granskog for their support in CDOM work. I would like to express my gratitude to other colleagues at the Alfred-Wegener-Institute, namely Ute Marx, Astrid Bracher, Christian Hohe and Sonja Wiegmann, for supporting me in the lab work. Thanks to Allison Fong, Clara Hoppe, Adam Ulfsbo, John Paul Balmonte, Jeff Bowman**,** Emelia Chamberlain, Jessie Creamean, Elise Droste, Lena Eggers, Oliver Müller, Lasse Mork Olsen, Sinhue Torres-Valdes and Laura Wischnewski for collecting Chlorophyll, CDOM or DOC samples during the MOSAiC expedition.

Last but not least, thanks to all my friends and my family for your company, support, and encouragements.

# TABLE OF CONTENTS

**Acknowledgement** ..... **I**

**Preface** ..... **1**

**List of Abbreviations** ..... **3**

**Abstract** ..... **7**

**1. Introduction** ..... **9**

1.1. Marine organic matter ..... 9

1.2. DOM reactivity and size ..... 10

1.3. DOM sources ..... 12

*1.3.1. Autochthonous sources* ..... *12*

*1.3.2. Allochthonous sources* ..... *13*

1.4. DOM sinks ..... 14

1.5. DOM in the Central Arctic Ocean ..... 17

1.6. Analytical methods for DOM characterization and quantification ..... 21

*1.6.1. Optical spectroscopy for DOM characterization* ..... *22*

*1.6.2. Solid-phase extraction for DOM desalting and enrichment* ..... *26*

*1.6.3. Applying mass spectrometry for DOM molecular characterization* ..... *27*

*1.6.4. Challenges of molecular-level analysis of DOM* ..... *28*

**2. Objectives** ..... **31**

**3. Manuscript I** ..... **33**

3.1. Abstract ..... 34

3.2. Introduction ..... 35

3.3. Methods and materials ..... 36

3.4. Results ..... 42

3.5. Discussion ..... 52

**4. Manuscript II** ..... **59**

4.1. Abstract: ..... 60

4.2. Introduction ..... 61

4.3. Materials and Methods ..... 63

4.4. Results ..... 68

*4.4.1. Spectral characteristics of FDOM components* ..... *68*
*4.4.2. Variations of DOC and FDOM at different sampling depths* ..... *69*
*4.4.3. Vertical profiles in the upper ocean* ..... *71*
*4.4.4. Optical Properties of DOM in the SML* ..... *73*
*4.4.5. Lead water samples from the Amundsen Basin* ..... *77*
4.5. Discussion ..... 78
*4.5.1. Spatial variability of DOM properties depends on the influence of the transpolar drift* ..... *78*
*4.5.2. Potential impact of the tCDOM-rich surface waters on primary production* ... *80*
*4.5.3. Potential impact of the tCDOM-rich surface waters on the sea ice melt and formation* ..... *82*
4.6. Conclusions ..... 83
**5. Manuscript III ..... 84**
5.1. Abstract ..... 85
5.2. Introduction ..... 87
5.3. Materials and Methods ..... 90
*5.3.1. Study area* ..... *90*
*5.3.2. DOC measurement* ..... *91*
*5.3.3. Optical spectroscopy* ..... *91*
*5.3.4. FT-ICR MS measurement hyphenated to UPLC* ..... *93*
*5.3.5. Statistical analysis* ..... *98*
5.4. Results ..... 99
*5.4.1. DOM quantification in original seawater using LC-FTMS* ..... *99*
*5.4.2. Relationship between MFs and terrigenous proxies* ..... *101*
*5.4.3. Polarity-based separation* ..... *105*
5.5. Discussion ..... 110
*5.5.1. DOM quantification in the Central Arctic* ..... *110*
*5.5.2. Identification and quantification of DOM subfractions in the Central Arctic* *111*
**6. Conclusions and perspective ..... 117**
**7. References ..... 119**

# Preface

The manuscripts that are part of this doctoral thesis are listed below. Chapters 3 to 5 are reprints of independent manuscripts of research articles including: one published manuscript (Manuscripts I), one submitted manuscript (Manuscript II, under review) and one manuscript in preparation (Manuscript III). The content is unchanged and the labels of figures and tables are adapted to the general format of this thesis. The references are included in the complete list at the end of the thesis.

**Chapter 3: Manuscript I**

Kong, X., Jendrossek, T., Ludwichowski, K.-U., Marx, U., Koch, B.P (2021). Solid-phase extraction of aquatic organic matter: loading-dependent chemical fractionation and self-assembly. Environ. Sci. Technol. 55, 15495–15504. https://doi.org/10.1021/acs.est.1c04535

I participated in the conception and design of the experiments, did most of the experimental work and data acquisition and analysis, prepared most of the figures and tables, draft the manuscript, and revised the manuscript with other co-authors.

This manuscript has been published in Environmental Science & Technology (contained in Nature Index). The supplementary figures have been merged into the main text, and the labeling of figures and tables has been adjusted.

**Chapter 4: Manuscript II**

Kong, X., Granskog, M.A., Hoppe, C.J.M., Fong, A.A., Stedmon, C.A., Tippenhauer, S., Ulfsbo, A., Vredenborg, M., Koch, B.P. (submitted). The composition of chromophoric dissolved organic matter in Central Arctic surface waters during the MOSAiC expedition depends on regional rather than seasonal differences.

I participated in the conception and design of the experiments, performed the analysis for chromophoric dissolved organic matter samples and data evaluation, prepared all figures and tables, draft the manuscript, and revised the manuscript with other co-authors.

This manuscript was submitted to Elementa: Science of the Anthropocene. Original data of this paper has been published open access in the World Data Center PANGAEA and is available at:

https://doi.pangaea.de/10.1594/PANGAEA.948019
https://doi.pangaea.de/10.1594/PANGAEA.948018
https://doi.pangaea.de/10.1594/PANGAEA.948016

**Chapter 5: Manuscript III**

Kong, X., Lechtenfeld, O.J., Koch, B.P. (in preparation). Quantitative characterization of dissolved organic matter in original Central Arctic seawater using liquid chromatography FT-ICR mass spectrometry.

I participated in the design of method analysis for MS sample, performed most of the data analysis and interpretation for MS, prepared all figures and tables, drafted the manuscript, and revised the manuscript with other co-authors.

This manuscript is in preparation for submission. Data will be available open-access via PANGAEA by the time of the final publication.

## List of Abbreviations

| | |
|---|---|
| $a_{CDOM}(350)$ | Absorption coefficient at 350 nm |
| AI | Aromaticity index |
| ANOVA | Analysis of variance |
| AO | Arctic Oscillation |
| AO+ | Positive Arctic Oscillation |
| AO− | Negative Arctic Oscillation |
| AW | Atlantic Water |
| AW1 | Upper Atlantic Water |
| AW2 | Lower Atlantic Water |
| BG | Beaufort Gyre |
| BIX | Biological index |
| BP | Biological pump |
| CAO | Central Arctic Ocean |
| CCD | Charge-coupled device detector |
| CDOM | Chromophoric dissolved organic matter |
| Chl-a | Chlorophyll a |
| $CH_2$ | Methylene unit |
| $CO_2$ | Carbon dioxide |
| CRAM | Carboxyl-rich alicyclic molecules |
| CTD | Conductivity temperature depth |
| DBE | Double bond equivalent |
| DBE-O | Double bond equivalent minus oxygen |
| DOC | Dissolved organic carbon |
| $DOC_{load}$ | Relative DOC loading weight of the sorbent |
| DOM | Dissolved organic matter |
| DON | Dissolved organic nitrogen |
| DOS | Dissolved organic sulfur |
| DMSP | Dimethylsulfoniopropionate |
| DI | Direct infusion |
| DIC | Dissolved inorganic carbon |

| | |
|---|---|
| DW | Deep waters |
| EEMs | Excitation-emission matrix spectrum |
| EGC | East Greenland Current |
| ESI | Electrospray ionization |
| Ex | Excitation |
| Em | Emission |
| FDOM | Fluorescent dissolved organic matter |
| $FDOM_{total}$ | Total fluorescence intensity |
| FI | Fluorescence index |
| FT-ICR MS | Fourier-transform ion cyclotron resonance mass spectrometry |
| GIN | Greenland-Iceland-Norwegian |
| $H_2O$ | Ultrapure water |
| HCl | Hydrochloric acid |
| HIX | Humification index |
| HL | Halocline layer |
| HMW | High molecular weight |
| HTCO | High temperature catalytic oxidation |
| KM | Kendrick mass |
| KMD | Kendrick mass defect |
| $int_{sum}$ | Summed peak magnitudes for one sample |
| $int_{sum, RT}$ | Summed peak magnitudes for each segment in one sample |
| $I_{DEG}$ | Degradation index |
| LC-FTMS | Fourier-transform ion cyclotron resonance mass spectrometry hyphenated with high performance liquid chromatography |
| LED | Light-emitting diodes |
| LHC | Lower Halocline |
| LMW | Low molecular weight |
| mDOM | Marine DOM |
| MCP | Microbial carbon pump |
| MF | Molecular formula |
| MFs | Molecular formulas |
| MOSAiC | Multidisciplinary Drifting Observatory for the Study of Arctic Climate |

| | |
|---|---|
| NADW | North Atlantic Deep Water |
| NM | Nominal IUPAC mass |
| NMR | Nuclear magnetic resonance |
| NOSC | Nominal oxidation state of carbon |
| NPP | Net primary production |
| OPA | orthophthal-aldehyde |
| PARAFAC | Parallel Factor Analysis |
| PCA | Principal component analysis |
| PC1 | Principal component 1 |
| POM | Particulate organic matter |
| POC | Particulate organic carbon |
| PPL | Priority PolLutant |
| RDOM | Refractory dissolved organic matter |
| RDOC | Refractory dissolved organic carbon |
| (RP-) HPLC | (Reversed phase-) high performance liquid chromatography |
| S/N | Signal to noise ratio |
| $S_{275-295}$ | Spectral slope between 275 and 295 nm |
| $S_{350-400}$ | Spectral slope between 350and 400 nm |
| $S_R$ | Spectral slope ratio |
| SEM | Scanning electron microscopy |
| SLDOC | Semi-labile dissolved organic carbon |
| SML | Surface mixed layer |
| SP | Solubility pump |
| SPE | Solid-phase extraction |
| SPE-DOM | Dissolved organic matter isolated using solid-phase extraction |
| SRFA | Suwannee River Fulvic Acid |
| SRDOC | Semi-refractory dissolved organic carbon |
| $SUVA_{254}$ | Specific UV absorbance at 254 nm |
| tCDOM | Terrestrially-derived chromophoric dissolved organic matter |
| tDOM | Terrestrially-derived dissolved organic matter |
| tDOC | Terrestrially-derived dissolved organic carbon |
| TDAA | Total dissolved amino acids |

| | |
|---|---|
| TDN | Total dissolved nitrogen |
| TEPs | Transparent exopolymer particles |
| THC | Thermohaline circulation |
| TIC | Total ion current |
| TPD | Transpolar Drift |
| UHC | Upper Halocline |
| UME | UltraMassExplorer |
| UPLC | Ultra-high performance liquid chromatography |
| URDOC | Ultra-refractory dissolved organic carbon |
| UV | Ultraviolet |
| UVB | Ultraviolet B |
| UVA | Ultraviolet A |
| wa | Intensity weighted average |
| WSC | West Spitsbergen Current |

## Abstract

Dissolved organic matter (DOM) in the ocean is a complex mixture of molecules derived from autochthonous (marine) or allochthonous (terrestrial) origins. DOM plays an important role in marine biogeochemical cycles by attenuating light available for primary production, serving as an energy and nutrient source for heterotrophic communities, regulating the ultraviolet and visible light absorption, undergoing photochemical processing, and acting as a trace metal ligand. DOM in the Central Arctic Ocean (CAO) is influenced by increased freshwater input and associated terrestrial materials in recent decades due to rapid climate change. The quantification of DOM sources (terrestrial versus marine) in the water column of the CAO is not well constrained. Few studies have systematically investigated the seasonality and spatial variability of DOM by combining optical and molecular-level analytical techniques in the CAO, especially during winter.

State of the art chemical characterization of DOM is subject to major challenges: Solid phase extraction (SPE) that is often used to desalt and pre-concentrate marine DOM introduces chemical fractionation effects, which limits the comparability between analytical results for original samples and those carried out for SPE-DOM. There is no specific method to quantify fractionation effects, nor specific guidelines to avoid fractionation. Using mass spectrometry, quantitative DOM analyses is challenged by selective ionization of molecules and the large number of unresolved structural isomers that prevent classical external calibration.

In the first part of this thesis, a method was developed to quantitatively track optical or chemical fractionation during SPE and investigate the potential mechanisms. We found a decrease in extraction efficiency of dissolved organic carbon (DOC), fluorescence and absorbance, and polar organic substances with increasing carbon loading on the SPE column. As the surface loading of the solid-phase increased, the dominant extraction mechanism shifted from PPL physisorption to increased DOM self-assembly, resulting in optical and chemical fractionation. The relative DOC loading ($DOC_{load}$) was used to assess the carbon loading during SPE, and a double sigmoid model was applied to our online permeate fluorescence data as a function of

$DOC_{load}$, which allowed us to assess the degree of variability induced by $DOC_{load}$. This finding has ample implications for the future processing and previous interpretation of chemical characteristics in SPE-DOM of aquatic organic matter.

For the second part of the thesis, original water samples were acquired from the "Multidisciplinary Drifting Observatory for the Study of Arctic Climate" (MOSAiC) expedition. The water column samples covered a full year (2019 / 2020) and included the regions Amundsen Basin, western Nansen Basin and Yermak Plateau and Fram Strait. Samples were analyzed using optical spectroscopy to determine chromophoric DOM (CDOM) and fluorescent DOM (FDOM). In addition, a new method was applied that used Fourier-transform ion cyclotron resonance mass spectrometry hyphenated to high performance liquid chromatography (LC-FTMS). The method allowed DOM analysis in original filtered water and thus avoided the chemical fractionation introduced by SPE. During the MOSAiC expedition, DOC concentrations and CDOM characteristics in the water column were primarily influenced by regional differences. These differences were largely dependent on terrestrially-derived DOM (tDOM) input by the transpolar drift (TPD) as indicative of average 136% and 45% higher $a_{CDOM}(350)$ and DOC concentration, respectively, in the Amundsen compared to the western Nansen Basin and Yermak Plateau, and slightly modified by seasonal changes. Despite the convenient identification of tDOM, optical spectroscopy was not suitable to quantify the contribution of tDOM to bulk DOC or to track sea ice derived DOM in the water column. In contrast, using LC-FTMS, we found quantitative linear correlation between the summed mass peak magnitudes for each sample ($int_{sum}$) and DOC concentration. By combing LC-FTMS and source identification with optical parameters, we were able to quantify DOM sources (terrestrial versus marine) in the water column: 83% of the summed peak magnitude of all samples could be related to marine or terrestrial sources. tDOM contributed ~17% (or 8 µmol $kg^{-1}$) to deep DOC (~2000 m) in the CAO and was more refractory and had a higher state of unsaturation compared to marine DOM. The quantitative characterization of DOM in original seawater from different origin is a major step in the field of research. It provides a unique and new insight into the molecular changes in marine DOM composition and an improved understanding of the terrestrial DOM distribution in the CAO.

# 1. Introduction

## 1.1. Marine organic matter

Dissolved organic matter (DOM) in the ocean is one of the largest active reservoirs of organic matter on earth, together with soil organic matter and plant biomass on land. The organic matter in the ocean occupies a molecular-size continuum (Figure 1), consisting of two operationally-defined phases: particulate organic matter (POM) and DOM (Verdugo, 2012). The fraction of organic matter that passes through a filter at a given pore size (typically 0.1–1 μm) is called DOM, which generally remains in the water column as a solute, and the fraction remaining on the filters is called POM, which can be suspended in the water column or prone to sink (Hedges, 2002; Perdue and Benner, 2009; Bolan et al., 2011). Many filter types and pore sizes have been applied according to different scientific purposes. Commonly used filters include pre-combusted glass fiber filters (with a pore size of 0.7 μm), silver filters (with a pore size of 0.45 μm), preconditioned polycarbonate filter (with a pore size 0.2 μm), and preconditioned mixed-ester filters (with a pore size 0.2 μm), which can remove most of living organisms except viruses and small bacteria (Perdue and Benner, 2009). POM is specifically quantified by its mass of carbon in the organic material and referred to as particulate organic carbon (POC). The POM in the ocean includes a major fraction of detritus (dead organisms and their remains) and a minor part of living biomass (phytoplankton, zooplankton and bacteria), which is mainly found in the euphotic zone in the ocean (Perdue and Benner, 2009; Stramska, 2009; Baltar et al., 2021). The living organisms within the POM pool mainly consist of proteins, lipids, carbohydrates, nucleic acids, and pigments (Anderson, 1995; Fraga et al., 1998). The DOM pool in the ocean is largely lifeless except for some prokaryotes and viruses (Hedges, 2002). DOM in the ocean is a heterogeneous mixture of organic compounds containing heteroatoms such as oxygen, nitrogen, phosphorus, and sulfur. DOM is specifically quantified by its mass of carbon in the organic material and referred to as dissolved organic carbon (DOC). which accounts for approximately 50% of DOM (Moody and Worrall, 2017). DOC represents the largest reservoirs of reduced carbon in the ocean comprising approximately 662 Pg C (1 Pg C = $10^{15}$ g C), which is

comparable in magnitude to the amount of carbon in atmospheric carbon dioxide ($CO_2$; Hedges, 2002; Hansell et al., 2009). Marine ecosystems play a crucial role in global climate and biogeochemical cycles by sequestering carbon into the deep ocean.

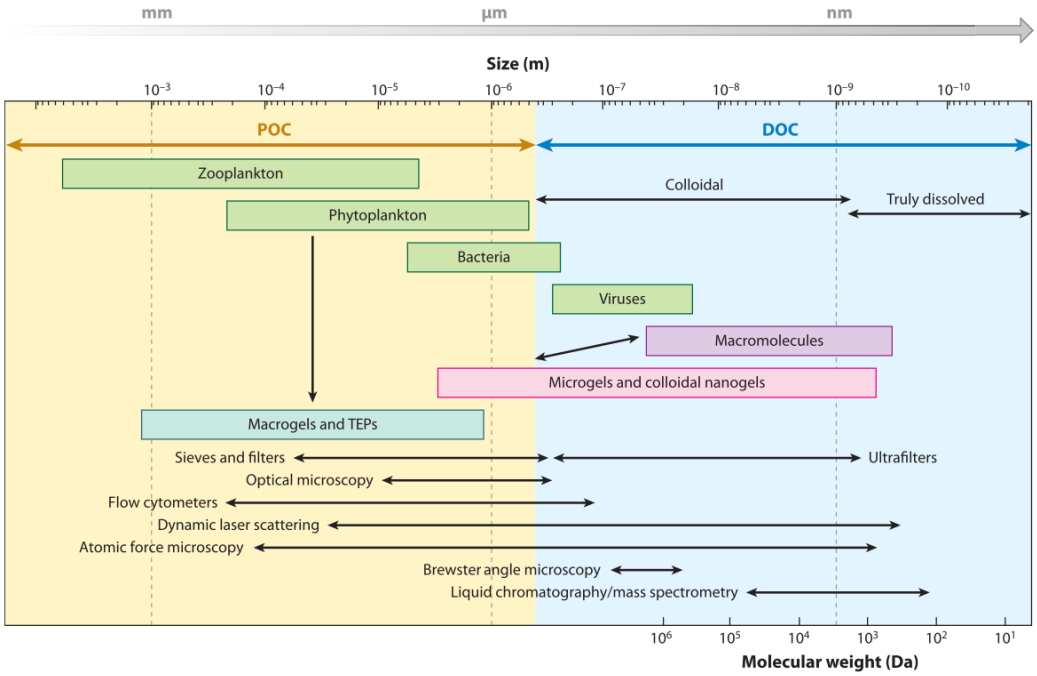


**Figure 1.** The continuum of molecular sizes and weight of organic matter in the ocean. Figure taken from (Verdugo, 2012) and adapted from (Hedges, 2002). The fraction retained by the filter with a 0.2 µm pore size is regarded as POC. The yellow color bar denotes POC pool. POC consists of all marine organisms, macrogels and transparent exopolymer particles (TEPs). The fraction that passes through the filter is categorized as DOC. The bule color bar denotes DOC pool. DOC comprises colloidal and truly dissolved materials. The different techniques that are used for different size of organic matter are also showed in the figures.

## 1.2. DOM reactivity and size

Marine DOM exhibits a wide range of turnover times and biological reactivity, from short-lived bioavailable organic matter in the upper ocean to long-lived organic material throughout the water columns (Hansell, 2013). The DOM pool can be divided into two major classes in the ocean, labile and recalcitrant DOM that are characterized by their lifetimes or reactivities (Figure 2; Hansell, 2013). The recalcitrant DOM is taken as the opposite of labile DOM, the latter being removed within hours to days

and not accumulated due to rapid microbial degradation. The recalcitrant DOM is resistant to rapid microbial degradation and can accumulate in the ocean. The recalcitrant DOM can be further distinguished in the sub-categories semi-labile (estimated turnover times of months to years), semi-refractory (estimated turnover times over decades to centuries), refractory (estimated turnover times of centuries to millennia), and ultra-refractory (estimated lifetime of ~40,000 years; (Hansell, 2013)

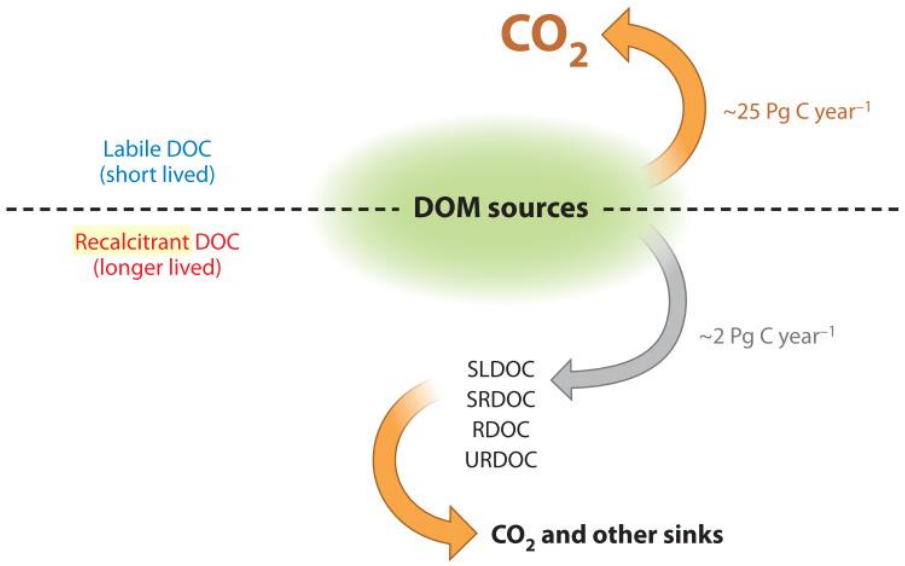


**Figure 2.** Two major classes (labile and recalcitrant DOM) of bulk DOM in the ocean. Figure taken from (Hansell, 2013). Recalcitrant DOM can be further subdivided into semi-labile DOC (SLDOC), semi-refractory (SRDOC), refractory (RDOC), and ultra-refractory DOC (URDOC).

The labile DOM only constitutes a smaller reservoir of around 0.2 Pg C but is produced at a high rate (~15–25 Pg C $y^{-1}$). It can be used by heterotrophic bacteria within days or even hours, thus the labile DOM does not accumulate in the ocean and has no direct contribution to the carbon sequestration (Azam et al., 1983; Ducklow, 1999; Hansell, 2013; Williams 2000). The semi-labile DOM persists in the ocean for months to years, which can be followed as seasonal variability in the euphotic zone and limited to the upper mesopelagic zone (to ~500 m) due to it relatively short lifetime (Carlson and Ducklow, 1995). The semi-refractory DOM, at an inventory of 14 ± 2 Pg C and a low production rate of 0.34 Pg C $yr^{-1}$, turns over on timescales of decades to centuries (Hansell, 2013). The refractory fraction represents more than 95%

of the total DOC reservoir in the ocean (~642 Pg C ± 32; distributed throughout the water columns), at a very low production rate of 0.043 Pg C $yr^{-1}$, and turns over on timescales of decades to millennia (Hansell, 2013). The refractory DOM in the ocean has an average radiocarbon age of 4000-6000 years (the average radio age of about 4000 yr in the Sargasso Sea and about 6000 yr in the central North Pacific; Williams and Druffel, 1987; Bauer et al., 1992). The ultra-refractory DOM has a total inventory of > 12 Pg C and a lifetime of 40,000 yr (Hansell, 2013). The ultra-refractory DOM may be thermogenic and it is also referred to as dissolved black carbon (Masiello and Druffel, 1998; Mannino and Rodger Harvey, 2004; Dittmar and Koch, 2006).

The DOC pool can be also operationally divided into colloids, macromolecules, and other high molecular weight (HMW) and low molecular weight (LMW) molecules based on its molecular weight (Benner et al., 1992; Hedges et al., 1997). In the ocean, the HMW (molecular weight > 1000 Da) of DOC comprises most colloids and gels rather than truly dissolved and constitutes ~22% of total organic carbon, while the HMW of DOC accounts for ~77% of total organic carbon at a molecular weight of < 1000 Da (Figure 1; Benner et al., 1992; Benner and Amon, 2015). A size-reactivity continuum model proposed by Amon and Benner, (1994, 1996) suggests that the bioreactivity of organic matter decreases continuously with the size from larger to smaller, thus, the HMW fraction of DOM is younger, semi-labile, and has a greater reactivity, while the LMW fraction of DOM is comprised of older, more biologically refractory molecules.

## 1.3. DOM sources

DOM in the ocean is a complex mixture of organic compounds that comes from both the autochthonous or allochthonous origins. DOM in the ocean is considered autochthonous when it is produced in the marine system by phytoplankton and plants, while DOM is considered allochthonous when it is derived from degraded terrestrial materials.

### *1.3.1. Autochthonous sources*

The major marine, or autochthonous, sources of DOM include the extracellular release by phytoplankton (Lancelot, 1979; Lignell, 1990; Marañón et al., 2005), release by

zooplankton grazing (excretion, sloppy feeding, egestion, and dissolution of fecal material; Strom et al., 1997), cell lysis from viral infection (Proctor and Fuhrman, 1990) and solubilization of particles (mostly from detritus or marine snow; Smith et al., 1992, 1995).

The major biomolecules and their building blocks in living organisms of the POC pool in the ocean, including proteins, lipids, and carbohydrates, can be released into the DOM pool (Lee et al., 2004; Perdue and Benner, 2009). These biochemical compounds are commonly hydrolyzed into their monomeric constituents (i.e., amino acids, amino sugars, monosaccharides, and fatty acids) prior to their measurements (Fitznar et al., 1999; Wakeham et al., 2003; Kaiser and Benner, 2009, 2012b; Nouara et al., 2019). Carbohydrates are key structural and energy storage components in photosynthetic organisms and constitute a carbon sink in the global oceans (Biersmith and Benner, 1998; Becker et al., 2020). Amino acids are the most abundant identifiable constituents in the living organisms in the POM pool and the main contributor to the dissolved organic nitrogen (DON) pool (Kaiser and Benner, 2009; Benner and Amon, 2015). Dissolved hydrolyzable neutral sugars, amino acids, and amino sugars consists of 5–18% of DOC and 4–5% of DON removed in the upper mesopelagic zone in the North Pacific (Kaiser and Benner, 2012b). Lipids are observed in the all living organisms and in sedimentary organic material, and the major fractions of dissolved lipids are fatty acids (Schubert and Stein, 1997; Wakeham et al., 2003; Parrish, 2013). Heterotrophic bacteria play a key role in the oceanic carbon cycle. The heterotrophic bacteria can utilize 10–50 % of carbon fixed by photosynthesis (Azam et al., 1983; Ducklow, 1999; Hansell, 2013). Carboxyl-rich alicyclic molecules (CRAM) are one of the most common forms of refractory DOM and have been related to microbial origin in the deep ocean (Hertkorn et al., 2006).

### *1.3.2. Allochthonous sources*

Allochthonous DOM in the ocean is initially produced on land and transported into ocean by rivers or the atmosphere. River discharges are the main source of terrigenous material and one of the largest contributors of carbon to the ocean, delivering ~170–250 Tg C $yr^{-1}$ (~1 Tg C = $10^{12}$ g C) of DOC and ~150–280 Tg C $yr^{-1}$ of POC into the global ocean (Raymond and Spencer, 2015; Kandasamy and Nath, 2016). The

DOM concentrations in rivers are mainly affected by soil carbon stocks, vegetation cover, land use, river floodplain, storms and precipitation (Raymond and Spencer, 2015; Keiluweit et al., 2017). The terrestrial organic matter is a heterogeneous mixture of recent vascular plant detritus, associated soil material, older fossil organic matter from carbonate rock erosion, and black carbon (Hedges, 1992; Galy et al., 2007; Bianchi, 2011). The terrigenous organic matter flowing into rivers is highly colored, aromatic and dominated by complex humic-rich constituents (referred as chromophoric dissolved organic matter (CDOM), see chapter 1.6.1; Dittmar and Stubbins, 2014). Lignin, a group of phenolic polymers uniquely produced by vascular plants, is commonly used as an organic tracer for terrestrial plant material (Hernes and Benner, 2006; Spencer et al., 2008, 2009b; Kaiser et al., 2017; Kharbush et al., 2020). Black carbon is ubiquitous in the environment and a chemically heterogeneous mixture produced by fossil fuel combustion and biomass burning (Masiello and Druffel, 1998; Kim et al., 2004; Follett et al., 2014). Black carbon is found in both dissolved and particulate pools in the ocean, and is released into ocean by aerosol and river deposition and has been detected in soils and in marine sediments (Masiello and Druffel, 1998; Dittmar, 2008).

## 1.4. DOM sinks

DOM removals and transformations in the ocean columns occur through degradation by marine heterotrophic prokaryotes, abiotic degradation via photochemical reactions, as well as DOM aggregation and subsequent flocculation (Dittmar and Stubbins, 2014).

Marine ecosystems are a major sink for atmospheric $CO_2$. The transfer of $CO_2$ from the atmosphere into the oceans interior and eventually into sediments, is mainly affected by the combination of the solubility pump (SP) and the biological pump (BP; Volk and Hoffert, 1985). A conceptual diagram is presented here to understand the major carbon cycling and storage in the ocean and the role of microbial processes in the production of refractory DOM (RDOM; Figure 3). The SP serves to describe the exchange of $CO_2$ between ocean surface and atmosphere. It redistribute and convert $CO_2$ into several compounds in equilibrium (e.g. $HCO_3^-$ and $CO_3^{2-}$; summarized as dissolved inorganic carbon (DIC)), within the ocean interior by thermohaline

circulation (THC; Hülse et al., 2017). The primary producers (phytoplankton and photoautotrophic bacteria) can assimilate atmospheric $CO_2$. The biomass produced contributes to sinking biogenic particles (i.e., POM) and DOM. The net primary production (NPP) is defined as the difference between the amount of carbon or energy fixed by autotrophs and their respiration (Dittmar and Stubbins, 2014). The world ocean contributes almost half of the global NPP (~50 Pg C $yr^{-1}$), with an average turnover time for the phytoplankton biomass of 2–6 days (Behrenfeld and Falkowski, 1997; Field et al., 1998; Behrenfeld et al., 2006; Carr et al., 2006). The BP is the main biological process for carbon sequestration and the major pathway to transfer both organic and inorganic carbon fixed by the photosynthesis in the euphotic zone to the ocean interior and eventually to the deep ocean or sediments (Ducklow et al., 2001). Most POM is remineralized to DIC and mineral nutrients during its transportation to the deep ocean or sediments via the BP (Jiao et al., 2010). Most of this newly produced DOM is biologically labile and reworked by microbial carbon pump (MCP), where most labile DOM is consumed and respired rapidly by heterotrophic bacteria into DIC (Hansell et al., 2009). The mixing of DOC in the upper layers is driven by wind forcing up to ~200 m depth. A small fraction of that DOM escapes rapid remineralization and is transformed into recalcitrant DOM (RDOM) and accumulates in the surface layer, and eventually is exported to the greater depth by the THC (Hansell et al., 2009). In the deep ocean, desorption and solubilization likely release particulate organics to the DOC pool, whereas adsorption and flocculation sequester DOC into particulate pool (Dittmar and Stubbins, 2014).

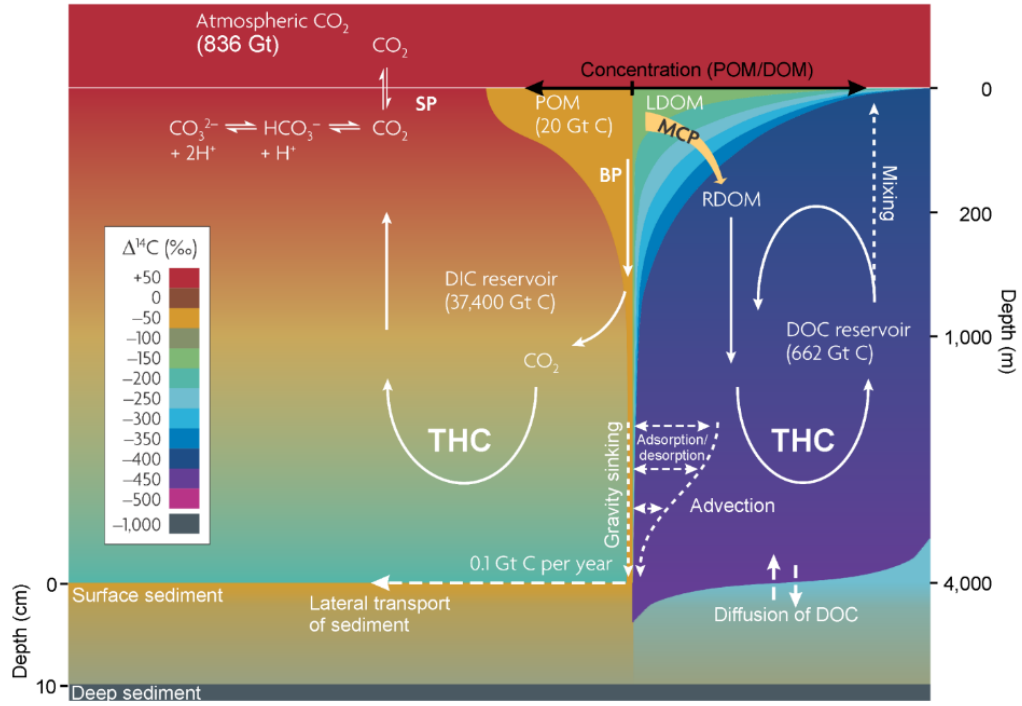


**Figure 3.** The major carbon cycling and storage in the ocean. Figure taken from (Lechtenfeld, 2012) and adapted from Jiao et al. (2010).

Photochemical degradation is a major abiotic process resulting in degradation and alteration of DOM in the ocean. The photochemical degradation could lead to CDOM photobleaching (i.e., the loss of light absorption) and the mineralization of organic carbon to inorganic carbon (Moran and Zepp, 1997; Osburn et al., 2009; Sulzberger and Durisch-Kaiser, 2009; Yamashita et al., 2013; Murphy et al., 2018). The influence of photochemical processes on the DOC pool depends on the chemical composition. Photochemical processes could lead to reduced bioavailability of freshly produced DOM or transform recalcitrant into labile DOC molecules that can be rapidly used by microbes (Benner and Ziegler, 1999; Holmes et al., 2008; Sulzberger and Durisch-Kaiser, 2009). A relatively minor impact of photodegradation on the terrigenous DOM is observed on Arctic shelves due to ice cover, and diminished sunlight and colder temperatures (Bélanger et al., 2006; Osburn et al., 2009). DOM biopolymers (e.g., carbohydrates, proteins and lipids) could spontaneously aggregate to nanogels, and microgels by noncovalent bonds such as electrostatic, hydrogen, hydrophobic, or van der Waals bonds in the ocean (Chin et al., 1998; Verdugo et al., 2004; Verdugo and Santschi, 2010; Verdugo, 2012). Nanogels and microgels can eventually grow further

to form larger macrogels and transparent exopolymer particles (TEPs), or even marine snow, which are considered as POM (Chin et al., 1998; Passow et al., 2001; Verdugo, 2012). Flocculation is a process during which DOM or suspended organic matter aggregate into particulate organic flocs which can be consumed by bacteria or grazers, or removed from the water column into the sediment (Tranvik and Sieburth, 1989; von Wachenfeldt et al., 2008, 2009; Zhou et al., 2021). Flocculation is often observed in the estuarine and coastal areas where the rapid shifts in salinity during the mixing of freshwater and seawater (Sholkovitz, 1976; Sholkovitz et al., 1978; Kohler et al., 2003; Asmala et al., 2014), which could reduce the contribution of riverine DOM into the ocean DOM pool.

## 1.5. DOM in the Central Arctic Ocean

The Arctic Ocean is experiencing increased freshwater loads and associated terrestrial matter inputs in recent decades due to rapid climate change, which has an impact on the stratification, vertical mixing, nutrient supply, heat flux, primary production, ocean acidification and biogeochemical cycles in the Arctic Ocean (Bates and Mathis, 2009; MacGilchrist et al., 2014; Carmack et al., 2016; Capelle et al., 2020; Woosley and Millero, 2020; Polimene et al., 2022). The freshwater in the Arctic Ocean is strongly influenced by river discharge and precipitation (Haine et al., 2015; Solomon et al., 2021). Precipitation minus evaporation delivers about $2200 \pm 220$ $km^3\ yr^{-1}$ (the average value during 2000–2010) of freshwater into Arctic Ocean (Haine et al., 2015). In addition, Pacific water enters the Arctic Ocean via the Bering strait and contributes water with a comparatively low salinity (Jones et al., 2008). It supplies an estimated of $2640 \pm 100$ $km^3\ yr^{-1}$ of freshwater (the average value during 2000–2010) into Arctic Ocean based on a reference salinity of 34.80 (Haine et al., 2015; Carmack et al., 2016). The DOC flux of Pacific water into Arctic Ocean was estimated to be around of 18 Tg C $yr^{-1}$ (Anderson and Amon, 2015). Large river discharges and their influences are evident in the Arctic Ocean. The Arctic Ocean (~1% of the global ocean volume) receives more than 10% of global riverine discharge (approximately 25 Tg C $yr^{-1}$), thus resulting in estuarine gradients and high DOC concentrations and terrestrial DOM proportions in surface polar waters across the Arctic basins (McClelland et al., 2012; Anderson and Amon, 2015). The most important discharge into the Arctic, the

Canadian Arctic Archipelago, and Baffin Bay from land (i.e., rivers, streams and groundwater) with a total amount of 4200 ± 420 $km^3$ $yr^{-1}$ is dominated by large rivers, mainly on the Eurasian side (Haine et al., 2015; Carmack et al., 2016). Total annual discharge from the six largest Artic rivers (i.e., Ob, Yenisei, Lena and Kolyma, Mackenzie and Yukon; Figure 4) is estimated up to 2348 $km^3$ $yr^{-1}$ (Holmes et al., 2012). Among these six rivers, the three largest Siberian rivers (i.e., Lena, Yenisei and Ob) alone contribute ~90% of the total lignin discharge or ~80% of total DOC to the Arctic Ocean (Amon et al., 2012).

The Arctic Ocean is divided into two major basins: the Eurasian Basin and the Amerasian Basin, separated by the Lomonosov Ridge (Rudels et al., 2015). The Eurasian Basin consists of two sub-basins: the Amundsen Basin and Nansen Basin with typical maximum depth of ~4000-4500 m, respectively, separated by the Gakkel Ridge (Figure 4). There are two major large-scale wind-driven surface currents in the Arctic Ocean, the Beaufort Gyre (BG) and the Transpolar Drift (TPD; Figure 4). The western Arctic (i.e., the Canada Basin and adjacent shelf seas) is dominated by the BG. It is estimated that runoff entering the BG has a much longer residence time of ~10 years (Yamamoto-Kawai et al., 2008; McClelland et al., 2012). The eastern Arctic (i.e., the Eurasian Basin and adjacent continental shelf seas) is dominated by the inflow of Atlantic water over the shelf seas, which is subsequently exported as the return flow of the TPD towards Fram Strait. The Pacific water not only circulates in the BG but also circulates along the transpolar drift route in the Arctic Ocean (Hu et al., 2019). The anticyclonic BG dominates in the circulation of the Surface Mixed Layer (SML) in the Canada Basin (Meincke et al., 1997). The TPD is the major surface current that transports sea ice and shelf surface waters from the Laptev and East Siberian shelves (Charette et al., 2020), carrying a large amount of freshwater and terrestrial DOM to the Central Arctic Ocean (CAO), indicated by elevated DOC and CDOM concentration (Slagter et al., 2017). The position of the TPD varies with the Arctic Oscillation index (Macdonald et al., 2005; Karcher et al., 2012; Smith et al., 2021). In a negative Arctic Oscillation (AO−), the TPD transports sea ice and shelf surface waters from the East Siberian Shelf and Laptev shelf across the Arctic Basin towards the Fram Strait and East Greenland Current (EGC; McClelland et al., 2012). The TPD affects the Amundsen Basin and Makarov Basin, which is separated by the

Lomonosov ridge, while the Nansen Basin, which are separated from the Amundsen Basin by the Gakkel Ridge, is largely unaffected by the TPD (Slagter et al., 2017). In a positive Arctic Oscillation (AO+), the TPD shifts eastward and into the BG, entraining more Pacific water from the Chukchi Sea and river runoff from the East Siberian Shelf waters, which are transported farther east along the shelf before entering the TPD (Anderson and Amon, 2015; Carmack et al., 2016).

The Arctic riverine drainage basins vary with variable vegetation and soil conditions. Most soils in the drainage basins of Arctic rivers typically contain old organic matter, with average radiocarbon ages ranging from centuries to millennia (Schirrmeister et al., 2002; Benner et al., 2004). Frozen permafrost soils represent a large reservoir of this old organic carbon (an estimated value of ~1700 Pg C). With extensive thawing of the permafrost due to a warmer climate, accelerate carbon losses and an increased export of aged organic matter to the Arctic ocean is expected (Tarnocai et al., 2009; Hugelius et al., 2014). It has been found that vegetation is a major source of terrigenous organic matter to the Arctic Ocean and little of aged organic carbon in the soils contributes to the Arctic Ocean (Opsahl et al., 1999; Benner et al., 2004). Several studies observed a largely conservative distribution of terrigenous DOM along a salinity gradient across the Arctic shelves, suggesting the predominantly recalcitrant character of terrestrial DOM (Guay et al., 1999; Kattner et al., 1999; Dittmar and Kattner, 2003; Kohler et al., 2003; Hölemann et al., 2021). However, Cooper et al. (2005) estimated that ~30% of terrestrial DOC is initially removed over the shelves before entering the Eurasian Arctic. Kaiser et al. (2017) showed that ~50% of the annual discharge of terrestrial-derived DOC from Siberian rivers is mineralized on the Eurasian shelves. Holmes et al. (2008) pointed out that the lability of terrestrial DOC transported by Alaska rivers to the Arctic Ocean has large seasonal variation, and 20%–40% of the terrestrially-derived DOM (tDOM) during the spring freshet in Alaskan rivers is labile on the timescale of months, while tDOM is more resistant to degradation during summer periods. Raymond et al. (2007) showed terrestrial DOC transported during spring floods is young based on radiocarbon age and likely consists of recently fixed carbon in leaf litter and soil, with about 50% 1–5 years old and about 35% 6–20 years old. River runoff has $3.5 \pm 2.0$ years of residence time on the Eurasian shelves before passing offshore to join the TPD (Schlosser et al., 1994). Then the transport time of

runoff from Eurasian shelves via TPD to reach Fram Strait is about three years (Jahn et al., 2010). Hence, the most labile tDOM may be removed in the Eurasian shelves before it transports into Central Arctic. The analysis on stable carbon isotope data, indicates that an estimate of 25–33% of the terrestrial DOC discharged by rivers to the Arctic Ocean is exported to the North Atlantic via the EGC (Benner et al., 2005), or 20–50% as estimated using DOM fluorescence (Amon et al., 2003), or 12–41% as estimated using the lignin content (Opsahl et al., 1999). The terrigenous DOC is estimated to be mineralized with a half-life of 7.1 ± 3.2 years in the western Arctic Ocean (Hansell et al., 2004). Therefore, except for the labile tDOM removal in the continental shelves, the remainder of tDOM can be removed in long timescales within the Arctic Ocean due to microbial or photochemical mineralization processes (Hansell et al., 2004).

The surface polar water in the Eurasian Basin is largely transported towards the Fram Strait via the TPD. Part of the polar surface water transported in the EGC mixes into the center of the convective gyres of the Greenland/Labrador Seas, and contributes to DOM export to North Atlantic Deep Water (NADW) formation (Schlosser et al., 1994; Rudels, 1995; Carmack et al., 2016). In addition, the Arctic deep waters (~2500 m) can be export to the Greenland-Iceland-Norwegian (GIN) seas through Fram Strait, and contribute to the formation of NADW (Bönisch and Schlosser, 1995). Terrigenous DOC of Arctic origin has been identified in components of NADW (Benner et al., 2005). The terrigenous DOC in Arctic polar surface waters has a modern radiocarbon age and a relatively short residence time (~1–6 yr) prior to export to the North Atlantic Ocean (Opsahl et al., 1999; Benner et al., 2004). Terrigenous DOM accounts for a much greater fraction of the DOM in the Arctic surface water (~5–33%) compared to the Pacific and Atlantic oceans (~0.7–2.4%; Opsahl et al., 1999). Hence a massive DOC export to the dark ocean with the NADW formation (~48 μmol $kg^{-1}$) and a subsequent DOC loss during thermohaline circulation because of DOM mineralization, reaching the minimum in the North Pacific (~34 μmol $kg^{-1}$; Hansell et al., 2009).

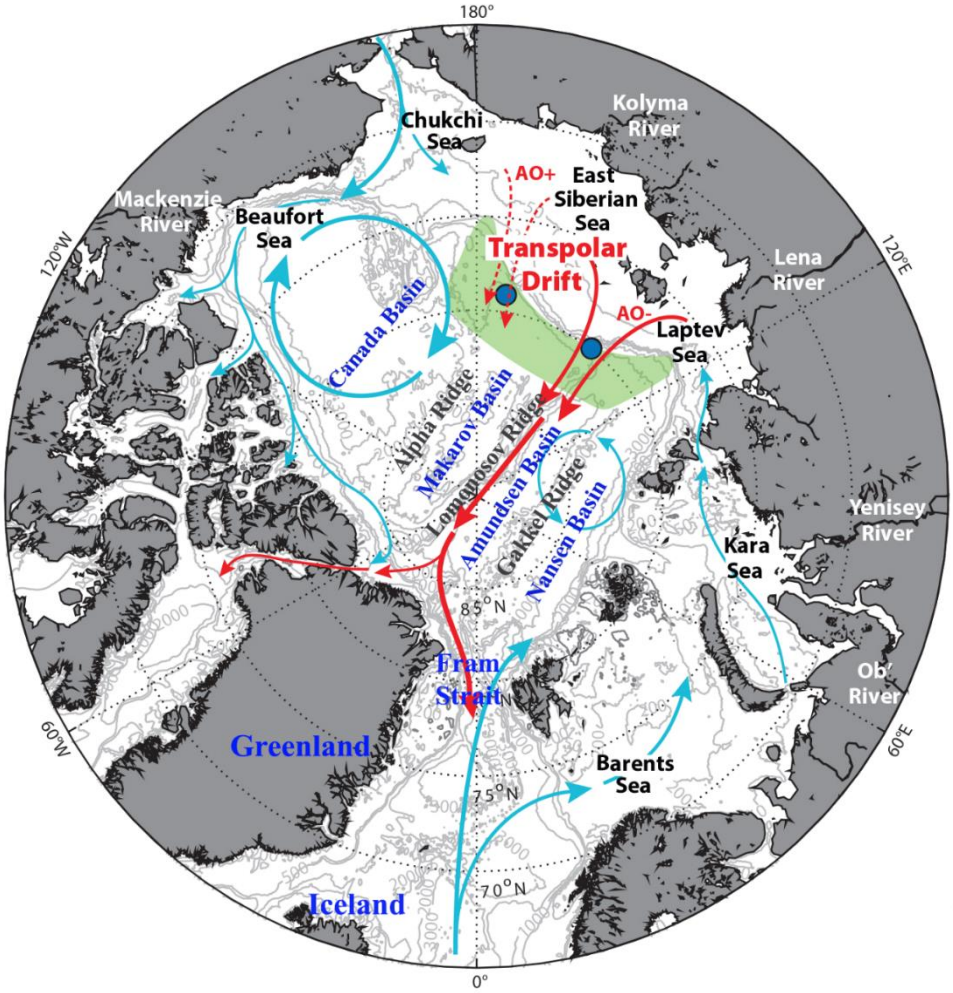


**Figure 4.** Map of the Arctic Ocean. Figure adapted from (Kipp and Charette, 2022). The light blue arrows indicate the major surface currents. The red arrows indicate approximate location of the TPD origin for the positive (AO+) and negative (AO−) modes of the Arctic Oscillation.

## 1.6. Analytical methods for DOM characterization and quantification

In the past, optical and molecular-level analytical techniques evolved and improved our mechanistic understanding of DOM fluxes. Optical spectroscopy (absorbance and fluorescence) has been widely used to investigate bulk changes of DOM in aquatic samples due to its simplicity and high sensitivity and cost-effectiveness (Parlanti et al., 2000; Baker and Spencer, 2004; Yamashita and Jaff , 2008). Parallel factor analysis (PARAFAC) is an efficient tool to decompose the fluorescence signal of the EEMs into the underlying individual fluorescent components and provides information about

the sources and composition of CDOM (McKnight et al., 2001; Stedmon et al., 2003; Murphy et al., 2008; Fichot et al., 2013). Fourier-transform ion cyclotron resonance mass spectrometry (FT-ICR) mass spectrometry (MS) provide great insight in the molecular-level characterization of DOM. Many studies have related FT-ICR MS based on SPE-DOM and optical parameters in natural waters (Herzsprung et al., 2012; Stubbins et al., 2014; Kellerman et al., 2015; Lavonen et al., 2015; Timko et al., 2015; Wagner et al., 2015; Martínez-Pérez et al., 2017; Wünsch et al., 2018a) to characterize the relevant molecular formulas (MFs) for different optical parameters or different sources of DOM. However, no studies have linked FT-ICR MS and optical parameters to investigate quantitative changes in different sources of DOM and their relative contributions in the Arctic.

### *1.6.1. Optical spectroscopy for DOM characterization*

In aquatic systems, a fraction of DOM that absorbs light in the ultraviolet (UV; 200-400 nm) and visible (400-800 nm) radiation is called colored, or chromophoric dissolved organic matter (CDOM; Stedmon and Nelson, 2015). Although the molecules that make up the CDOM pool are poorly defined, it is estimated that CDOM constitutes up to ~70% of the DOC pool (Laane and Koole, 1982) and is dominated by aromatic carbon content (Chin et al., 1994; Weishaar et al., 2003; Stubbins et al., 2008). CDOM, the optically active and ubiquitous constituent in the ocean, can have negative feedback on primary production by attenuating light penetration and absorbing light, that otherwise would be available for photosynthesis. A positive feedback of CDOM on marine organisms is via the protection of plankton from harmful ultraviolet B (UVB; 280–320 nm) or ultraviolet A (UVA; 320–400 nm) radiation (Arrigo and Brown, 1996; Williamson et al., 1996; Granskog et al., 2007; Hill, 2008). CDOM can be recorded by satellite remote sensing (Glukhovets et al., 2020; Lewis and Arrigo, 2020) and participates in a wide range of photochemical reactions (Miller and Zepp, 1995; Osburn et al., 2009; Gonsior et al., 2013; McKay et al., 2018). High CDOM concentration is found in the Arctic Ocean, subarctic North Atlantic and Pacific, intermediate values are observed in Equatorial upwelling regions and the Southern Ocean, and lower abundance in the subtropical gyres (Siegel et al., 2005; Nelson et al., 2010). High CDOM concentration is observed in the Arctic Ocean,

due to the large inputs of color-rich DOM by river discharge and the inefficient photo-degradation of CDOM in the sunlight-diminished and often ice-covered waters (Bélanger et al., 2006; Osburn et al., 2009; Dittmar and Stubbins, 2014). After the absorption of light (energy), a part of CDOM that emits a fraction of the absorbed energy as fluorescence, is called fluorescent dissolved organic matter (FDOM). DOM molecules are excited by photons of specific wavelengths and emitted light has a longer wavelength due to energy loss (Coble et al., 2014). The relationship between DOM, CDOM, and FDOM are display in Figure 5.

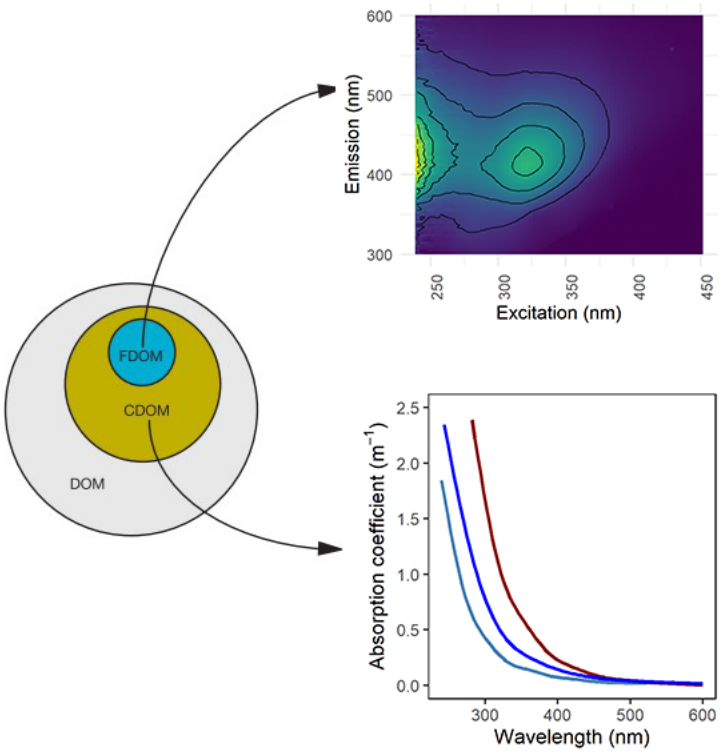


**Figure 5.** The optically active pools of CDOM and FDOM as subfractions of the total DOM pool. Figure adapted from (Dittmar and Stubbins, 2014).

CDOM can be quantified rapidly by the strength of its optical signals in the laboratory, in situ, or remotely sensing and directly measured in the original water (Spencer et al., 2009b; Zielinski et al., 2018; Glukhovets et al., 2020; Lewis and Arrigo, 2020). The UV-visible light absorption spectrum of CDOM often decreases exponentially from 240 to 600 nm wavelengths (Stedmon and Nelson, 2015). The concentration of CDOM can be expressed in terms of its absorption coefficient at a specific wavelength.

Wavelengths in the range of 280–450 nm are commonly used for this purpose (Perdue and Benner, 2009). The absorption coefficient at λ nm ($a_{CDOM}(\lambda)$ in $m^{-1}$) can be calculated by the equation: $a_{CDOM}(\lambda) = 2.303A(\lambda)/l$, where the factor 2.303 is the natural logarithm of 10, A(λ) is the absorbance at wavelength λ in nm, and $l$ is the optical path length in meters (Stedmon and Markager, 2001). The quality of CDOM is often assessed by the spectral slope of the absorption spectrum, such as the spectral slope between 275 and 295 nm ($S_{275-295}$ in $nm^{-1}$), and between 350 and 400 nm ($S_{350-400}$ in $nm^{-1}$), and the spectral slope ratio $S_R$ (calculated by the ratio between $S_{275-295}$ and $S_{350-400}$). These parameters provide insight concerning the source, molecular weight, and aromaticity of DOM (Helms et al., 2008; Stubbins et al., 2012; Hansen et al., 2016). An additional qualitative measure of CDOM is the specific UV absorbance at 254 nm ($SUVA_{254}$ in L $mg^{-1}$ $m^{-1}$), which is calculated by the UV absorbance at 254 nm (given in $m^{-1}$) divided by the DOC concentration in mg $L^{-1}$ (Weishaar et al., 2003). $SUVA_{254}$ has been previously used as a proxy for aromaticity of aquatic humic substances and is positively correlated with molecular weight (Weishaar et al., 2003).

The concentration of FDOM can be expressed as its fluorescence intensity, which is a function of the wavelengths of excitation and emission. The fluorescence intensity can be measured at a single pair of wavelengths for excitation and emission, a single excitation wavelength over a range of emission wavelengths, or a single emission wavelength over a range of excitation wavelengths. The most comprehensive measurement of fluorescence intensity is the combination of a number of fluorescence emission scans at different excitation wavelengths to obtain an excitation-emission matrix spectrum (EEMs; Perdue and Benner, 2009). The fluorescence properties of FDOM are largely restricted to excitation wavelengths of 240-500 nm and emission wavelengths of 300-600 nm (Stedmon and Nelson, 2015). In general, the data can be characterized by visual identification of peaks (peak picking), signal integration in different wavelength regions, or developing indices from ratios of fluorescence at specific wavelengths (Stedmon and Nelson, 2015). Peaks are typically categorized into two groups: protein-like and humic-like substances (Coble, 2007). In these two groups, six general types of fluorescence peaks in different wavelength regions of DOM are displayed in Table 1. The protein-like fluorescence is typically narrower and at wavelengths shorter than 350 nm and often categorized into tyrosine-like

(Ex. 275/Em. 305 nm; peak B), tryptophan-like (Ex. 275/Em. 340 nm; peak T) and phenylalanine-like (Ex. 280/Em. 370 nm; peak N) substances. The term protein-like is used because it resembles the three fluorescent aromatic amino acids: tryptophan, tyrosine, and phenylalanine (Determann et al., 1998). The fluorescence of tyrosine is difficult to detect when both tyrosine and tryptophan coexist in the same peptides because the emission energy of tyrosine is transferred to tryptophan and quenching by neighboring groups (Stedmon and Nelson, 2015). The humic-like fluorescence has been characterized by a broad range of emissions exceeding 350 nm. The term humic-like is used because the similar fluorescence was originally detected in soil organic matter and fulvic acid XAD extracts (Stedmon and Nelson, 2015). Compared to protein-like fluorescence, the humic-like fluorescence is ubiquitous in all aquatic environments and is detected at higher emission wavelengths, which is commonly referred to peak A, peak C and peak M. Peaks A and C are often considered as terrestrial-derived humic-like materials, and peak M is characterized as marine-derived humic-like substances (Coble, 2007). It is well known that humic-like peaks A and C can be generated in situ in the oceans by phytoplankton and bacteria (Romera-Castillo et al., 2010, 2011). Terrestrial humic-like materials show excitation and emission maxima at longer wavelengths than marine humic-like materials, as predicted from their more aromatic chemistry and assumed higher molecular weight (Coble, 2007). Parallel Factor Analysis (PARAFAC) is the most common method to statistically decomposes fluorescence EEMs into underlying individual, independently components that represent groups of fluorophores with similar spectra (Stedmon et al., 2003; Murphy et al., 2008, 2013; Stedmon and Bro, 2008).

**Table 1.** Spectral characteristics for major fluorescent components identified by peak-picking method. Table adapted from (Coble, 2007)

| Peak name | Excitation (nm) | Emission (nm) | Source |
|---|---|---|---|
| B | 275 | 305 | Tyrosine-like, autochthonous |
| T | 275 | 340 | Tryptophan-like, autochthonous |
| N | 280 | 370 | Phenylalanine-like, autochthonous |
| A | 260 | 400-460 | Terrestrial humic-like |
| M | 290-310 | 370-410 | Marine humic-like |
| C | 320-360 | 420-460 | Terrestrial humic-like |

In addition, three fluorescence parameters are widely applied to the analysis of FDOM. The fluorescence index (FI) is calculated, based on the ratio of the emission intensity at a wavelength of 450 nm and that at 500 nm, obtained for a fixed excitation wavelength of 370 nm (McKnight et al., 2001). FI is commonly used as an indicator to identify the relative contribution of microbial and terrestrial sources to the DOM pool: Low FI values suggest that water samples are dominated by terrestrially-derived substances, whereas high values are indicative of microbially-derived DOM (Johnson et al., 2011; Murphy et al., 2018). The biological index (BIX) is calculated by the ratio of the emission intensity at 380 nm divided by that at 430 nm with a fixed excitation wavelength of 310 nm (Huguet et al., 2009). BIX is an indicator of autotrophic productivity, with high values (>1) corresponding to recently produced DOM of autochthonous origin (Huguet et al., 2009). The humification index (HIX) is calculated by the area under the emission spectra 435–480 nm divided by the peak area 300–345 nm with a fixed excitation wavelength of 254 nm (Ohno, 2002). It is an indicator of humic substance content or extent of humification, with high values indicating an increasing degree of humification (Ohno, 2002).

### *1.6.2. Solid-phase extraction for DOM desalting and enrichment*

Solid-phase extraction (SPE) is one of the most widely used techniques to concentrate and desalt DOM in marine and freshwater prior to DOM analysis, which is widely used method of sample extraction for the ultrahigh-resolution mass spectrometry

(FT-ICR MS; Dittmar et al., 2008; Li et al., 2017; Tfaily et al., 2012). PPL (styrene divinyl benzene polymer) has become a popular extraction adsorbent for SPE with the ability to retain moderately polar to nonpolar DOM at relatively high recoveries for DOC from seawater and freshwater (Dittmar et al., 2008; Raeke et al., 2016; Broek et al., 2017; Johnson et al., 2017). However, PPL extractions are not quantitative and recover ~20–90% of DOC in aquatic samples, which could result in molecular differences when comparing DOM composition between original water and extracts (Koch et al., 2008; Chen et al., 2016a; Li et al., 2016a; Wünsch et al., 2018b). Many studies have compared compositional or structural differences for original and extracted DOM, and some compared the influence of enrichment volume on the extraction efficiency (Dittmar et al., 2008; Sleighter and Hatcher, 2008; Chen et al., 2016a; Li et al., 2016b; Raeke et al., 2016; Wünsch et al., 2018b). However, few studies have looked at the mechanistic details of potential fractionation and adsorption mechanisms that are caused by different loadings in SPE (Li et al., 2016b). Hence, it is worth investigating the potential chemical fractionation mechanisms for PPL-extracted DOM induced by different loadings.

### *1.6.3. Applying mass spectrometry for DOM molecular characterization*

The composition of the DOM is highly complex, and with common analytical techniques only a small fraction can be analyzed at the molecular level, such as amino acids, carbohydrates, lipids and lignin, which are present in DOM only in trace amounts (Kaiser and Benner, 2009, 2012b). The largest fraction of DOM remains molecularly uncharacterized due to its resistance to isolation, chromatographic separation and hydrolysis, oxidation and other preparation processes (Hedges et al., 2000). Recent advances in technology, especially of ultrahigh resolution Fourier-transform ion cyclotron resonance (FT-ICR) mass spectrometry (MS) with direct infusion (DI) electrospray ionization (ESI) has emerged as an important analytical technique to characterize the compounds making up the DOM reservoir on a molecular level. FT-ICR MS has been successfully applied to distinguish thousands of molecules of different elemental composition in marine DOM, with peak locations ranging from 200 to 1,000 m/z and the most abundant masses concentrated between

300 and 400 m/z (Flerus et al., 2012; D'Andrilli et al., 2015; Hawkes et al., 2016; Arakawa et al., 2017).

### *1.6.4. Challenges of molecular-level analysis of DOM*

Nuclear magnetic resonance (NMR) spectroscopy is the most used technique for the structural characterization of DOM molecules, and major structural characteristics have been revealed (Hertkorn et al., 2006; Mopper et al., 2007). The broad signals are unresolved in conventional $^{1}$H- or $^{13}$C-NMR due to the overlapping spectra of thousands of individual compounds in DOM (Dittmar and Stubbins, 2014). Even though most advanced NMR techniques could reveal more detailed molecular structures within DOM, the resolving capacities are still surpassed due to the molecular diversity and heterogeneity of DOM (Hertkorn et al., 2007). Hence, it is not possible to obtain structural information for individual molecules within the DOM pool.

FT-ICR MS provides much higher resolution than other MS techniques and is now capable of determining the mass of an intact molecule with an mass accuracy of better than 0.1 mDa from complex natural mixtures of organic compounds and mostly approximates the compositional diversity of DOM (Petras et al., 2017). Although FT-ICR MS provides valuable insight into the molecular diversity, the molecular information within DOM is restricted to exact molecular masses and subsequently MFs that assigned to mass peaks. The MFs have provided further information about elemental ratios and thus compound diversity (Koch et al., 2008), but it is unable to differentiate between structural isomers of a molecular formula (MF), hence the molecular structures capable of understanding of sources, sinks, and turnover processes of DOM remain elusive. Even the number of structural isomers behind each detected MF in the DOM is unknown, but the underlying structural features can still be inferred from the MF and its relative abundance pattern (Dittmar and Stubbins, 2014).

Ultrahigh resolution DI-ESI FT-ICR MS has revealed the molecular complexity within the marine and terrigenous DOM (Koch et al., 2005, 2007; Flerus et al., 2012), but quantitation of terrestrial and marine sources in the DOM pool has not be well

defined. Two major chemical fractionation effects so far challenged the representative and quantitative characterization of DOM by ESI FT-ICR MS measurement: (i) desalting and pre-concentration via SPE (cf. Kong et al., 2021) and (ii) selective ionization of molecules in the ionization process of the mass spectrometer (Kiontke et al., 2016). Normally, these advanced techniques such as NMR or mass spectrometry require sample isolation prior to analysis. Three common methods include ultrafiltration (Skoog and Benner, 1997), reverse osmosis coupled with electrodialysis (Koprivnjak et al., 2009) and SPE using various resins (Stuermer and Harvey, 1974; Lara and Thomas, 1994; Dittmar, 2008). All of these methods are primarily based on molecular size or polarity to separate operationally defined DOM fractions, and a considerable fraction of DOM still escapes molecular characterization. A subfraction of DOM isolated using SPE, referred as SPE-DOM, has been widely used for FT-ICR MS measurements (Hertkorn et al., 2007; Koch et al., 2007; Mopper et al., 2007; Capley et al., 2010; Sleighter et al., 2012; Kellerman et al., 2014). SPE-related fractionation results in molecular compositional differences between SPE-DOM and original samples (Kong et al., 2021), which limits the comparison between MS data and bulk optical parameters. In addition, using FT-ICR MS requires ionization of the DOM prior to MS analysis. An ideal ionization source for quantitative characterization of DOM by the FT-ICR MS should be non-selective (i.e., ionization efficiency of all compounds equally) and soft (i.e., ionize compounds without fragmentation; Mopper et al., 2007). Electrospray ionization (ESI) has been a widely used ‘soft’ ionization technique that allows the molecular ions to be detected by the mass spectrometer without fragmentation (Novotny et al., 2014). It has been shown that ionization efficiency is related to compound properties such as basicity, polarity, volatility and molecular size on ESI-MS response (Oss et al., 2010; Kiontke et al., 2016). The assigned MFs include heteroatoms like N, S, and P, and each of the assigned formulas can cover a large number of structures (Hawkes et al., 2018a). The MFs in the DOM with heteroatom contents or the MFs with diverse structural isomers may present different ionization efficiencies, which can also influence the quantification of DOM on the molecular level. SPE-DOM samples analyzed by DI-ESI FT-ICR MS leads to an ionization suppression and competition of many molecules due to the homogeneity

and complexity of DOM (Lechtenfeld et al., 2015; Zark and Dittmar, 2018), preventing the discrimination of isobaric and isomeric structures.

High performance liquid chromatography (HPLC) separation offers a promising alternative for MS analysis since it physically separates DOM based on the polarity prior to detection (Reemtsma, 2001; Dittmar et al., 2007; Mopper et al., 2007; Brown et al., 2016; Petras et al., 2017; Lu et al., 2018; Lu and Liu, 2019). Some studies utilize offline HPLC separation for FT-ICR MS for SPE-DOM analysis (Koch et al., 2008; Spranger et al., 2019), which is laborious and time-consuming. Few recent studies applied Fourier-transform ion cyclotron resonance mass spectrometry hyphenated with high performance liquid chromatography (LC-FTMS) to analyze the original waters (Hawkes et al., 2018b; Kim et al., 2019), which introduces a new fractionation effect in ESI due to a changing solvent matrix along the HPLC gradient. Han et al. (2021) utilizes the LC-FTMS using a counter gradient to stabilize the solvent matrix for transient ESI-MS signals and successfully detects more polar compounds using original the Suwannee River Fulvic Acid (SRFA) and peat pore water compared to DI SPE-DOM measurement.

## 2. Objectives

My thesis was organized in a methodological objective (Part 1) that addressed chemical mechanisms during SPE and a research objective (Part 2) that focused on spatiotemporal changes of DOM in the Central Arctic Ocean and was based on samples acquired during the MOSAiC expedition.

**Part 1**

Solid-phase extraction (SPE) has been widely applied for DOM analyses techniques that lack sufficient sensitivity and / or require desalting of samples. Here, a method was developed to investigate and quantify the potential chemical fractionation and adsorption mechanisms that potentially occur during SPE. Specifically, we wanted to assess the effect of increased column loading on the chemical characteristics of the extracts. The study aimed at providing a best practice recommendation for solid-phase extraction of DOM to minimize compositional variability introduced by SPE. We tested the hypotheses as follows:

a) Increased carbon loading results in decreasing extraction efficiency of DOC concentration and in optical and chemical fractionation;

b) The predominant extraction mechanism shifts from DOM-PPL physisorption to DOM self-assembly with increasing carbon loading on the PPL surface.

**Part 2**

The quantification of terrestrial DOM in the ocean and the contribution of DOM derived from sea ice production are not well constrained. Climate warming related changes in DOM chemical characteristics and terrestrial DOM contributions may alter DOM budgets not only in the Arctic but also in the deep Atlantic Ocean. Due to the severe conditions in the Central Arctic Ocean, very few seasonal DOM observations are available compared to the remainder of the world oceans, especially in the winter season. Chemical characterization and quantification by mass spectrometry is primarily challenged by the fact that all previous studies relied on sample preparation by SPE that is subject to chemical fractionation (cf. Part 1) and hampers quantitation.

My overall objective was to quantify spatiotemporal differences in the DOM composition and bioavailability in the Central Arctic Ocean. We combined optical spectroscopy and an online high performance liquid chromatography separation that was hyphenated to FT-ICR MS and allowed analyses of original seawater.

Specifically, we wanted to quantify the changes in DOM sources (terrestrial versus marine) throughout the water column and between regions and seasons. Key hypotheses were:

a) The chemical composition of DOM varies much more with spatial rather than seasonal changes during the MOSAiC expedition;

b) The DOM compositions can be significantly modulated by seasonality during the MOSAiC expedition;

c) DOM from original Central Arctic water samples can be quantitatively characterized using the LC-FTMS analysis;

d) DOM derived from sea ice production can be tracked using LC-FTMS and optical spectroscopy;

e) The chemical properties of DOC derived from different origins can be compared by the LC-FTMS and optical spectroscopy.

## 3. Manuscript I

# Solid-phase extraction of aquatic organic matter: loading-dependent chemical fractionation and self-assembly

*Xianyu Kong*, Thomas Jendrossek, Kai-Uwe Ludwichowski, Ute Marx, and Boris P. Koch**

Alfred Wegener Institute Helmholtz Centre for Polar and Marine Research, Am Handelshafen 12, 27570 Bremerhaven, Germany

* Corresponding author: Email: Xianyu.Kong@awi.de

Email: Boris.Koch@awi.de

## 3.1. Abstract

Dissolved organic matter (DOM) is an important component in marine and freshwater environments and plays a fundamental role in global biogeochemical cycles. In the past, optical and molecular-level analytical techniques evolved and improved our mechanistic understanding about DOM fluxes. For most molecular chemical techniques, sample desalting and enrichment is a prerequisite. Solid-phase extraction (SPE) has been widely applied for concentrating and desalting DOM. The major aim of this study was to constrain the influence of sorbent loading on the composition of DOM extracts. Here we show that increased loading resulted in reduced extraction efficiencies of dissolved organic carbon (DOC), fluorescence and absorbance, and polar organic substances. Loading-dependent optical and chemical fractionation induced by altered adsorption characteristics of the sorbent surface (PPL) and increased multilayer adsorption (DOM self-assembly) can fundamentally affect biogeochemical interpretations, such as the source of organic matter. Online fluorescence monitoring of the permeate flow allowed to empirically model the extraction process, and to assess the degree of variability introduced by changing the sorbent loading in the extraction procedure. Our study emphasizes that it is crucial for sample comparison to keep the relative DOC loading ($DOC_{load}$ [wt%]) on the sorbent always similar to avoid chemical fractionation.

**Keywords:** dissolved organic matter; fluorescence spectroscopy; EEMs; PARAFAC; RP-HPLC; scanning electron microscopy; polarized light microscopy; multilayer adsorption.

## 3.2. Introduction

Dissolved organic matter (DOM) is a highly complex heterogeneous mixture of compounds comprising a large range of molecular size, polarity, or elemental composition all of which varying considerably between freshwater and saltwater (Hopkinson and Vallino, 2005; Ksionzek et al., 2016, 2018). DOM plays an essential role as a large carbon reservoir in global biogeochemical carbon cycles and an improved understanding of DOM biogeochemistry relies on molecular characterization (Hockaday et al., 2009; Perminova et al., 2014; Lewis et al., 2020). Water sample desalting and enrichment is a prerequisite for many analytical techniques, such as ultrahigh-resolution mass spectrometry (FT-ICR MS; Mopper et al., 2007; Chen et al., 2011; Green et al., 2014).

Solid-phase extraction (SPE) is one of the most widely used techniques to concentrate and desalt DOM in marine and freshwater (Dittmar et al., 2008; Tfaily et al., 2012; Li et al., 2017). Although other SPE sorbent also exhibited high recoveries (Swenson et al., 2014; Rho et al., 2019), PPL (styrene divinylbenzene polymer) has become a popular extraction sorbent with the ability to retain moderately polar to nonpolar DOM at relatively high recoveries for dissolved organic carbon (DOC; Dittmar et al., 2008; Raeke et al., 2016; Broek et al., 2017; Johnson et al., 2017). However, PPL extractions are not quantitative and recover ~20–90% of DOC in aquatic samples, resulting in molecular differences when comparing DOM composition between original water and extracts (Koch et al., 2008; Chen et al., 2016a; Li et al., 2016a; Wünsch et al., 2018b). Unlike in one-compound systems, the efficiency of DOM extraction via SPE is not only driven by the interaction with the stationary phase, but also affected by the concentrations, size and polarities of molecules in DOM. Intermolecular effects and competition affect the equilibria between mobile and stationary phase. Many studies have compared compositional or structural differences for original and extracted DOM, and some compared the influence of enrichment volume on the extraction efficiency (Dittmar et al., 2008; Sleighter and Hatcher, 2008; Chen et al., 2016a; Li et al., 2016b; Raeke et al., 2016; Wünsch et al., 2018b). However, few studies have looked at the mechanistic details of potential fractionation and adsorption mechanisms that are caused by different loadings in SPE (Li et al.,

2016b).

Chromophoric dissolved organic matter (CDOM), the optically active fraction of bulk DOM, also plays an important role in biogeochemical cycles (Nelson and Gauglitz, 2016; Martias et al., 2018; Cao et al., 2020). Optical spectroscopy (absorbance and fluorescence) has been widely used to characterize properties and dynamics of CDOM in the original matrix because of its relative ease of use, and high sensitivity (Hansen et al., 2016; Yamashita et al., 2017; Zherebker et al., 2020). Fluorescence excitation-emission matrices evaluated with parallel factor analysis (EEM-PARAFAC) is an effective tool for tracking and characterizing the source, distribution, composition, and turnover of fluorescent dissolved organic matter (FDOM) (Ishii and Boyer, 2012; Murphy et al., 2018; Schittich et al., 2018; Carr et al., 2019). Moreover, targeted analysis of specific DOM compounds (such as amino acid) or untargeted analysis (such as polarity assessment) using e.g. reversed-phase high-performance liquid chromatography (RP-HPLC) are also used to chemically characterize DOM (Fitznar et al., 1999; Koch et al., 2008).

The main objective of this study was to reveal the potential chemical fractionation mechanisms for PPL-extracted DOM induced by different loadings. For this, we established an online fluorometric monitoring of the permeate and applied microscopy to visualize the loading on the surface of PPL beads. We hypothesize that increased loading results in decreasing extraction efficiency and in optical and chemical fractionation. Based on the online monitoring data, we aimed at establishing an extraction model that helps to assess the analytical variability introduced by changing extraction mechanisms along increased sorbent loading.

## 3.3. Methods and materials

**Sampling.** Samples were collected at lower River Weser (Ws1, riverine sample) near the town of Minden, the outer River Weser estuary (Ws2, estuarine sample), the Southern North Sea (Ws3, Ms1, marine sample), and the fishery harbor near the Alfred Wegener Institute in Bremerhaven, Germany (Es1, Es2, estuarine sample). Es1 was used to carry out online fluorometric detection of the permeate DOM using PPL extraction. Es2 served to visualize PPL sorbent surface using microscopy. Ms1 (high

microbial degradation) was used to examine FDOM self-assembly on PPL sorbent, and Ws1, Ws2, and Ws3 to explore loading and sorbent-type dependent changes in DOM extracts. All samples were filtered using pre-combusted glass fibre filters (GF/F, 1825-047, Whatman), and stored at 4 °C in the dark until analysis. All sampling material was previously either pre-combusted at 450 °C or treated with 10% hydrochloric acid and well-rinsed with ultrapure water. The relative DOC loading weight of the sorbent ($DOC_{load}$) was calculated as:

$$\mathrm{DOC_{load}(wt\%) = DOC_{conc}(mg\,L^{-1}) \times Volume_{sample}(L) \div Mass_{sorbent}(mg) \times 100} \quad (1)$$

where $DOC_{conc}$ is the DOC concentration of the original sample, $Volume_{Sample}$ is the volume of the extracted samples, and $Mass_{Sorbent}$ is the weight of the sorbent material.

**Experimental setup.** For online fluorometric detection (USB2000-FLG, 200 µm slit, Ocean Optics spectrometer) of DOM in the permeate flow of a large volume (8.2 L) estuarine sample Es1 extraction, SPE cartridge (PPL; 200 mg; Bond Elut, Agilent Technologies) was conditioned with methanol (3 mL each, LiChrosolv, Merck) and acidified ultrapure water (3 mL, pH 2; HCl 30% suprapure, Merck). The acidified water sample (pH 2; HCl 30% suprapure, Merck) was filled into reservoirs, which were connected by Luer adaptors to SPE cartridge. The cartridge was fixed using an extraction support device (Visiprep, Supelco). Sample was drawn through the cartridge using Tygon tubings (SC0015, ISMATEC) and a peristaltic pump (ISM931C, ISMATEC) at a flow rate of 4.0 mL $min^{-1}$. The permeate flow was passed through a flow-through cell (V = 750 µL, 175 050-QS, Hellma) and DOM was excited using light-emitting diodes (LLS LED, Ocean Optics) at 365 nm during the entire extraction. The emitted fluorescence signal was measured with a fiber optic spectrometer (USB2000-FLG, 200 µm slit, Ocean Optics spectrometer) and integrated over a wavelength range of 420–600 nm. Processing and visualization of the data were performed using the instrument software (spectra suite, Ocean Optics, Table 1). Subsamples were collected from the permeate at the exit of the flow-through cell and measured for DOC concentration, excitation emission matrices (EEMs), and absorbance (see below). Process blanks for each sorbent were performed by extracting acidified ultrapure water with same procedure.

**Table 1.** Spectrasuite-parameters for online fluorescence measurement

| Parameters | Setting |
|---|---|
| Integration time (s) | 2 |
| Scans to average | 3 |
| Boxcar width | 5 |
| *Non*-linearity correction | active |
| Stray light correction | active |
| Integration method | rectangular |

To further investigate FDOM self-assembly on PPL sorbent (200 mg; Bond Elut, Agilent Technologies), we collected the permeate for the volumes 0–200 mL (0–0.1 wt% $DOC_{load}$) and 200–400 mL (0.1–0.2 wt% $DOC_{load}$) for Ms1 SPE process. PPL extractions were performed in triplicate and the EEMs of permeate were averaged for each treatment and the EEMs extraction efficiency was calculated by subtracting the permeate EEMs from the EEMs of the original sample.

In addition, four discrete enrichment volumes (100, 250, 500 and 1000 mL) of samples Ws1 - Ws3 were extracted using PPL and C8 cartridges (200 mg; Bond Elut, Agilent Technologies). All cartridges were eluted with 1.5 mL of methanol and stored at -18 °C until analysis to prevent esterification (Flerus et al., 2011).

**Microscopy.** To visualize DOM adsorption on the surface of PPL sorbent, three treatments of PPL sorbents were used for scanning electron microscopy (SEM), and polarized light microscopy. PPL cartridges were conditioned and (i) not loaded at all, (ii) loaded with 0.5 L, or (iii) loaded with 5 L estuarine water (Es2). All PPL sorbents were dried with $N_2$ prior to the microscope visualizations. PPL particles were mounted on stubs, sputter coated (Emscope SC500; Ashford, UK) with gold-palladium and viewed at 10 kV under a SEM (FEI Quanta FEG200; Eindhoven, the Netherlands). For polarized light microscopy, a mercury vapor lamp was used as light source (Axioskop50, Axiocam, Axiovision software; all Zeiss, Germany).

**Dissolved organic carbon measurement.** DOC and total dissolved nitrogen (TDN) were determined by high-temperature catalytic oxidation and non-dispersive infrared

spectroscopy and chemiluminescence detection (TOC-VCPN, Shimadzu). For determination of the sample DOC content in the methanol extracts, a 50 µL aliquot of each methanol extract was evaporated under $N_2$ and subsequently redissolved in 6.5 mL ultrapure water (Ksionzek et al., 2018). DOC extraction efficiency was calculated for all samples as DOC concentration in extract divided by DOC concentration in the corresponding original sample and considering the enrichment factor. DOC extraction efficiency for Es1 was additionally acquired by subtracting the permeate DOC from the original DOC.

**Optical spectroscopy measurement.** EEMs and absorbance were measured for permeate samples collected at discrete time intervals during SPE using a fluorometer (Horiba Aqualog) equipped with a CCD detector. Excitation and absorbance wavelengths ranged from 240 to 600 nm in 3 nm increments, and emission wavelengths from 220 to 620 nm (increment ~3.3 nm). EEMs and absorbance data were processed by staRdom package in R studio (Version 3.5.1) (Pucher et al., 2019). The fluorescence spectra were performed by ultrapure water blank correction, inner filter effect correction, and Raman normalization (dividing by Raman peak of pure water at integrated excitation of 350 nm with an emission wavelength interval of 371 to 428 nm; Lawaetz and Stedmon, 2009). Based on the acquired data, a PARAFAC analysis was carried out (Murphy et al., 2013). The fluorescence index (FI) is calculated, based on the ratio of the emission intensity at a wavelength of 450 nm and that at 500 nm, obtained for a fixed excitation wavelength of 370 nm (McKnight et al., 2001), and the biological index (BIX) is calculated by the ratio of the emission intensity at 380 nm divided by that at 430 nm with a fixed excitation wavelength of 310 nm (Huguet et al., 2009). Spectral slopes ($S_{275\text{-}295}$ and $S_{350\text{-}400}$) were calculated using nonlinear least-squares fit and spectral slope ratio ($S_R$) was calculated by the ratio of $S_{275\text{-}295}$ and $S_{350\text{-}400}$ (Helms et al., 2008). The fluorescence extraction efficiency was calculated using the extracted fluorescence signal divided by the fluorescence signal of the corresponding original sample.

**Polarity profile measurement.** The polarity profile of methanol extracts was analyzed using an HPLC method (Koch et al., 2008). Chromatographic separation was performed on an RP-HPLC system (Hitachi) equipped with an autosampler (L-2200),

pump (L-2130), column oven (L-2300), fluorescence detector (L-2485), and diode array detector (L-2450). In each analysis, 5 µL of methanol extracts were injected and separated according to polarity using a C18 reversed-phase column (PLRP-S column 3u 300Å, 150 x 2.1 mm, Agilent Technologies). The mobile solvents ultrapure water and methanol are used in a gradient program (Table 2). The separated substances were characterized optically by a fluorescence detector with excitation at 260 nm and emission at 430 nm. The amount of the separated organic substances was estimated by absorbance at a wavelength of 210 nm using a diode array detector. This wavelength was chosen, because it is sensitive to most functional groups that dominate in DOM (Lechtenfeld et al., 2011).

**Table 2.** Gradient program for polarity profile analysis

| Time (min) | Ultrapure water (%) | Methanol (%) | Flow rate (mL $min^{-1}$) |
|---|---|---|---|
| 0 | 99 | 1 | 0.2 |
| 1 | 99 | 1 | 0.2 |
| 10 | 0 | 100 | 0.4 |
| 20 | 0 | 100 | 0.4 |
| 30 | 99 | 1 | 0.4 |
| 50 | 99 | 1 | 0.3 |
| 55 | 99 | 1 | 0.2 |

**Amino acid measurement.** Amino acid analysis in methanol extracts was based on a previous method (Fitznar et al., 1999). Amino acid derivatization and separation were performed on the RP-HPLC system (Agilent Technologies) equipped with an autosampler (1200 Series G1329A), pump (1200 Series G1312A), column oven (1260 Infinity G1316A), fluorescence detector (1200 Series G1321A), and diode array detector (1260 Infinity G1315D). Amino acids were identified based on the mechanism that amino acids form highly fluorescent derivatives after reacting with orthophthal-aldehyde (OPA) and mercaptoethanol. For pre-column amino acid hydrolysis and derivatization, 20 µL methanol extracts firstly were pipetted and evaporated in precombusted glass ampoules, 400 µL of 4.5 M hydrochloric acid were added and sealed for 24 hours at 110 °C. Then ampoules were opened and the liquid slowly evaporated at 70 °C, and 200 µL of ultrapure water was added to the dried

hydrolyzate and again evaporated at 70 °C to remove traces of HCl. After that, 400 µL of borate buffer (30.91 g of boric acid in 1 L of sodium hydroxide (32%, Merck)) were added to the hydrolyzed amino acids, homogenized, and transferred into 2 mL HPLC vials. Finally, 20 µL of the hydrolyzed sample was derivatized to hydrophobic fluorescent amino acid derivatives with 3 µL of a mixture of 26 µL OPA and 1 mL mercaptoethanol in the autosampler.

After two minutes of derivatization, the sample was injected into the HPLC system for chromatographic separation and determination. The stationary phase used for the separation was a C18 reverse-phase column (Kinetex 2.6u 100 Å, 150 × 4.6 mm, Phenomenex) heated to 32 °C. The mobile phase consisted of two eluents, sodium acetate buffer (3.4 g $L^{-1}$, pH 6.0, Merck) and acetonitrile, which were used in a gradient program (Table 3). The flow rate of the gradient was 0.7 mL $min^{-1}$. The derivatized amino acids were monitored by the fluorescence detector at excitation/emission wavelengths of 330 / 445 nm and identified by amino acid standards (Agilent Technologies: 5061-3333). Twelve amino acids (Asx: aspartic acid/asparagine, Glx: glutamic acid/glutamine, Ser: serine, Gly: glycine, Thr: threonine, Arg: arginine, Ala: alanine, Tyr: tyrosine, Val: valine, Ile: isoleucine, Phe: phenylalanine, and Leu: leucine) were determined after acid hydrolysis and derivatization with o-phthalaldehyde and methanol.

**Table 3.** Gradient program for amino acid measurement

| Time (min) | Sodium acetate (%) | Acetonitrile (%) |
|---|---|---|
| 0 | 92 | 8 |
| 10 | 90 | 10 |
| 60 | 66 | 34 |
| 65 | 0 | 100 |
| 67 | 0 | 100 |
| 74 | 92 | 8 |
| 76 | 92 | 8 |

**Statistical analyses.** Cluster analysis based on the group-average method was performed by the “pvclust” package in R studio (Version 3.5.1). The Bray-Curtis

dissimilarity measures based on relative abundances were used to visualize sample similarities. For FDOM changes in the permeate of Es1 extraction, six PARAFAC components were used. For amino acid data, the proportion of individual amino acids in the extracts was used. The double sigmoid model was calculated using the software Origin (2018).

### 3.4. Results

**Online and offline analysis of the permeate.** Online monitoring of FDOM in the permeate allowed tracking quantitative and qualitative changes related to increased DOC loading (Figures 1, 3). Inherently, this also yields information on optical changes of the extracted DOM, as these can be deduced from the difference between FDOM in the original water and the permeate. Despite previous study suggested that varying flow rate had little influence on DOC extraction efficiency and composition (Li et al., 2016b), we used a pump to keep the flow rate constant and hence eliminated flow rate as a factor in the extraction model. A double sigmoid model given an excellent representation (coefficient of determination was 0.999 and reduced chi-squared was near to zero; The estimates of the quality of the model fit were evaluated by the adjusted coefficient of determination and reduced chi-squared, which is also known as mean squared weighted deviation and closest to zero is the best fit. The adjusted coefficient of determination was 0.999 and reduced chi-squared was near to zero, indicating the double sigmoid model was suitable for describing the PPL-based solid-phase extraction process) of changes in the permeate fluorescence integrals (y) with increased SPE column loading (Figure 1):

$$y = y_0 + A[\frac{p}{1+e^{\frac{x-x_{01}}{k1}}} + \frac{1-p}{1+e^{\frac{x-x_{02}}{k2}}}] \quad (2)$$

where $y_0$ and A are the left and right asymptotes of y, and A is the maximum value of y corresponding to the limit $x \rightarrow \infty$ and constrained to $\leq 1$ in this case; p is the fraction of the first phase, 1 - p is the fraction of the second phase; $x_{01}$ and $x_{02}$ are the centers of the two phases; and k1 and k2 are the slope factors that determine the rise of the first and second phase (Aferni et al., 2021).

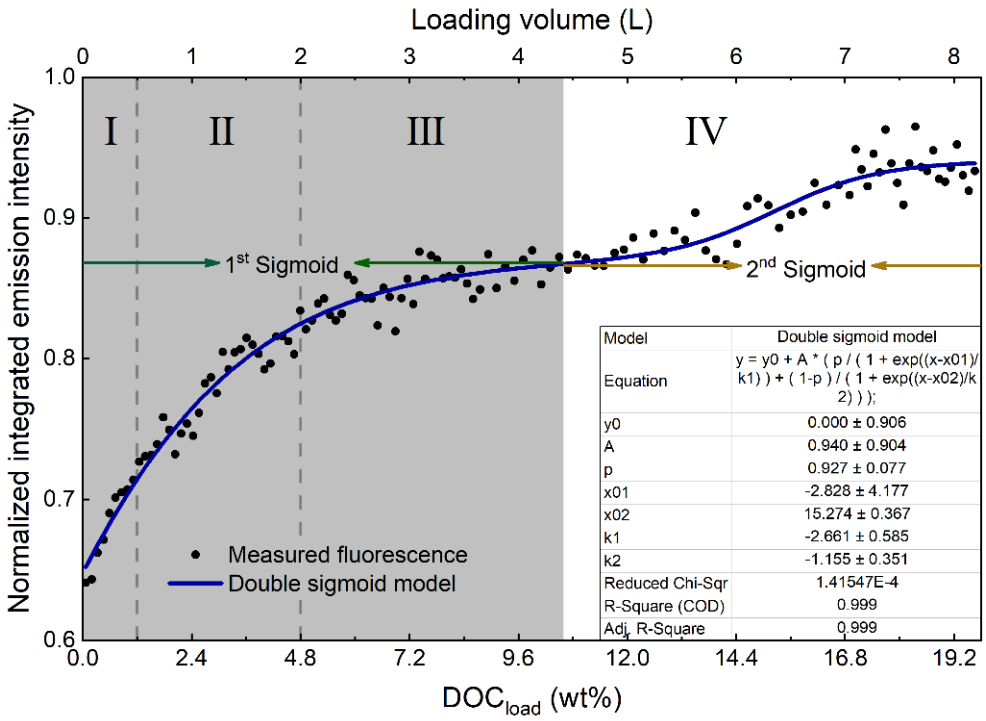


**Figure 1.** Online fluorometric detection (dots; Ex: 365 nm; Em: 420–600 nm) of solid-phase extraction (PPL, 200 mg) of a large-volume estuarine water sample (Es1): a double sigmoid model (blue line) was fitted to the normalized integrated emission intensity in the permeate as a function of $DOC_{load}$ (DOC mass loading versus PPL mass in wt%). Normalized permeate integrated emission intensity was calculated by dividing the integrated emission intensity of the permeate by the original sample. The 1st sigmoid transitioned to the 2nd sigmoid process at the local minimum of $DOC_{load}$ of 10.6 wt% (equivalent to 4.4 L loading volume). Gray and white areas denote 1st and 2nd sigmoid, respectively. Dashed vertical lines denote different loading stages as derived from the cluster analysis (cf. **Figure 3b)**. The double sigmoid approach highlights a transition of adsorption characteristics after 10.6 wt% $DOC_{load}$ where the 2nd sigmoid process starts to deviate from the 1st sigmoid.

Applying PARAFAC analysis to EEMs of discrete permeate samples resulted in six underlying components (Figure 2). Based on fluorescence maxima, components C2, C3, and C5 can be attributed to terrestrial humic-like sources (Stedmon et al., 2007a; Murphy et al., 2008; Baghoth et al., 2011; Kong et al., 2017; Madonia et al., 2020; Zabłocka et al., 2020), while C4 was previously interpreted as representing marine and microbial humic-like fluorophores (peak M; Coble, 1996; Cao et al., 2020). C1

represents terrestrial and marine humic-like sources (Stedmon et al., 2003; Murphy et al., 2008; Baghoth et al., 2011), and C6 was categorized as protein-like component (tryptophan-like peak T) with biological autochthonous origin (Coble, 1996; Carr et al., 2019; Kim et al., 2020). The average extraction efficiency for each component varied from 88.0% at the beginning to 24.6% at the end. A cluster analysis based on six components revealed most pronounced changes of the permeate fluorescence after the first 0.5 L and 2 L of extraction. Guided by multivariate statistics and double-sigmoid model, we split our data into four different intervals of $DOC_{load}$ (Figure 1): 0–1.2 wt% (I), 1.2–4.8 wt% (II), 4.8–10.6 wt% (III), 10.6–19.7 wt% (IV).

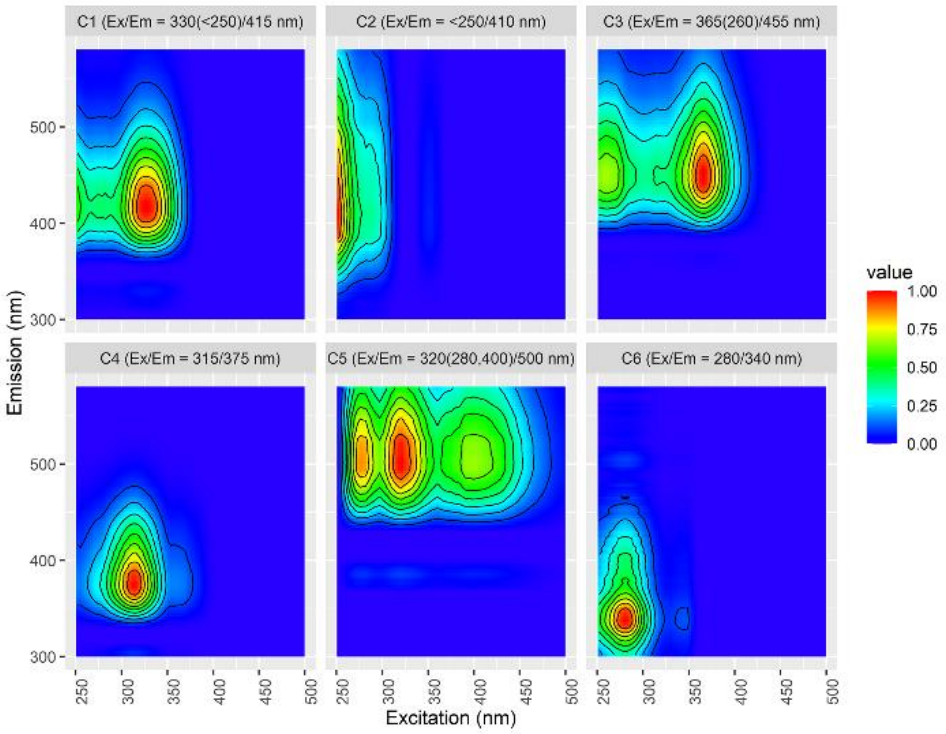


**Figure 2.** Excitation and emission matrix spectral characteristics of six PARAFAC components in the permeate during solid-phase extraction (PPL, 200 mg) of a large volume (loading) estuarine DOM sample (Es1).

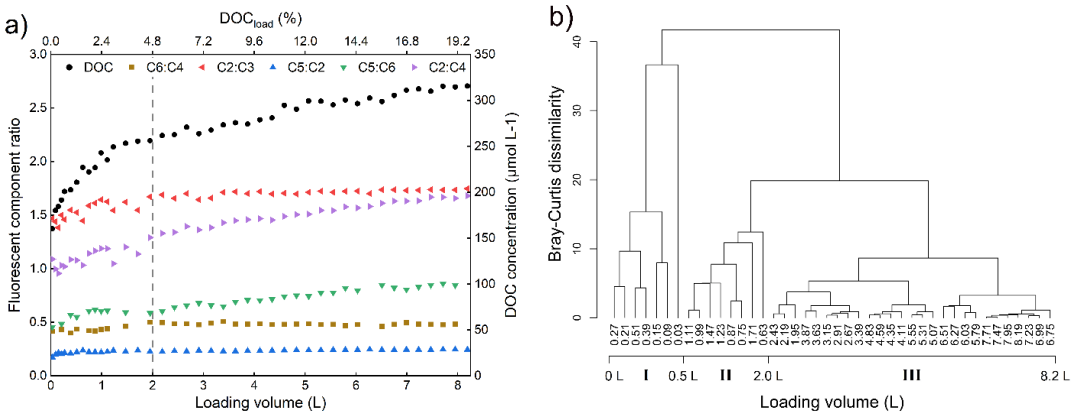


**Figure 3.** Loading-related changes in permeate DOC concentration and fluorescence: (a) DOC concentration and fluorescent component ratios derived from PARAFAC analysis, and (b) cluster analysis of different enrichment volumes based on six fluorescent components in the permeate during solid-phase extraction (PPL, 200 mg) of a large volume (loading) estuarine DOM sample (Es1).

For permeate flow, we observed a continuous increase in DOC concentration, PARAFAC component intensity, and absorbance at 254 nm (a254) with increased column loading (Figure 3a and Figure 4a, b). At the beginning of SPE, virtually all fluorescent compounds were retained and DOC concentration, absorbing and fluorescing compounds were very low in the permeate and continuously increased with DOC loading. Since absolute changes in these parameters could be simply related to a yield change, we evaluated ratio changes in the permeate that undoubtedly highlight compositional changes: for example, ratios of terrestrial components (C2: C3 and C5:C2) and microbial components (C6:C4) increased strongly during the first 4.8 wt% of $DOC_{load}$, and only increased slightly thereafter (Figure 3a). However, ratios between terrestrial and microbial components (i.e., C5:C6 and C2:C4) still showed a continuous increase thereafter. Hence, FDOM components derived from different sources had different sorbent affinities and FDOM composition with similar sources showed little chemical fractionation after 4.8 wt% of $DOC_{load}$.

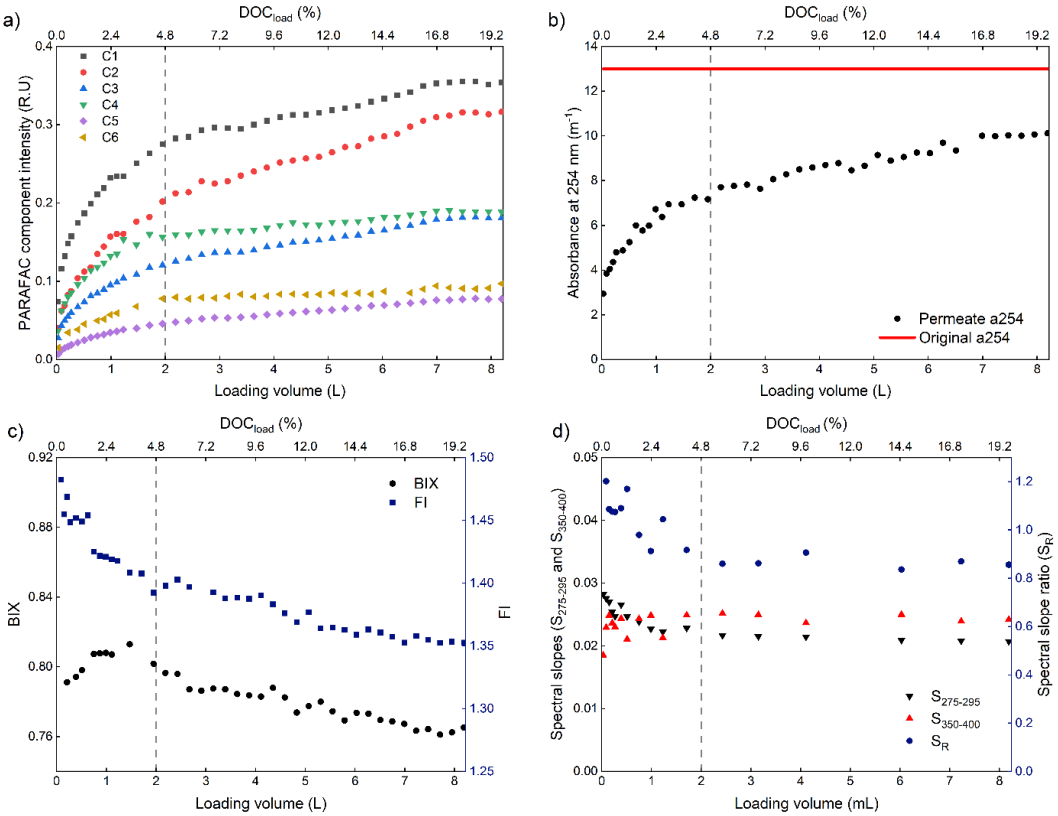


**Figure 4.** Chemical changes in the permeate during solid-phase extraction (PPL, 200 mg) of a large volume (loading) estuarine DOM sample (Es2): (a) maximum fluorescence intensity ($F_{max}$) of six PARAFAC components, (b) absorbance at 254 nm, (c) fluorescence index (FI) and biological index (BIX), and (d) spectral slopes and slope ratio. Note: $S_R$ was calculated by the ratio of $S_{275-295}$ and $S_{350-400}$.

Furthermore, spectral slopes and optical indices were calculated to investigate changes in chemical composition. During the first 2 L of enrichment, the permeate showed a pronounced decrease in $S_{275-295}$, $S_R$ and FI, while $S_{350-400}$ and BIX increased (Figure 4c, d). After 2 L extraction, spectral slopes and spectral slope ratio showed only little variation, whereas BIX and FI decreased continuously in the permeate.

Motivated by results from the large volume experiment (Figure 3) and to better understand FDOM self-assembly, we extracted and analyzed a marine sample (Ms1) that was subject to higher microbial degradation due to ~3 months storage at room temperature and showed higher ultraviolet A (UVA) fluorescence ($Ex_{max}$ < 300 nm, $Em_{max}$ < 400 nm) (Figure 5a). Compared to first 200 mL of the collected permeate, we observed that the permeate collected between 200 and 400 mL sample extraction (0.1–0.2 wt% DOC$_{load}$) showed a lower extraction efficiency in high excitation

wavelength region (peak at Ex/Em: 335/380 nm), while it is higher in UVA region (peak at Ex/Em: 275/330 nm; Figure 5b).

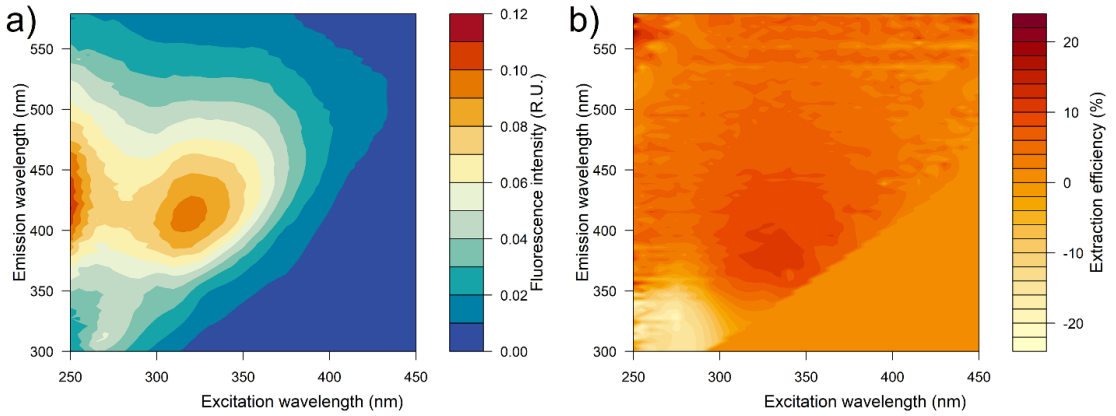


**Figure 5.** EEMs contour for (a) original seawater Ms1 (84 µmol DOC $L^{-1}$), and (b) wavelength-depended difference of the FDOM extraction efficiency for 0-200 mL ($DOC_{load}$ of 0–0.1 wt%) minus 200–400 mL ($DOC_{load}$ of 0.1–0.2 wt%) permeate (Ms1 extraction). Compared to the first 200 mL sample loading, 200–400 mL loading showed a higher loss of FDOM at higher excitation wavelengths, but little loss in the UVA region. This indicates that particularly UVA fluorescent compounds might be involved in the self-assembly, consistent with our result that protein-like and microbial humic-like components have a higher affinity for self-assembly than terrestrial humic-like components.

**Loading and sorbent-type dependent changes in DOM extracts.** To further evaluate how loading affected composition and chemical properties of solid-phase extracted DOM, four discrete water volumes (100 mL, 250 mL, 500 mL, and 1000 mL) from three aquatic locations (riverine Ws1 and estuarine Ws2 and marine Ws3) were extracted using PPL and C8 cartridges. PPL sorbents showed a much larger extraction efficiency than C8 sorbents (Table 4). For both sorbent materials, comparing 100 mL ($DOC_{load}$ = 0.09–0.18 wt%) with 1000 mL sample volume ($DOC_{load}$ = 0.89 – 1.81 wt%), DOC extraction efficiency decreased by 11.5–17.7% for riverine and marine samples, and only by 5.4–9.6% for estuarine sample.

**Table 4.** Comparison of DOM extracts based on sorbent-type and sample origin

| Source | Extraction volume (mL) | $DOC_{load}$ (wt%) | PPL | | C8 | |
|---|---|---|---|---|---|---|
| | | | DOC extraction efficiency (%) | Polarity ratio | DOC extraction efficiency (%) | Polarity ratio |
| Ws1 Riverine | 100 | 0.16 | 57.3 | 1.1 | 35.9 | 0.7 |
| | 250 | 0.40 | 48.5 | 1.0 | 27.5 | 0.6 |
| | 500 | 0.80 | 45.0 | 0.9 | 26.5 | 0.5 |
| | 1000 | 1.60 | 42.5 | 0.5 | 24.4 | 0.5 |
| Ws2 Estuarine | 100 | 0.18 | 61.2 | 3.4 | 39.8 | 2.7 |
| | 250 | 0.45 | 60.9 | 2.5 | 37.2 | 2.3 |
| | 500 | 0.91 | 59.8 | 2.1 | 34.1 | 1.7 |
| | 1000 | 1.81 | 55.8 | 1.2 | 30.2 | 1.2 |
| Ws3 Marine | 100 | 0.09 | 65.7 | 3.1 | 45.0 | 1.5 |
| | 250 | 0.22 | 58.9 | 2.2 | 32.9 | 1.6 |
| | 500 | 0.44 | 55.2 | 1.9 | 29.7 | 1.0 |
| | 1000 | 0.89 | 51.7 | 1.7 | 27.3 | 1.1 |

Note: stationary phase was 200 mg for both cartridges; DOC concentrations for Ws1, Ws2, and Ws3 were 267, 302, and 148 μmol $L^{-1}$, respectively. Previous studies with larger sample numbers reported a standard deviation for DOC extraction efficiency of about 2–7% (Dittmar et al., 2008; Lechtenfeld et al., 2014).

The polarity profile of methanol extracts for Ws1, Ws2, and Ws3 was determined by RP-HPLC. According to the gradient program (Table 2), the first fraction was defined as polar water-soluble substances (retention time < 16 min), whereas a fraction of less polar compounds eluted in the methanol soluble fraction (retention time > 16 min). Polarity ratio was calculated by the area of polar fraction versus less polar fraction to illustrate polarity changes (Table 4). It was noteworthy that polarity ratio decreased with increasing sample volumes ($DOC_{load}$). Comparing 100 mL with 1000 mL extraction volume, the average decrease of polarity ratio was approximately 18% and 12% for all samples extracted with PPL and C8, respectively. As expected, PPL sorbent extracted more polar compounds than C8 sorbent (Ws1: 1–14%, Ws2: 0–4%, Ws3: 7–15%).

To explore the loading-related qualitative changes of the amino acid composition in solid-phase extracts, we evaluated proportional changes of individual amino acids: Compared to the changes in fluorescence characteristics of the permeate, individual

amino acid proportions only varied by 1–3% between different volumes, independent of sample origin and sorbent type used (Table 5). Although, these results were also generally supported by a cluster analysis (Figure 6), the statistical method revealed that amino acid composition in 100 mL extractions differed most strongly from 1000 mL, emphasizing that also amino acid composition varies with extraction volume.

**Table 5.** Amino acid distribution (relative proportion of individual amino acid) in methanol extracts of the riverine (Ws1), estuarine (Ws2), and marine (Ws3) samples enriched with PPL and C8 cartridges.

| Sample type | Volume (mL) | Asx | Glx | Ser | Gly | Thr | Arg | Ala | Tyr | Val | Ile | Phe | Leu |
|---|---|---|---|---|---|---|---|---|---|---|---|---|---|
| S1 - PPL | 100 | 23.0 | 11.9 | 4.3 | 14.1 | 7.8 | 2.8 | 10.2 | 0.2 | 11.2 | 6.7 | 2.7 | 5.1 |
| | 250 | 23.6 | 11.1 | 4.1 | 14.1 | 8.2 | 2.5 | 10.1 | 0.7 | 11.1 | 6.7 | 2.7 | 5.0 |
| | 500 | 23.8 | 12.3 | 7.2 | 13.3 | 7.3 | 2.1 | 9.9 | 1.1 | 10.0 | 5.8 | 2.4 | 4.6 |
| | 1000 | 26.9 | 10.9 | 5.0 | 12.8 | 8.2 | 2.3 | 9.6 | 1.0 | 10.2 | 6.0 | 2.4 | 4.6 |
| S2 - PPL | 100 | 17.4 | 9.9 | 6.6 | 32.8 | 3.8 | 0.8 | 15.8 | 2.3 | 4.7 | 2.5 | 1.3 | 2.0 |
| | 250 | 19.0 | 10.7 | 5.5 | 31.7 | 4.1 | 1.1 | 15.6 | 2.1 | 4.8 | 2.4 | 1.2 | 1.9 |
| | 500 | 19.2 | 10.9 | 5.4 | 30.1 | 4.9 | 1.1 | 15.6 | 2.0 | 5.0 | 2.6 | 1.2 | 2.0 |
| | 1000 | 19.1 | 11.1 | 5.3 | 28.7 | 5.3 | 1.7 | 15.8 | 1.9 | 5.1 | 2.7 | 1.2 | 2.1 |
| S3 - PPL | 100 | 17.6 | 10.2 | 7.3 | 30.3 | 4.5 | 1.7 | 14.8 | 1.6 | 5.4 | 2.7 | 1.5 | 2.4 |
| | 250 | 18.4 | 10.4 | 6.6 | 29.7 | 4.6 | 1.4 | 15.1 | 1.7 | 5.4 | 3.0 | 1.4 | 2.3 |
| | 500 | 19.7 | 10.6 | 6.4 | 27.4 | 5.3 | 1.2 | 15.4 | 1.7 | 5.6 | 3.0 | 1.4 | 2.3 |
| | 1000 | 19.6 | 10.0 | 6.6 | 29.1 | 5.2 | 1.0 | 15 | 1.6 | 5.4 | 3.0 | 1.3 | 2.2 |
| S1 – C8 | 100 | 18.9 | 14.0 | 6.8 | 10.3 | 6.9 | 3.3 | 9.7 | 0.8 | 12 | 7.6 | 3.7 | 6.4 |
| | 250 | 17.2 | 13.3 | 6.3 | 9.6 | 7.0 | 3.5 | 9.2 | 0.7 | 16 | 7.3 | 3.3 | 6.4 |
| | 500 | 16.1 | 13.7 | 6.6 | 10.7 | 7.7 | 3.7 | 9.9 | 1.2 | 13 | 7.5 | 3.3 | 6.6 |
| | 1000 | 16.8 | 13.0 | 6.7 | 10.6 | 8.4 | 4.2 | 10.5 | 1.2 | 12 | 7.4 | 3.4 | 6.4 |
| S2 – C8 | 100 | 20.9 | 11.0 | 7.5 | 28.4 | 4.4 | 1.4 | 14.7 | 0.4 | 3.6 | 3.4 | 1.6 | 2.6 |
| | 250 | 20.5 | 10.8 | 6.3 | 26.9 | 4.3 | 1.5 | 13.9 | 2.0 | 6.0 | 3.4 | 1.6 | 2.7 |
| | 500 | 21.0 | 11.2 | 5.7 | 26.8 | 4.7 | 1.4 | 13.7 | 1.9 | 6.0 | 3.7 | 1.5 | 2.5 |
| | 1000 | 19.7 | 10.9 | 5.8 | 27.9 | 5.0 | 1.2 | 13.8 | 1.9 | 5.9 | 3.7 | 1.5 | 2.7 |
| S3 – C8 | 100 | 21.2 | 12.2 | 9.1 | 25.1 | 3.3 | 1.2 | 11.2 | 0.5 | 6.7 | 4.1 | 1.9 | 3.5 |
| | 250 | 21.0 | 12.2 | 9.8 | 23.3 | 3.7 | 1.0 | 11.5 | 0.8 | 7.1 | 4.1 | 2.0 | 3.6 |
| | 500 | 20.5 | 12.6 | 5.8 | 25.8 | 4.0 | 1.1 | 12.8 | 1.2 | 6.7 | 4.3 | 1.9 | 3.4 |
| | 1000 | 20.4 | 12.3 | 6.2 | 25.2 | 4.0 | 1.1 | 12.7 | 1.3 | 6.9 | 4.6 | 1.9 | 3.4 |

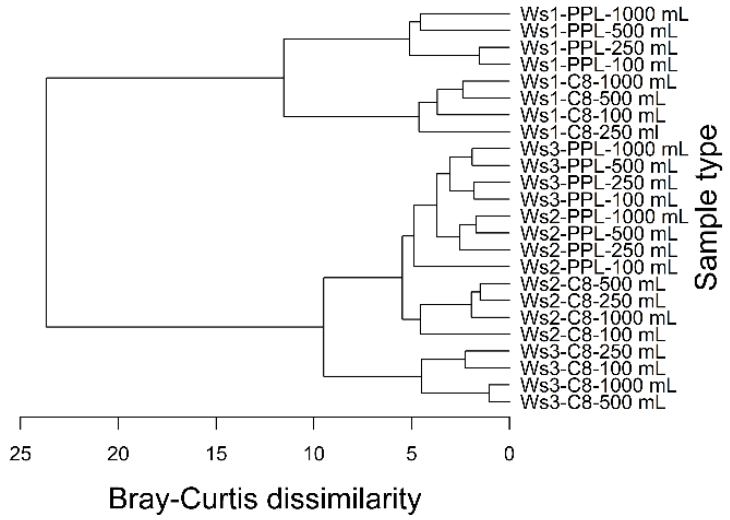


**Figure 6.** Cluster analysis (Bray Curtis dissimilarity) based on relative distributions of total hydrolysable amino acids from the solid-phase extraction of riverine (Ws1), estuarine (Ws2) and marine (Ws3) samples using four different sample volumes with PPL and C8 cartridges.

**Imaging of loading-related changes of the sorbent surface.** Microscopic visualizations of PPL surface were performed using 200 mg cartridges that were either unloaded or loaded with Es2 (530 µmol DOC $L^{-1}$) at 1.6 wt% or 15.9 wt% $DOC_{load}$ (equivalent to 0.5 and 5 L loading volume, respectively). Images of PPL surface from polarized light microscopy and SEM were compared between 0.5 L and 5 L loading. The continuous change of surface color (Figure 7a−c), the decrease of texture (Figure 7d–f) and the visible DOM surface layer (Figure 8d) was an illustrative representation how the porous surface of PPL is increasingly covered from unloaded state to 0.5 L and 5 L loading.

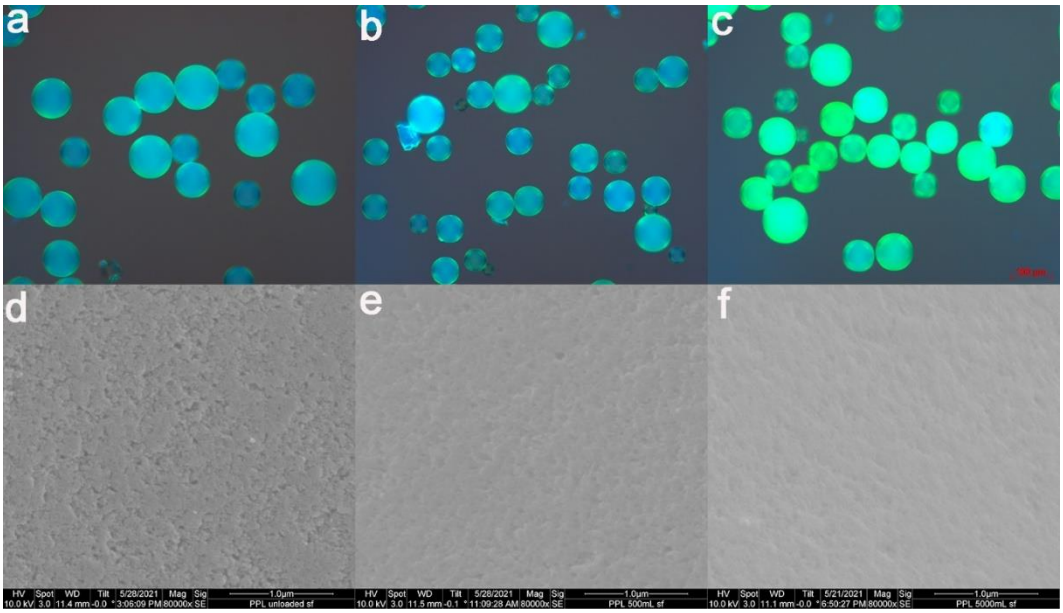


**Figure 7.** Images of polarized light microscopy at 10× magnification (a, b and c), and SEM at 80,000× magnification (d, e and f) for the surface of unloaded PPL (a and d), PPL loaded with 0.5 L (b and e), and PPL (c and f) of estuarine sample Es2.

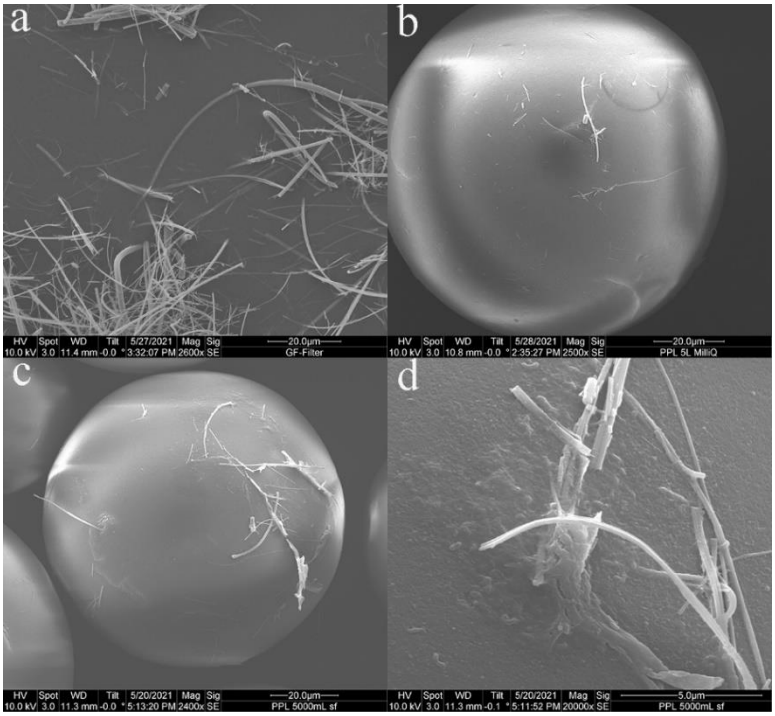


**Figure 8.** SEM images for the surface of (a) GF/F filter at 2,600× magnification, (b) PPL loaded with 5 L ultrapure at 2,500× magnification, (c) PPL loaded with 5 L of sample Es2 ($DOC_{load}$ of 15.9 wt%) at 2,400× magnification, and (d) PPL loaded with 5 L of sample Es2 at 20,000× magnification. All samples were filtered with GF/F filters

(Whatman glass fibre filter, 0.7 µm pore size) prior to SPE and traces of the GF/F filters were leached and deposited on the surface of the PPL beads. The images of the PPL beads loaded with DOM revealed that some GF/F fibres were hidden under a DOM extract layer covering the PPL surface.

### 3.5. Discussion

**Inverse online-monitoring of the extraction procedure and empirical modelling.** In our study, we used an inverse online-monitoring approach to track chemical changes during aquatic DOM SPE extraction. We think that this simple procedure can be easily applied for other sorbents and environmental samples so that methodological biases introduced by SPE in aquatic research can be more conveniently assessed in future. It should be noted that classical adsorption models such as Thomas model (Mahmoud, 2016), Langmuir isotherm (Edet and Ifelebuegu, 2020) or Dubinin-Astakhov isotherm (Moritz and Geszke-Moritz, 2020) are difficult to apply due heterogeneous and complex nature of aquatic DOM. Although we don't know precisely, how many organic compounds are contained in water, mass spectrometry yields at least ten thousand different molecular masses and an unknown dimension of structural isomers within each sample. For this reason, we chose an exclusively empirical modelling approach of the permeate fluorescence. Starting with a sigmoid Boltzmann model for breakthrough curve of single compound solid-phase extraction (Bielicka-Daszkiewicz and Voelkel, 2009; Tartaglia et al., 2019) that was similar to e.g., non-linear Langmuir isotherm, our online-monitoring experimental data highlighted a considerable deviation, which led to double sigmoid model that better reconstructed the measured data. In this model, we assumed that DOM extraction equilibria are controlled by unequal contributions of PPL physisorption and multilayer adsorption (DOM self-assembly), we modelled the permeate fluorescence by double sigmoid equation (Figure 1). Given the choice of sample and sorbent type in our experiment, the 2$^{nd}$ sigmoid process deviated from the 1$^{st}$ sigmoid process at a $DOC_{load}$ > 10.6 wt% (equivalent to 4.4 L loading volume of Es1).

Self-assembly - an important mechanism during DOM solid-phase extraction. Despite a very large ratio of sample volume (8.2 L) versus mass of sorbent (200 mg PPL) in our online monitoring experiment, we did not observe a capacity limit of stationary

phase that would have been indicated by a constant fluorescence signal towards the end of SPE. Although we found a notable decrease in DOC extraction efficiency from lower to higher extraction volumes, we still observed considerable DOC extraction (21.2%) at a sample volume of >8 L. According to the manufacturer, PPL can extract up to 12 wt% of the sorbent mass (pers. comm. Agilent Technologies). In order to facilitate comparisons between extractions of varying sorbent amounts, sample volume and concentrations, the relative DOC loading weight on the column ($DOC_{load}$) is a very helpful parameter: in our experiment, for 200 mg PPL and a sample volume of 8.2 L having a DOC concentration of 400.7 µmol $L^{-1}$, $DOC_{load}$ was 19.7 wt%. Assuming that DOC contributes half of total DOM mass and given an overall DOC extraction efficiency of ~31.0% for Es1 (calculated by integral of permeate DOC concentration in Figure 3a), the maximum capacity of stationary phase was exceeded in our experiment. The discontinuous changes in DOC extraction efficiency as well as absorbing and fluorescing compounds suggested a change in the predominant extraction mechanism with increased loading. Additional extractions using four discrete smaller volumes (Table 4) confirmed the online monitoring results and a previous study that reported decreasing DOC recovery with increasing sample volume (Li et al., 2016b).

The discontinuous changes we observed could not be explained by just an increased coverage of the stationary PPL phase. Despite reaching the capacity of the sorbent towards the end of our extraction, DOC extraction efficiency was still relatively high (Figure 3a). We therefore hypothesized that with increasing loading of PPL surface the predominant extraction mechanism shifts from DOM-PPL physisorption to an increased multilayer adsorption of DOM adsorbate. In aquatic science, a mechanism similar to multilayer adsorption is known as DOM “self-assembly”. This important process contributes to particle formation in aquatic environment: DOM polymers assemble into microgels by noncovalent bonds such as electrostatic, hydrogen, hydrophobic, or van der Waals bonds (Chin et al., 1998; Verdugo et al., 2004; Verdugo and Santschi, 2010). In the following, we therefore use the term “self-assembly” as a synonym for multilayer adsorption.

Polarized light and scanning electron microscopy revealed a gradual change of surface texture and color, clearly showing the increasing and homogenous loading of DOM on PPL surface (Figure 7). Based on the assumption that the density of DOM and PPL is comparable and that the weight of DOM is approximately double of DOC weight, it can be roughly estimated that the radius of PPL particles increased by 5% given a 31.8 mg DOC loading (equivalent to 5L loading of Es2) on 200 mg of PPL. This massive surface coverage combined with the observation that DOC is still extracted at larger loadings supports our assumption that self-assembly is responsible for the ongoing DOC extraction beyond the capacity of the sorbent. Given that DOM adsorption and self-assembly will be competing processes, self-assembly likely also contributes to chemical fractionation at smaller loadings. However, looking at the differences of the gradients in the first and second sigmoid phase (Figure 1), we assume that the average enthalpy yielded by DOM adsorption on PPL is considerably higher than the enthalpy of DOM self-assembly. Therefore, both processes unequally contribute to the overall DOC extraction efficiency and chemical fractionation along the extraction process.

**Chemical fractionation of complex organic matter during solid-phase extraction.** Most importantly for molecular DOM studies, our results show a loading-dependent qualitative chemical change in the permeate that can be considered as inverse changes of the extracted organic matter. It should be noted though, that we expect our online permeate monitoring to be more sensitive to compositional changes compared to changes analyzed in the extracts. The reason for this is that the extracts represent cumulated changes over a larger loading, which might contribute to the low variability observed in our amino acid composition experiment (Figure 6 and Table 5). In consistence with previous studies (Dittmar et al., 2008), a preferential extraction of terrestrial DOC was observed by slightly higher efficiencies for estuarine samples compared to marine samples (Table 4). Different from previous studies, we found unexpectedly low DOC extraction efficiencies for riverine samples, for which we only can speculate that salt discharge or locally different organic matter sources at respective section of River Weser are possible explanations.

Although fluorescence analysis of DOM typically does not require an extraction step, it is a helpful technique to document loading-related chemical changes. In particular,

the change of ratios of fluorescent components during the first 2 L of SPE ($DOC_{load}$ <= 4.8 wt%, Figure 3a) highlight substantial chemical fractionation. At the beginning of extraction (0–0.5 L, $DOC_{load}$: 0–1.2 wt%) fluorescent substances were almost quantitatively retained on the unloaded PPL. Between 0.5–2 L sample volume ($DOC_{load}$: 1.2–4.8 wt%), the increasing fluorescence signal in the permeate reflected fewer available polymer binding sites, and after 2 L of extraction DOM self-assembly dominated. Such loading-dependent fractionations can also affect interpretations on aquatic organic matter composition, e.g., with respect to the contribution of organic-matter sources: the estuarine water used for the online extraction experiment (salinity of 11.6) contained a mixture of terrestrial and marine-derived organic matter that is partially reworked by microbial activity. We observed a stronger decrease in the extraction efficiency of microbial and protein-like components (i.e., C4 and C6) within the first 2 L extraction ($DOC_{load}$ of <= 4.8 wt%), whereas the extraction efficiency for terrestrial humic-like components (i.e., C2, C3 and C5) declined more at higher loadings where self-assembly predominated (Figure 4a). FI (McKnight et al., 2001) is commonly used as an indicator to distinguish DOM source: Low FI values suggest that water samples are dominated by terrestrially-derived substances, whereas high values are indicative of microbially-derived DOM (Johnson et al., 2011; Murphy et al., 2018). FI value of 1.3 for the original estuarine water Es1 showed that bulk DOM was mainly derived from terrestrial sources. In the permeate of our online experiment, FI decreased continuously, indicating a higher loss of terrestrially-derived organic matter with increasing loading. In addition, the index of recent autochthonous (microbial-derived) contribution (BIX; Huguet et al., 2009) showed a loading-dependent increase of microbial-derived DOM in the permeate before 2 L of the enrichment, and a loss at higher volumes (Figure 4c). These observations are in agreement with our interpretation that terrestrial DOM has a high affinity to PPL, whereas microbial humic-like and protein-like components were preferentially extracted by self-assembly. Amino acid analysis with four discrete enrichment volumes showed that the relative amino acid composition in methanol extracts changes slightly with different enrichment volumes (Figure 6 and Table 5), an observation supporting that peptide or proteins showed higher self-assembly

capabilities (Passow, 2002; Kerner et al., 2003; Verdugo et al., 2004; Verdugo and Santschi, 2010).

The slope ratio $S_R$ was previously shown to be negatively correlated with molecular weight and DOM aromaticity (Helms et al., 2008; Hansen et al., 2016; Mann et al., 2016), and therefore also a good indicator for changes in chemical composition along the extraction. During the first 2 L of extraction, $S_R$ decreasing in the permeate indicated increasing loss of aromatic content. At higher volumes we only observed little changes for $S_R$ and assume that π-π interactions between PPL and aromatic DOM decreased as a consequence of increased loading of the polystyrene surface. It has been previously shown that marine DOM is characterized by a larger contribution of aliphatic structural features in comparison to terrestrially derived DOM, which is characterized by a higher aromaticity and more hydroxyl and carboxyl functionalities (Sleighter and Hatcher, 2008; Chen et al., 2016b; Wang et al., 2019). An earlier study (Chen et al., 2016a) revealed higher PPL recoveries for fluorescing terrestrial DOM compared to marine DOM, and lower recoveries for biopolymers (i.e., proteins, polysaccharides, and amino sugars).

Increased loading also resulted in a decreased average polarity of organic substances in the extracts. It has been reported that PPL preferentially extracts more hydrophobic DOM, and has a low capacity for highly polar substances (Dittmar et al., 2008; Li et al., 2016b; Lewis et al., 2020). A previous study that performed a large scale extraction (12.5 L) showed a compositional shift along increasing methanol elution volumes, from relatively polar and marine-derived to relatively nonpolar and terrestrial-derived DOM (Lewis et al., 2020). Given the results of our study, these results might also be related to an increasing contribution of DOM self-assembly. Previous studies demonstrated that biopolymers including proteins, polysaccharides and nucleic acids are more likely to assemble into microgels (Chin et al., 1998; Verdugo et al., 2004; Verdugo and Santschi, 2010). DOM self-assembly is therefore highly dependent on DOM origin and composition and is favored in samples that were subject to microbial degradation (Chin et al., 1998; Xu and Guo, 2018; Xu et al., 2018). Microbial degradation promotes the production of carboxyl-rich alicyclic molecules (CRAM) by consuming the bioavailable DOM in the euphotic layer

(Mathew et al., 2021). CRAM is an important chemical feature in PPL-extracted DOM (Chen et al., 2016b, 2016a; Hertkorn et al., 2016) that also can facilitate aggregation and microgel formation (Hertkorn et al., 2006). This general observation is in agreement with our findings that self-assembly increases the relative recovery of protein-like and microbial humic-like DOM. It is also consistent with the results of our experiment that compared optical features of permeates at different $DOC_{load}$ (Figure 5), which suggested particularly strong self-assembly for UVA fluorescent compounds.

**Implications for solid-phase extraction of aquatic natural organic matter.** Our findings have important implications for procedure and interpretation of solid-phase extraction of aquatic organic matter. All of the bulk and optical / chemical changes we observed, were dependent on $DOC_{load}$. Different from solid-phase extraction of single compounds, increased loading of the sorbent affected the adsorption equilibria for each compound contained in complex organic matter. If similar volumes of samples with vastly different organic carbon concentration are extracted, analyzed and compared for molecular features (Singer et al., 2012), it is therefore critical to minimize variances introduced by different loadings. Ideally, this could be achieved by harmonizing the $DOC_{load}$ by analyzing the sample DOC concentration first and adjusting the sample extraction volume accordingly so that similar sorbent loading is reached for all samples in the sample set (Kellerman et al., 2014). Alternatively, absorption or fluorescence measurements of original sample before extraction might serve as a rough proxy for organic carbon concentration. If the sample processing is performed in field studies, this might be a feasible alternative to determine suitable loading volumes, compared to the elaborate determination of organic carbon concentration. It is important to note that, for reasons of feasibility, we defined the $DOC_{load}$ by DOC concentration, sample volume and sorbent mass. DOM samples derived from different sources will have different affinities to the sorbent and self-assembly, both affecting the overall extraction efficiency and therefore the effective loading of the stationary phase.

Online optical monitoring of the permeate flow was a simple and effective tool to track performance and qualitative chemical changes in the permeate. The resulting data allowed modelling the extraction process, which in turn allowed to assess the

variability introduced by different sorbent loadings. Within our estuarine sample extraction, an increase of the $DOC_{load}$ from $x_1$ wt% to $x_2$ wt%, resulted in a calculated increase of total fluorescence in the permeate of:

$$94.0\left[\frac{0.927}{1+e^{\frac{x_2+2.828}{(-2.661)}}}+\frac{0.073}{1+e^{\frac{x_2-15.274}{(-1.155)}}}-\frac{0.927}{1+e^{\frac{x_1+2.828}{(-2.661)}}}-\frac{0.073}{1+e^{\frac{x_1-15.274}{(-1.155)}}}\right]\ \% \quad (3)$$

If the total fluorescence would be used to compare samples in a sample set, the model can help to compare the variability introduced by differences in loading versus the variability between samples in the sample set.

Our results also underpin that different loading affects the quantification of single compounds that are solid-phase extracted from water samples with complex organic matrices, such as natural aquatic environments, effluents or aquaculture systems. The quantification of specific analytes such as organic pollutants, metabolites, or ligands are affected by the overall sorbent loading because the complex organic matrix alters the surface of the sorbent and therefore changes the adsorption equilibrium of the analyte. At very high DOC loading, PPL preferentially extracted nonpolar and terrestrially-derived compounds as the target DOM. However, self-assembly may lead to more accumulation of interfering components (e.g., polar and microbial-derived compounds) than the analytes of interest. For comparison of samples, it must be considered that the choice of elution solvent and changing ionic strength (salinity) of the matrix can affect DOM composition. Different mechanisms such as van der Waals forces, hydrophobic interactions, hydrogen bonding, and $Ca^{2+}$ bridging regulate DOM self-assembly and might be altered by sample matrix-effects (Kruger et al., 2011). DOM self-assembly fundamentally changes the quality of the extracted DOM in SPE process, resulting in (i) increased DOM molecular weight by non-covalent bonds, change in the (ii) molecular composition and (iii) optical properties, and (iv) significant reduced carbon extraction efficiency (Chin et al., 1998; Romera‐Castillo et al., 2014; Xu and Guo, 2018). By applying the online fluorometric modeling, we can optimize the $DOC_{load}$ and respective sample volume by following these steps: (i) modelling PPL-based solid-phase extraction processes; (ii) calculate the targeted $DOC_{load}$ that yields the least chemical fractionation for the target parameter; (iii) finally determine the optimal sample volume.

## 4. Manuscript II

# The composition of chromophoric dissolved organic matter in Central Arctic surface waters during the MOSAiC expedition depends on regional rather than seasonal differences

Xianyu Kong[1]*, Mats A. Granskog[2], Clara J. M. Hoppe[1], Allison A. Fong[1], Colin A. Stedmon[3], Sandra Tippenhauer[1], Adam Ulfsbo[4], Myriel Vredenborg[1], Boris P. Koch[1,5]

[1] Alfred Wegner Institute Helmholtz Centre for Polar and Marine Research, Bremerhaven, Germany

[2] Norwegian Polar Institute, Fram Centre, Tromsø, Norway

[3] National Institute of Aquatic Resources, Technical University of Denmark, Kongens Lyngby, Denmark

[4] Department of Marine Sciences, University of Gothenburg, Gothenburg, Sweden

[5] University of Applied Sciences, Bremerhaven, Germany

* Corresponding author: Email: Xianyu.Kong@awi.de

## 4.1. Abstract:

Chromophoric dissolved organic matter (CDOM), the optically active constituent of dissolved organic matter (DOM), can have a profound effect on light penetration and primary production in Arctic surface waters. Here, we present a comprehensive, seasonal observation of CDOM in the Central Arctic Ocean (CAO) surface waters based on the year-round (November 2019–September 2020) expedition "Multidisciplinary Drifting Observatory for the Study of Arctic Climate" (MOSAiC). CDOM absorbance spectra and fluorescence excitation-emission matrices (EEMs) combined with parallel factor analysis (PARAFAC) model were applied to characterize the changes in DOM sources and composition. CDOM characteristics in the surface waters were affected by differences in regions (primary water masses) rather than seasonal changes. CDOM in the surface of the TPD-influenced part of the drift study (i.e., Amundsen Basin) was dominated by terrestrially-derived CDOM (as indicative of average 136% and 45% higher absorption coefficient $a_{CDOM}(350)$ and dissolved organic carbon (DOC) concentration, respectively, compared to the western Nansen Basin and Yermak Plateau), while CDOM outside the TPD-influenced regions (i.e., western Nansen Basin and Yermak Plateau) were characterized by a predominance of autochthonous DOM (as indicative of average 25% higher biological index (BIX) value compared to the Amundsen Basin). Surface waters in the Fram Strait, influenced by Polar Water and Atlantic Water, were characteristic by high terrestrial and autochthonous CDOM in summer.

**Keywords:** Transpolar Drift; CDOM; Optical spectroscopy; EEMs; PARAFAC.

## 4.2. Introduction

Dissolved organic matter (DOM), the largest pool of organic material in the ocean (Hansell et al., 2009), is a heterogeneous mixture of allochthonous (terrestrially-derived) and autochthonous (in situ biological production) materials (Stedmon et al., 2007b). It is a key component for biogeochemical processes and global carbon cycling (Battin et al., 2009) by attenuating light (Morris et al., 1995), regulating the UV and visible light absorption (Osburn et al., 2001), serving as an energy and nutrient source for heterotrophic communities (Wetzel, 1984), and acting as a trace metal ligand (Hirose, 2007). The distribution and dynamics of DOM in the Arctic have received considerable attention over the past several decades. An increase of DOM flux induced by climate warming and permafrost thawing have been reported in the Arctic Ocean (Frey and Smith, 2005; Spencer et al., 2015; O'Donnell et al., 2016). The fraction of DOM that absorbs light within the ultraviolet and visible light spectrum is called chromophoric dissolved organic matter (CDOM). CDOM, the optically active constituent ubiquitously in the Arctic Ocean, has a profound effect on penetration of ultraviolet radiation and its impact on primary production (Guéguen et al., 2005; Granskog et al., 2007; Hill, 2008). Optical spectroscopy (absorbance and fluorescence) has been widely used to characterize the properties and dynamics of CDOM in aquatic samples (Parlanti et al., 2000; Baker and Spencer, 2004; Yamashita and Jaff , 2008). Fluorescence excitation-emission matrices (EEMs) evaluated with parallel factor analysis (PARAFAC) is an effective tool for distinguishing the terrestrial (allochthonous) and autochthonous sources of fluorescent dissolved organic matter (FDOM), a subfraction of CDOM that emits a fraction of the absorbed energy as fluorescence (Stedmon et al., 2003; Murphy et al., 2008).

The upper ocean (upper 500 m of the water column) in the Arctic Ocean generally consists of three layers: The surface mixed layer (SML) of the Arctic Ocean is characterized by relatively low salinity and cold temperatures (Rudels et al., 1996). In the halocline layer (HL) salinity increases rapidly with depth, separating surface waters from the relatively warm and saline Atlantic Water (AW) layer beneath (Rudels et al., 2004). Less saline Pacific Water entering through the Bering Strait, precipitation over the Arctic region, and river runoff are three major suppliers of

freshwater to the Arctic Ocean (Yamamoto-Kawai et al., 2005; Watanabe and Hasumi, 2009). River discharge additionally provides high loads of terrestrial organic matter into the Arctic surface waters and upper halocline (Bélanger et al., 2006; Stedmon et al., 2011). In the eastern Arctic Ocean, the Transpolar Drift (TPD, Figure 1) is the major surface current that transports sea ice and shelf surface waters from the Laptev and East Siberian Seas across the CAO towards the Fram Strait (Charette et al., 2020), carrying a large amount of freshwater and terrestrially-derived CDOM (tCDOM) to the CAO, indicated by elevated CDOM concentration (Slagter et al., 2017) and lower salinities (Paffrath et al., 2021). The TPD affects the Amundsen Basin and Makarov Basin, which is separated by the Lomonosov ridge, while the Nansen Basin, which are separated from the Amundsen Basin by the Gakkel Ridge, is largely unaffected by the TPD (Slagter et al., 2017). The position of the TPD varies with the Arctic Oscillation (Macdonald et al., 2005; Karcher et al., 2012; Smith et al., 2021). Seasonal sea ice formation and melt influence the dynamics and stratification in the SML. Melting of sea ice in summer leads to a freshening of the SML causing a stronger stratification, and in winter brine is rejected during sea ice formation which increases the density of the SML (Rudels, 1995; Kikuchi et al., 2004; Granskog et al., 2015). In addition to physical processes, primary production in the Arctic Ocean contributes to the DOM distribution in surface waters and undergoes strong seasonal changes (Mathis et al., 2007). Some studies have investigated the seasonality of CDOM in the Amerasian sector of the CAO (Matsuoka et al., 2011; Lewis and Arrigo, 2020), but few CDOM measurements exist in the Eurasian sector of the CAO (Gonçalves-Araujo et al., 2018; Boles et al., 2020), especially in winter.

The expedition “Multidisciplinary Drifting Observatory for the Study of Arctic Climate” (MOSAiC) was the year-round (October 2019–September 2020) passive sea ice drift of RV Polarstern across the CAO. The objective of MOSAiC was to better quantify and decipher physical, biological and chemical processes and their feedbacks within the coupled atmosphere-ice-ocean system in the CAO (Nicolaus et al., 2022; Rabe et al., 2022; Shupe et al., 2022). Here, we present the first comprehensive, year-round CDOM observations in the CAO, with the aim to determine the spatial and seasonal variation of the CDOM composition and sources in the surface waters. Two hypotheses were tested: (i) CDOM characteristics in the surface waters mainly differ

by the contribution from terrestrial input. Therefore, changes in CDOM composition are mainly linked to whether or not samples were taken within the TPD and (ii) these differences on CDOM characteristics can be significantly modulated by seasonality.

## 4.3. Materials and Methods

**Study Area.** Water samples were collected on RV Polarstern (Knust, 2017) expedition PS122 (MOSAiC) from October 2019 to July 2020 for Legs 1–4 during which vessel passively drifted with one ice flow from the Amundsen Basin, via the western Nansen Basin and Yermak Plateau, towards the Fram Strait. After steaming back to the Amundsen Basin (near the North Pole) RV Polarstern drifted again with a second ice floe for Leg 5 from August to September 2020 (Figure 1; Nicolaus et al., 2022). To compare the MOSAiC results with previous observations and end-member information, we used CDOM absorption and fluorescence data acquired during the Norwegian young sea ICE (N-ICE2015) expedition that was carried out in the western Nansen Basin and Yermak Plateau (Figure 1; January to June 2015; Granskog et al., 2018), and data from the Bering Strait, Laptev Sea, and East Siberian Sea that were acquired during the expedition TA19_4 (Figure 1; September to October 2019; Hölemann et al., 2021).

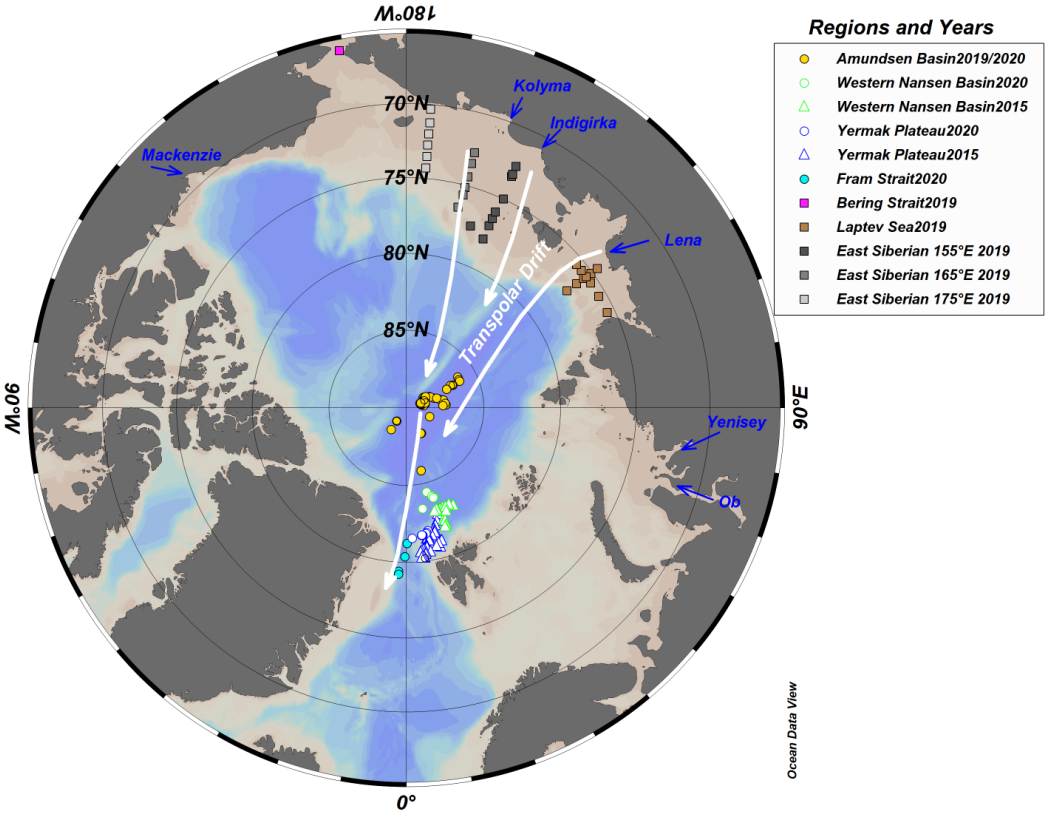


**Figure 1.** Map of the study area. Circles: stations of the MOSAiC PS122 expedition from October 2019 to September 2020, covering the Amundsen Basin, western Nansen Basin, Yermak Plateau, and Fram Strait. Triangles: stations of the N-ICE2015 expedition from January 2015 to June 2015, covering the western Nansen Basin and Yermak Plateau. Squares: stations of the TA19_4 expedition from September 2019 to October 2019, covering the Laptev Sea, the East Siberian Sea and the Bering Strait. Filled white symbols for MOSAiC and N-ICE2015 expeditions denote stations that were not affected by TPD, and filled symbols for the MOSAiC expedition denote stations that were affected by the TPD. Blue arrows indicate major Arctic River inflows. White arrows indicate the approximate location of TPD current. Note that the Arctic Oscillation (Macdonald et al., 2005) can result in a substantial interannual spatial variability of the TPD.

**Water mass definitions.** Based on the profiles of potential temperature and salinity from CTD/rosette, six water masses were identified along the drift track during the MOSAiC expedition which slightly differed from previous studies in the region (Korhonen et al., 2013; Rabe et al., 2022): the Surface Mixed Layer (SML) from surface to the potential temperature minimum layer, the Upper Halocline (UHC) from

the potential temperature minimum layer to salinity = 34, the Lower Halocline (LHC) from salinity = 34 to potential temperature = 0 °C, the Upper Atlantic Water (AW1) from potential temperature = 0 °C to the potential temperature maximum layer, the Lower Atlantic Water (AW2) from the potential temperature maximum to potential temperature = 0 °C, and deep waters (DW) for depth ≥ 1000 m. We did not further classify the deep waters into different water masses as the number of observations below 1000 m was comparably low. The SML is typically about 50 m thick in the Eurasian Arctic Ocean (Rudels et al., 1996), and it is generally thickest in the Nansen Basin (Korhonen et al., 2013). During the MOSAiC expedition, the mixed layer deepened from shallower than 40 m in Legs 1–2 to 60 m in Leg 3, on average. Leg 4 (Yermak Plateau and in the Fram Strait), exhibited deeper mixed layers (100–120 m) (Rabe et al., 2022). Our sampling depths were typically approximately 2 m, 10 m, 20 m, 50 m, 100 m, 200 m, 500 m, 1000 m, 2000 m, 3000 m, 4000 m and 4400 m. The samples in the upper 20 m were in the SML during most of the MOSAiC expedition, so we chose the upper 20 m water column for SML analysis in this paper. Further, we chose a sample depth of 200 m for AW1, of 500 m for AW2, and ≥ 1000 m for samples from the DW for our study.

**Season definitions.** Based on near-surface air temperature (2 m) changes during MOSAiC as well as sea ice melt onset and freeze onset times (Shupe et al., 2022), four seasons were identified: the winter season was set from late November 2019 to Mid-April 2020 (near-surface air temperature below −20 °C), subsequently the spring transition season was until late May 2020 (onset of sea ice melt), followed by the summer season until early September (sea ice freeze-up), and finally the autumn season was from early September (near-surface temperature consistently below 0 °C).

**Sampling.** Samples for water columns taken from the CTD/rosette on Polarstern or the one based on the ice floe ('Ocean City', Rabe et al., 2022) were filtered through pre-combusted (450 °C, 5 h) glass fiber filters (Whatman; GF/F). Temperature and salinity profiles for water column samples were acquired with a CTD attached to a rosette system. The 60 mL filtered water column samples were stored in acid-washed high-density polyethylene bottles at −20 °C for dissolved organic carbon (DOC) and total dissolved nitrogen (TDN; sum of dissolved inorganic and organic components)

measurements, in which samples from November 2019 to February 2020 (Legs 1–2) were also used for absorbance and EEMs measurements. The 40 mL filtered water column samples from January 2020 to September 2020 (Legs 2–5) were stored in pre-combusted amber glass vials at 4 °C for absorbance and EEMs measurements. Samples from lead waters were collected using the peristatic pump (Master flex E/S portable sampler) from the surface 0.1 m down to 2 m between August 25$^{th}$ and September 4$^{th}$ 2020 in summer in the Amundsen Basin (Leg 5), then filtered through an in-line 0.2 µm pore size Sterivex cartridge filter (polyethersulfone membrane) and stored in acid-washed high-density polyethylene bottles at −20 °C for DOC and TDN measurements, and in pre-combusted amber glass vials at 4 °C for absorbance and EEMs measurements. Salinity for lead water samples was measured with a hand-held multi-parameter meter (Cond 340i, WTW). For the analysis of surface chlorophyll a (Chl-a) concentrations, 2 to 4 L of seawater were filtered onto glass fiber filters (Whatman, GF/F) in duplicates or triplicates from the ships underway intake system located at 11 m water depth and filters were frozen at −80 °C until further analyse

**DOC analysis.** DOC and TDN were determined by high temperature catalytic oxidation (HTCO) and non-dispersive infrared spectroscopy and chemiluminescence detection (TOC-VCPN, Shimadzu; for details see Ksionzek et al., 2018). Water samples were directly poured into well-rinsed vials and placed in the autosampler. In the autosampler, the sample was acidified (0.1 M HCl Suprapur, Merck) and sparged with oxygen for 5 min to remove inorganic carbon. 50 µL sample volume was injected directly on the catalyst (680 °C). Detection of the generated $CO_2$ was performed with an infrared detector at a limit of determination of 7 µmol DOC kg$^{-1}$ and a precision of ± 5%. Total nitrogen was quantified by a chemiluminescence detector at a limit of determination of 11 µmol TDN kg$^{-1}$.

**Optical spectroscopy.** FDOM EEMs were measured using a spectrofluorometer (Aqualog, Horiba) equipped with a charge-coupled device (CCD) detector. Excitation wavelengths were performed from 240 to 600 nm at 3 nm increments, and emission from 220 to 620 nm (~3.3 nm increments). CDOM absorbance spectra were acquired by a spectrophotometer (UV2700, Shimadzu) in a quartz cuvette with an optical path length of 10 cm in the spectral range of 200−800 nm. FDOM EEMs and CDOM

absorbance spectra were processed by the *staRdom* package in R studio (Version 3.5.1) (Pucher et al., 2019). The fluorescence spectra were blank corrected using ultrapure water (Whatman, Milli-Q), inner filter effect correction and Raman normalization by dividing by the Raman peak of ultrapure water at an integrated excitation of 350 nm and an emission between 371 and 428 nm (Raman Units (R.U.); Lawaetz and Stedmon, 2009). Subsequently, we applied a PARAFAC (Stedmon et al., 2003) to decompose EEMs into different underlying fluorescent components (Murphy et al., 2013). The biological index (BIX) was calculated by the ratio of the emission intensity at 380 nm divided by that at 430 nm with a fixed excitation wavelength of 310 nm (Huguet et al., 2009). BIX is a proxy of freshly produced autochthonous DOM and higher values indicate a higher proportion of freshly produced DOM (Huguet et al., 2009).The specific ultraviolet absorbance ($SUVA_{254}$ in $L\ mg^{-1}\ m^{-1}$) was calculated by the ultraviolet absorbance at 254 nm (given in $m^{-1}$) divided by the DOC concentration in $mg\ L^{-1}$ (Weishaar et al., 2003). $SUVA_{254}$ has been previously used as a proxy for aromaticity of aquatic humic substances and is positively correlated with molecular weight (Weishaar et al., 2003). The spectral slope between 275 and 295 nm ($S_{275-295}$ in $nm^{-1}$) is calculated using nonlinear least-squares (Helms et al., 2008). $S_{275-295}$ is a CDOM proxy that is negatively correlated with molecular weight and DOM aromaticity (Helms et al., 2008; Hansen et al., 2016).

The absorption coefficient at λ nm ($a_{CDOM}(\lambda)$ in $m^{-1}$) was calculated by the following equation:

$$a_{CDOM}(\lambda) = 2.303A(\lambda)/l$$

where the factor 2.303 is the natural logarithm of 10, A(λ) is the absorbance at wavelength λ in nm, and *l* is the optical path length in meters (Stedmon and Markager, 2001). The absorption coefficient $a_{CDOM}(350)$ has been suggested as a proxy for CDOM concentration, and used to estimate the inputs of terrigenous DOM and lignin phenol concentrations in the Arctic (Spencer et al., 2009a; Walker et al., 2013; Fichot et al., 2016).

**Chlorophyll a measurement.** Samples were extracted in 90% acetone over night at 4 °C and subsequently analyzed on a fluorometer (TD-700; Turner Designs, USA),

including an acidification step (1 M HCl) to determine phaeopigments (Knap et al., 1996).

**Statistical analysis.** Principal component analysis (PCA) and analysis of variance (ANOVA) were performed using the software Origin (Version 2018. OriginLab Corporation, Northampton, MA, USA.). PCA was used to assess spatial variability in optical properties (three humic-like fluorescent components C474, C435, C395, BIX, absorption coefficient at 350 nm $a_{CDOM}(350)$ and the spectral slope $S_{275-295}$ of CDOM in the SML samples (upper 20 m water column) and lead water samples. A two-way ANOVA was computed to assess the effect of regions and seasons on the optical parameters using a significance level of 0.1. The degree of statistical significance of the seasonality in different regions was estimated by applying a one-way ANOVA test with a significance level of 0.05.

## 4.4. Results

### *4.4.1. Spectral characteristics of FDOM components*

Applying PARAFAC analysis to EEMs of all samples (MOSAiC, N-ICE2015 and TA19_4 expeditions) resulted in five underlying components, subsequently named as C475, C440, C395, C340, and C320 according to their fluorescence emission maxima (Figure 2). Based on fluorescence maxima, the components C475 and C440 are often assigned as humic-like components with terrestrial origin (Coble, 1996; Murphy et al., 2011; Gonçalves-Araujo et al., 2016). Component C395 has been assigned as humic-like substance with marine and microbial origin (Coble, 1996; Wagner et al., 2015; Brogi et al., 2019), or with terrestrial origin (Gonçalves-Araujo et al., 2016; Lin and Guo, 2020). In this study, C395 had a significant correlation with C475 and C440 ($R^2 > 0.9$), indicating similar characteristics and allochthonous origins. According to previous studies, C340 is a protein-like component (tryptophan-like peak T) of autochthonous origin (Coble, 1996), and C320 was similar to protein-like (tyrosine-like peak B) component of autochthonous origin (Coble, 1996).

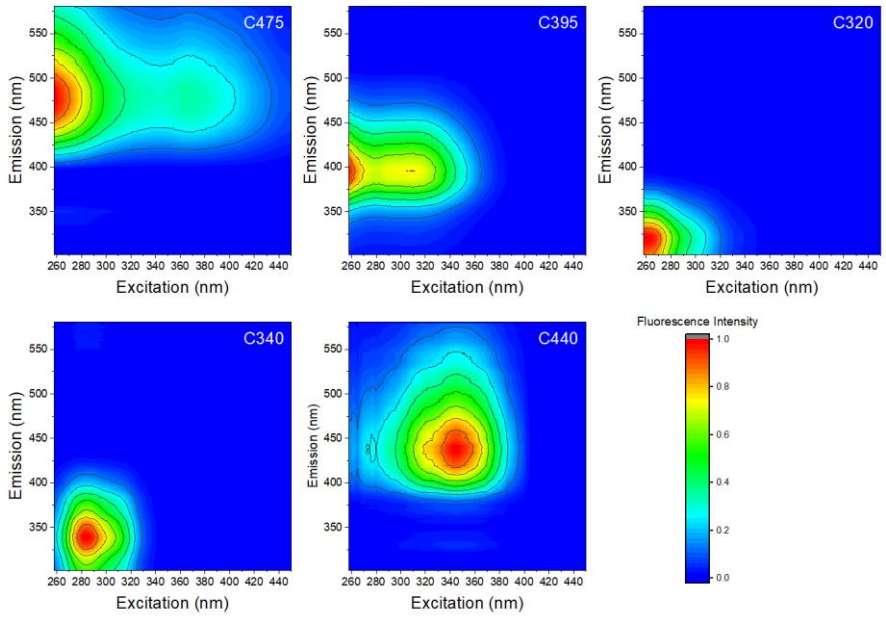


**Figure 2.** Contour plots of the five-component PARAFAC model developed from Fluorescence excitation-emission matrices (EEMs) recorded for all samples during MOSAiC, N-ICE2015 and TA19_4 expeditions.

### *4.4.2. Variations of DOC and FDOM at different sampling depths*

To evaluate the how the DOM changes for different depths during the five Legs of the MOSAiC expedition, we examined the standard deviation of the DOC concentration and FDOM components at different water column depths (Figure 3). For the rather invariant DW (≥ 1000 m water column), the coefficient of variation for different depths and all Legs was ≤ 4.9% for DOC concentrations, and ≤ 12.8% for all FDOM humic-like components, for comparison, to the analytical coefficient of variation was ≥ 10% for DOC concentration and ≥ 22.8% for all FDOM humic-like components for different depths in the surface waters (upper 200 m water column). The low variability in DW measurements indicated the seasonal or regional differences had large influence in the surface waters, but less in the deep over the course of the MOSAiC expedition.

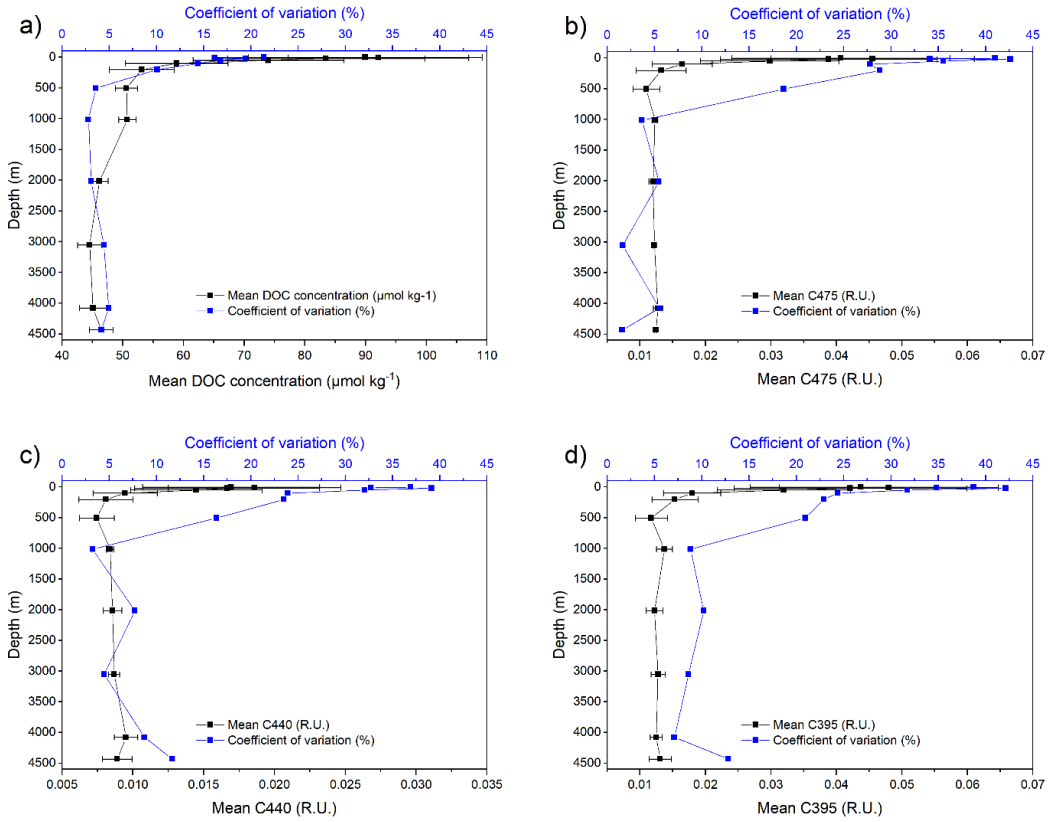


**Figure 3**. Mean values and coefficient of variation of (a) DOC concentration, (b) FDOM component C475, (c) C440 and (d) C395 for different sampling depths during MOSAiC. Error bars indicate standard deviations of all samplings for each depth.

Mean values of temperature, practical salinity, DOC and TDN concentration, C/N ratio, and optical parameters for different water masses in different regions are given in Table 1. Distinct differences between different regions were found in the SML. The DOC concentrations, C/N, $SUVA_{254}$, $a_{CDOM}(350)$, humic-like component C475, C440 and C395 values were higher in the SML in the Amundsen Basin compared to those from the SML in the western Nansen Basin and Yermak Plateau (Table 1). At the same time, higher TDN concentration was observed in the western Nansen Basin and Yermak Plateau compared to the Amundsen Basin and Fram Strait (Table 1). In the Amundsen Basin, the AW1 had an average winter temperature of 1.16 ± 0.04 °C, with temperatures being higher in summer (mean value of 1.30 ± 0.20 °C).

**Table 1.** Mean temperature (T; °C), practical salinity ($S_P$), DOC and TDN concentration (μmol $kg^{-1}$), C/N (calculated by the ratio of DOC and TDN concentration) and optical parameters $SUVA_{254}$ (L $mg^{-1}$ $m^{-1}$), $a_{CDOM}(350)$ ($m^{-1}$), BIX and FDOM components C475(R.U.), C440(R.U.), C395(R.U.), C340 (R.U.) and C320 (R.U.) for different water masses in different regions. SML denotes Surface Mixed Layer (upper 20 m), AW1 denotes Upper Atlantic Water (200 m), AW2 denotes Lower Atlantic Water (500 m), and DW denotes deep water (≥1000 m).

| | Amundsen Basin (Legs 1-2) | | | | Amundsen Basin (Leg 5) | | Western Nansen Basin and Yermak Plateau | | | Fram Strait | | | |
|---|---|---|---|---|---|---|---|---|---|---|---|---|---|
| | SML | AW1 | AW2 | DW | SML | AW1 | SML | AW1 | AW2 | SML | AW1 | AW2 | DW |
| T | -1.75 | 1.16 | 0.87 | -0.54 | -1.55 | 1.33 | -1.76 | 2.01 | 0.64 | -1.50 | 1.66 | 0.97 | -0.29 |
| $S_P$ | 31.9 | 34.8 | 34.9 | 34.9 | 29.9 | 34.8 | 33.9 | 34.9 | 34.9 | 31.8 | 34.8 | 34.9 | 34.9 |
| DOC | 92.4 | 49.0 | 50.4 | 47.2 | 111.0 | 54.2 | 68.1 | 56.8 | 49.3 | 98.2 | 55.9 | 50.2 | 51.7 |
| TDN | 6.0 | 15.8 | 15.0 | 16.7 | 5.6 | 14.9 | 9.2 | 14.1 | 17.9 | 6.9 | 16.0 | 15.7 | 17.0 |
| C/N | 15.7 | 3.2 | 3.4 | 2.8 | 20.5 | 3.6 | 7.4 | 4.2 | 2.8 | 14.3 | 3.5 | 3.2 | 3.1 |
| $SUVA_{254}$ | 1.91 | 0.98 | 0.98 | 0.93 | 1.92 | 1.04 | 1.16 | 0.89 | / | 1.82 | 0.88 | / | / |
| $a_{CDOM}(350)$ | 0.76 | 0.19 | 0.18 | 0.16 | 0.86 | 0.19 | 0.33 | 0.21 | / | 0.75 | 0.12 | / | / |
| BIX | 0.81 | 0.95 | 0.99 | 0.89 | 0.78 | 1.00 | 1.10 | 1.00 | / | 1.09 | 1.07 | / | / |
| C475 | 0.052 | 0.013 | 0.011 | 0.012 | 0.057 | 0.013 | 0.020 | 0.013 | / | 0.050 | 0.013 | / | / |
| C440 | 0.021 | 0.008 | 0.007 | 0.009 | 0.023 | 0.008 | 0.009 | 0.007 | / | 0.023 | 0.008 | / | / |
| C395 | 0.054 | 0.015 | 0.012 | 0.013 | 0.061 | 0.015 | 0.022 | 0.015 | / | 0.054 | 0.014 | / | / |
| C340 | 0.016 | 0.007 | / | / | 0.020 | 0.007 | 0.030 | 0.032 | / | 0.105 | 0.017 | / | / |
| C320 | 0.004 | 0.001 | / | / | 0.011 | 0.013 | 0.012 | 0.008 | / | 0.007 | 0.024 | / | / |

### *4.4.3. Vertical profiles in the upper ocean*

The oceanographic parameters (temperature and practical salinity), the optical indices BIX, $SUVA_{254}$, $a_{CDOM}(350)$ and the terrestrial humic-like FDOM components C475 and C440 were utilized to trace changes in the upper ocean (≤ 500 m water column) along the MOSAiC drift track (Figure 4). In the Amundsen Basin, DOC concentrations, C/N ratios, $SUVA_{254}$, $a_{CDOM}(350)$ and the terrestrial humic-like FDOM component C475 and C440 were higher in the SML than in deeper waters below. In contrast, TDN concentrations in the SML were lower compared to deeper waters below in all regions. In addition, BIX was relatively high values in surface waters of the western Nansen Basin and Yermak Plateau, with an average value of 1.10 ± 0.20,

and the Fram Strait, with an average value of 1.09 ± 0.27, compared to the Amundsen Basin, with an average value of 0.80 ± 0.02 for Legs 1–2, and 0.78 ± 0.02 for Leg 5. On March 6th 2020, strong storms in the Amundsen Basin led to mixing and stronger terrestrial signals in the deeper water, which becomes apparent as higher DOC, $SUVA_{254}$ and C475 down to 200 m water column (Figure 4). We estimated that the contribution of DOC, $SUVA_{254}$ and C475 in the storm-influenced sample at 200 m depth were on average 27%, 41% and 126% higher, respectively, compared to the regular wind conditions.

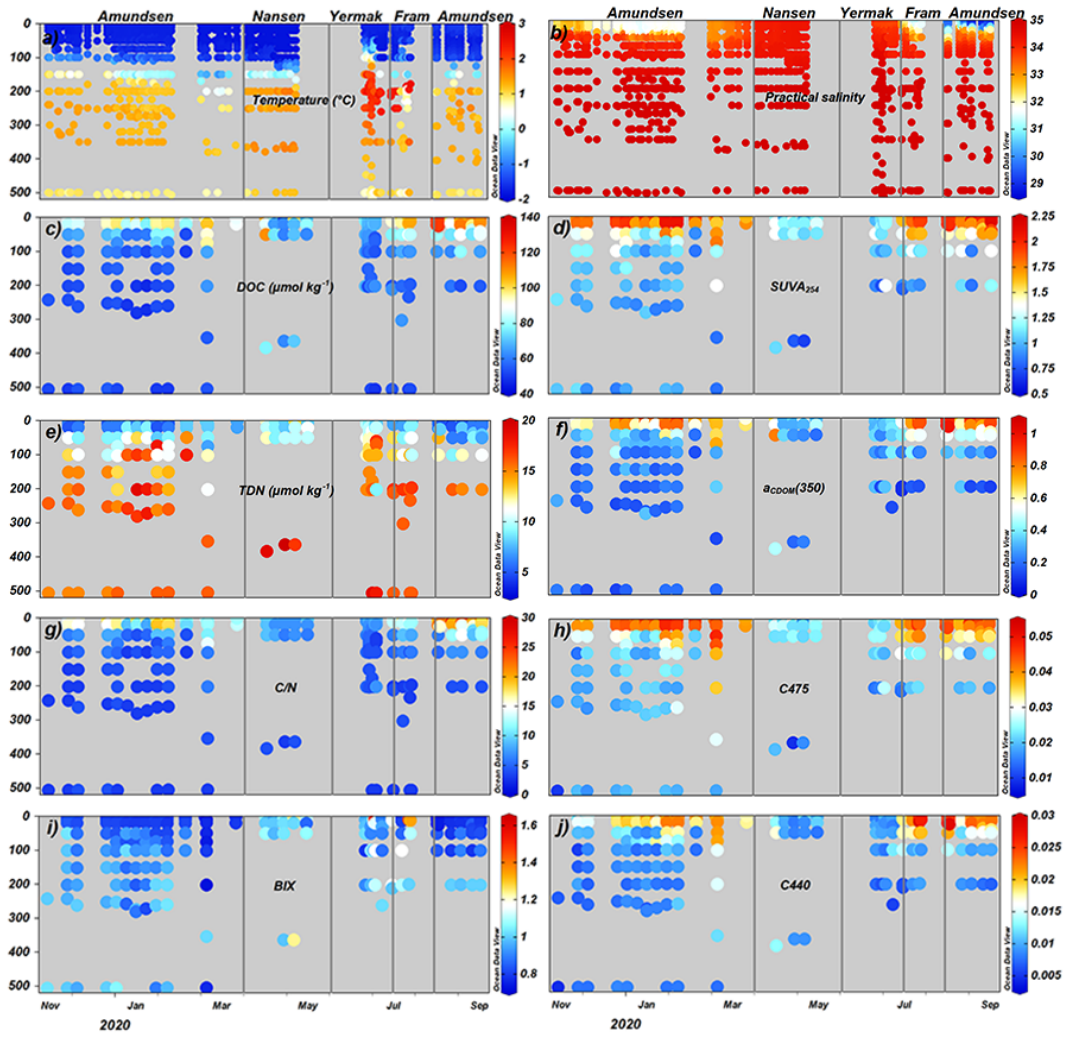


**Figure 4.** Vertical profiles of (a) temperature, (b) practical salinity, (c) DOC concentration, (d) $SUVA_{254}$, (e) TDN, (f) $a_{CDOM}(350)$, (g) C/N (calculated by the ratio of the molar DOC and TDN concentration), (h) C475, (i) BIX, and (j) C440 in the upper 500 m water column over time. X axis indicates sampling depths (m).

### *4.4.4. Optical Properties of DOM in the SML*

The optical parameters in the SML, including the three humic-like fluorescent components C475, C440 and C395, as well as BIX, absorption coefficient $a_{CDOM}(350)$, and spectral slope $S_{275\text{-}295}$ were chosen for a principal component analysis (PCA) to illustrate spatial variability of DOM (Figure 5). Principal component 1 (PC1) accounted for 81% of the total variance, separating surface samples collected in the Laptev Sea, the East Siberian Sea and the Amundsen Basin from surface samples collected in the western Nansen Basin and Yermak Plateau. PC1 showed strong positive loadings for parameters associated with tCDOM (i.e., humic-like components (C475, C440 and C395) and $a_{CDOM}(350)$) and negative loadings for parameters associated with BIX and $S_{275\text{-}295}$. Samples with positive PC1 scores were largely characterized as material with terrestrial sources, with samples located towards the top right of the PCA biplot showing Siberian shelf end members (Figure 5). In contrast, samples from the western Nansen Basin and Yermak Plateau with negative PC1 scores were characterized by low molecular weight and a greater proportion of autochthonous CDOM, representing the marine end member.

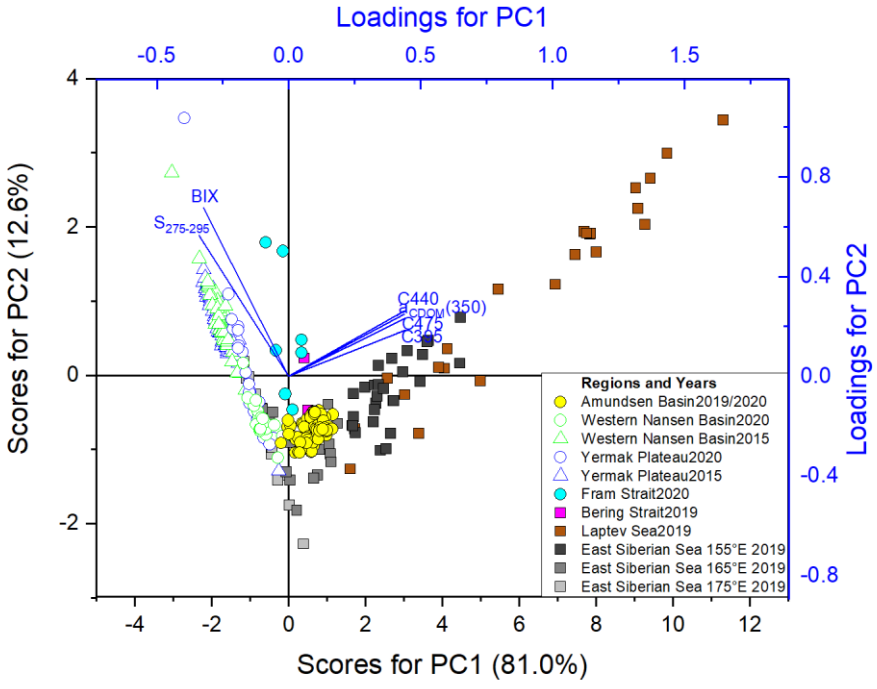


**Figure 5.** Principal component analysis (PCA) biplot based on optical parameters (three humic-like fluorescent component C475, C440 and C395, BIX, absorption

coefficient $a_{CDOM}(350)$ and $S_{275-295}$) in the SML. Scores are shown as colored symbols according to sample locations (similar symbols as in Figure 1 for station locations). Loadings for the six variables are represented in blue.

To assess the imprint of regions and seasons on optical DOM properties in the SML, a two-way ANOVA was performed using regions and seasons as factors (Table 2). The result indicated no statistically significant difference in humic-like components C475, C440 and C395, $a_{CDOM}(350)$ between seasons ($p > 0.1$), but there were statistically significant differences between regions ($p < 0.1$). Additionally, a statistically significant difference in C475, C440, C395, and $a_{CDOM}(350)$ was observed in combined interaction from regions and seasons, indicating at least some influence of seasons on the variability of these CDOM parameters.

**Table 2**. Two-way ANOVA for regions, seasons and a combination of both based on optical DOM properties in the SML. Two asterisks denote differences at a significance level of $p < 0.05$, and one asterisk denotes differences at a significance level of $p < 0.1$.

| | *p value* | | |
|---|---|---|---|
| Variables | Region | Season | Region-Season Interaction |
| C475 | 0.017** | 0.564 | 0.001** |
| C440 | 0.009** | 0.387 | 0.001** |
| C395 | 0.075* | 0.641 | 0.009** |
| $a_{CDOM}(350)$ | 0.060* | 0.833 | 0.050* |
| $S_{275-295}$ | 0.229 | 0.491 | 0.321 |
| BIX | 0.982 | 0.993 | 0.998 |

Monthly average optical parameters as well as salinity and Chl-a concentrations in the SML are presented in Figure 6. Low monthly average DOC concentration and $SUVA_{254}$ values were observed in the western Nansen Basin and Yermak Plateau (ranging from $66.2 \pm 2.7$ to $74.8 \pm 13.8$ μmol $kg^{-1}$ for DOC concentration, and $1.12 \pm 0.06$ to $1.20 \pm 0.11$ L $mg^{-1}$ $m^{-1}$ for $SUVA_{254}$), compared to the Amundsen Basin and Fram Strait (ranging from $82.7 \pm 1.4$ to $112.0 \pm 9.6$ μmol $kg^{-1}$ for DOC concentration, and $1.67 \pm 0.08$ to $1.97 \pm 0.11$ L $mg^{-1}$ $m^{-1}$). BIX (Figure 6c) exhibited

much higher values from April to July in the western Nansen Basin, Yermak Plateau and Fram Strait (ranging from 0.97 ± 0.07 to 1.21 ± 0.0.22 µg $L^{-1}$). Chl-a (Figure 6d) exhibited quite higher values in June and July on the Yermak Plateau and Fram Strait (ranging from 0.70 ± 0.19 to 1.09 ± 0.53 µg $L^{-1}$).

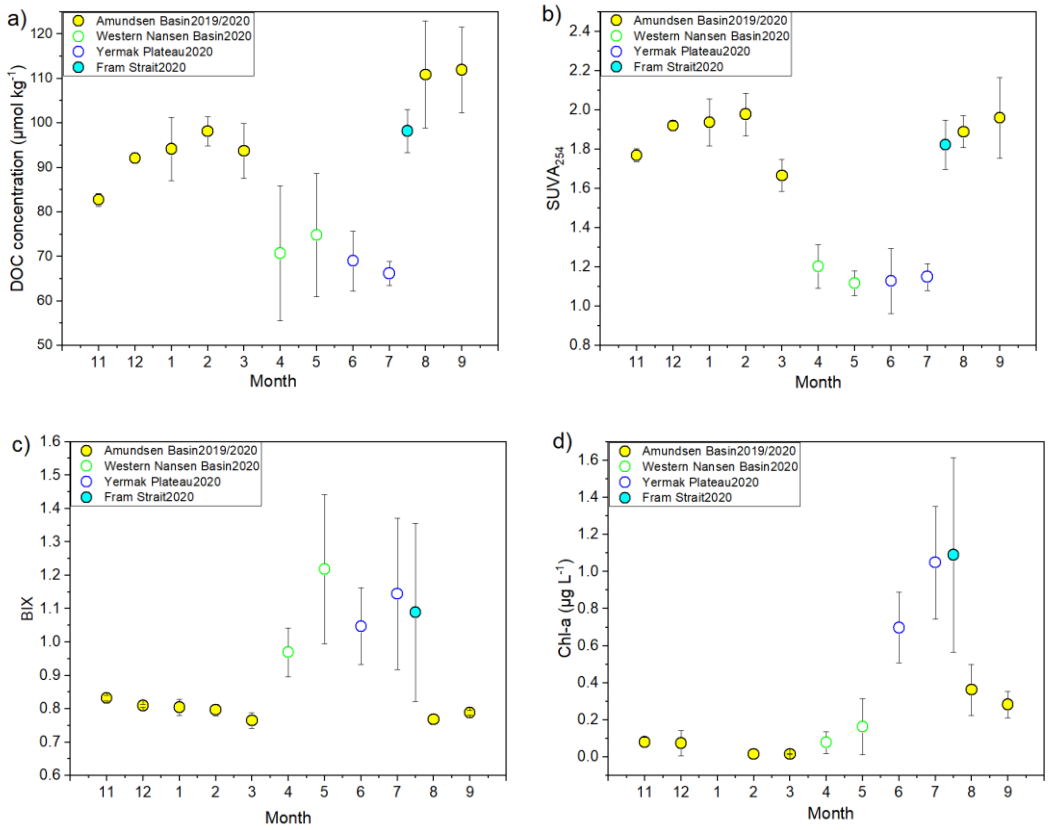


**Figure 6.** Monthly averages (Nov 2019 – Sep 2020) in the SML of (a) DOC concentration, (b) $SUVA_{254}$, (c) BIX and (s) Chl-a during MOSAiC. Unfilled circles denote samples outside the Transpolar Drift (TPD) influence, and filled circles denote samples within the TPD influence. Note that for July 2020, averages were calculated for two shorter periods 01.07. – 09.07.2020 (Yermak Plateau) and 16.07. – 29.07.2020 (Fram Strait).

Seasonal changes in optical parameters as well as salinity and Chl-a concentrations in the SML at different regions are presented in Figure 7. Under the influence of the TPD (i.e., Amundsen Basin), summer exhibited high freshwater input (likely from sea-ice melt and river runoff) as reflected by low practical salinity values (mean value of 30.0 ± 0.7; Figure 7a). Additionally high Chl-a concentrations (mean value of 0.35 ± 0.12 µg $L^{-1}$; Figure 7d) indicate a high phytoplankton biomass in summer.

However, we could not observe a coincident change in BIX (Figure 7c). Outside the influence of the TPD (i.e., western Nansen Basin and Yermak Plateau), summer SML in 2020 was characterized by lower practical salinity (mean value of 33.8 ± 0.08) compared to spring (mean value of 34.3 ± 0.05; Figure 7a). In addition, summer SML exhibited higher Chl-a concentration and BIX values, with mean values of 0.83 ± 0.29 μg $L^{-1}$ and 1.12 ± 0.22, respectively, compared to spring, with mean values of 0.14 ± 0.13 μg $L^{-1}$ and 1.06 ± 0.18, respectively (Figure 7c, d). BIX (at ~10 m depth) exhibited a positive correlation with Chl-a (at 11 m depth) with $R^2$ of 0.69 in summer. The proxies for tCDOM ($a_{CDOM}(350)$ and humic-like component C475) showed a similar trend. Using $a_{CDOM}(350)$, we can estimate that the contribution of terrestrial material in summer within the TPD influence was on average 136% higher than outside the TPD influence during the MOSAiC expedition. In summer, Chl-a concentration was higher on the Yermak Plateau (mean value of 0.83 ± 0.29 μg $L^{-1}$) and the Fram Strait (mean value of 1.04 ± 0.48 μg $L^{-1}$) compared to the Amundsen Basin (mean value of 0.35 ± 0.12 μg $L^{-1}$) (Figure 7d). In addition, summer BIX values during the MOSAiC expedition were higher on the Yermak Plateau (mean value of 1.12 ± 0.22) and the Fram Strait (mean value of 1.09 ± 0.27) compared to the Amundsen Basin (mean value of 0.77 ± 0.02) (Figure 7c). Furthermore, higher terrestrial contribution, lower BIX values and Chl-a concentrations were found in summer 2020 on the Yermak Plateau (MOSAiC; mean values of 1.12 ± 0.22 and 0.83 ± 0.29 μg $L^{-1}$ for BIX and Chl-a concentration, respectively) compared to summer 2015 (N-ICE2015; mean values of 1.54 ± 0.22 and 4.17 ± 1.21 μg $L^{-1}$ for BIX and Chl-a concentration, respectively).

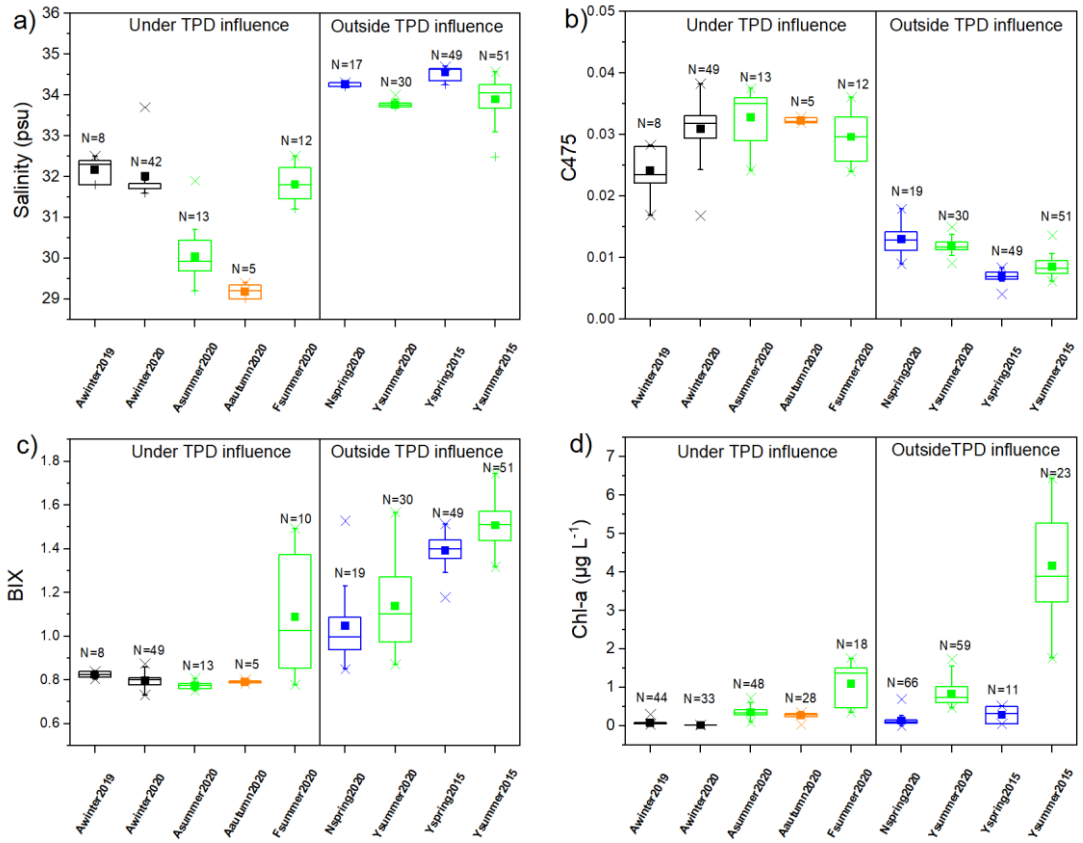


**Figure 7.** The SML seasonality (one-way ANOVA at a 95% confidence level) of (a) practical salinity, (b) FDOM component C475, (c) BIX and (d) Chl-a concentration at different regions and years for MOSAiC and N-ICE2015. $p < 0.05$ for all parameters above. N indicates the number of samples in each category. The mean (solid squares), median (horizontal lines), 25$^{th}$ to 75$^{th}$ percentile (boxes), total range (whiskers) and outliers (cross marks) for each sample population are shown. Black=Winter; Blue=Spring; Green=Summer; Orange=Autumn. Labels on the x-axis denote regions of the Amundsen Basin (A), western Nansen Basin (N), Yermak Plateau (Y), and Fram Strait (F) at which the ship was located during the respective season and year.

### *4.4.5. Lead water samples from the Amundsen Basin*

Low-salinity ($2.4 \leq$ salinity $\leq 20$) lead water samples showed a significant positive correlation between salinity and DOC ($R^2$=0.89, Figure 8a), as well as a significant positive correlation between salinity and C475, C440 and C394 ($R^2$ = 0.92, 0.89 and 0.83, respectively). High-salinity ($28 \leq$ Salinity $\leq 30$) lead water samples, which supposedly have a low contribution of meltwater, had much higher DOC concentrations than the low-salinity waters (Figure 8a). Based on the optical

parameters, principal component 1 (PC1) accounted for 81.1% of the total variance, separating high-salinity from low-salinity lead water samples (Figure 8b). High-salinity lead water samples were dominated by tCDOM as indicative of strong positive loading for humic-like components (C475, C440 and C395) and $a_{CDOM}(350)$ in PC1, and low-salinity lead water samples were dominated by autochthonous DOM as indicative of strong negative loading for BIX and $S_{275-295}$ in PC1.

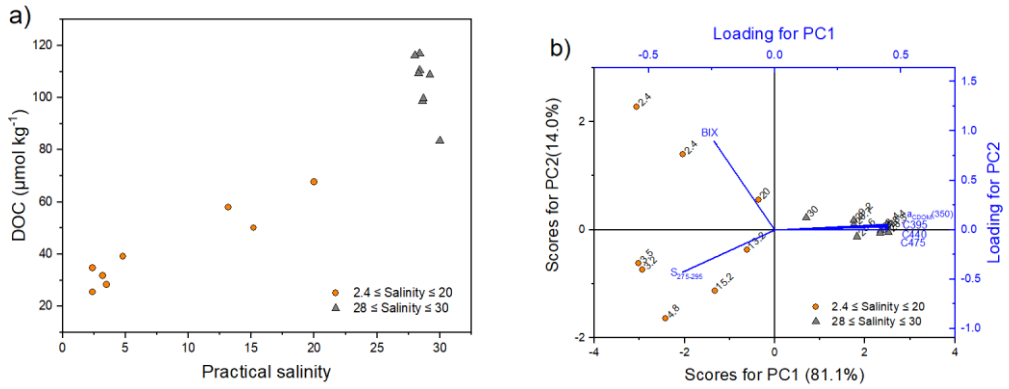


**Figure 8**. (a) Relationship between DOC concentration and practical salinity ($S_P$) for MOSAiC lead water samples in the Amundsen Basin, (b) PCA biplot based on optical parameters (C475, C440, C395, BIX, $a_{CDOM}(350)$ and $S_{275-295}$) for the lead water samples. Black numbers indicate the value of practical salinity.

## 4.5. Discussion

### *4.5.1. Spatial variability of DOM properties depends on the influence of the transpolar drift*

During the MOSAiC expedition, optical DOM indices and PARAFAC components in the SML showed pronounced differences between regions, particularly between those that were located within and outside the influence of the TPD.

In the TPD-influenced regions (i.e., Amundsen Basin), the SML was largely characterized by a high contribution of tCDOM (indicated by on average 136% and 45% higher values for $a_{CDOM}(350)$ and DOC concentration, respectively, compared to the western Nansen Basin and Yermak Plateau; Figures 4–6). This is in agreement with previous studies reporting that the tCDOM input to surface waters in the Amundsen Basin can be high compared to the western Nansen Basin (Slagter et al., 2017; Boles

et al., 2020). Higher $SUVA_{254}$ values in the Amundsen Basin (mean value of $1.91 \pm 0.13$ L mg$^{-1}$ m$^{-1}$) during our study indicate a predominance of humic-like substances with higher molecular weight from allochthonous input (Weishaar et al., 2003; Walker et al., 2013) by the large Siberian rivers and shelf. Our studies emphasizes that this terrestrial contribution is also predominant in the Central Arctic winter in 2020. However, it should be considered that the location of the transpolar drift can vary substantially between years as a response of the Arctic oscillation (Mysak, 2001; Karcher et al., 2012; Smith et al., 2021). Outside the TPD-influenced regions (i.e., western Nansen Basin and Yermak Plateau), the SML was characterized by a much greater proportion of freshly generated autochthonous CDOM (indicated by on average 25% higher BIX values compared to the Amundsen Basin). The surface waters in the western Nansen Basin and Yermak Plateau were generally affected by the inflow of relatively warm, salty and nutrient-rich AW having a low terrestrial organic matter content (Rudels et al., 2015; Pavlov et al., 2017). Lower $SUVA_{254}$ values (mean value of $1.16 \pm 0.09$ L mg$^{-1}$ m$^{-1}$) in the western Nansen Basin and Yermak Plateau are also associated to more autochthonous or modified tCDOM with lower aromaticity (Weishaar et al., 2003; Walker et al., 2013).

The surface waters of the Fram Strait also showed a substantial contribution of terrestrial material but also a large proportion of newly generated DOM. The Fram Strait is a region that is affected by two contrasting water masses, the Polar Water in the East Greenland Current (EGC) and the Atlantic Water in the West Spitsbergen Current (WSC; Pavlov et al., 2015). In the western Fram Strait, relatively fresh and cold Polar Water is exported to the North Atlantic by the EGC. This water was formerly transported across the Arctic Ocean via the TPD, exhibiting a relatively high load of terrestrial DOM (Opsahl et al., 1999; Amon et al., 2003; Granskog et al., 2012). In the eastern Fram Strait, warm and saline Atlantic Water is transported northwards into the Arctic Ocean by the WSC (e.g., Beszczynska-Möller et al., 2012). Part of the Atlantic Water recirculates (Return Atlantic Water) in the Fram Strait and joins the EGC in the West (Amon et al., 2003). The observations during the MOSAiC expedition in our study were taken from the central to western part of the Fram Strait (Figure 1), and thus were influenced by Polar Water and Atlantic Water.

With increasing sampling depth, the variability in the DOC concentration and FDOM humic-like components decreased (Figure 3). DW (≥ 1000 m water column) showed the lowest variability. This was in agreement with the fact that DOM is more labile (i.e., susceptible to microbial degradation) in the upper water column and more refractory (i.e., resistant to microbial degradation) in the deep ocean below 1000 m (Hansell et al., 2012). As expected, for samples in the upper 200 m, the variability of DOC and FDOM over all the observations was relatively high due to the seasonal and regional variations. Our two-way ANOVA results (Table 2) confirmed that CDOM in the SML across the year-round MOSAiC expedition was mainly affected by regional differences, which were modulated to an extent by seasonal changes.

### *4.5.2. Potential impact of the tCDOM-rich surface waters on primary production*

CDOM characteristics in the SML strongly differed between regions within and outside the TPD, which has a potential impact on primary production. Compared to the Yermak Plateau, surface waters in the Amundsen Basin exhibited a lower proportion of freshly generated DOM (average 31 % lower BIX value) and lower phytoplankton biomass (average 58 % lower Chl-a concentration) in summer 2020 (Figure 7). BIX (at ~10 m depth) exhibited a positive correlation ($R^2$ = 0.69) with Chl-a concentration (at 11 m depth) in summer. Freshly generated autochthonous DOM in the ocean originates from extracellular release by phytoplankton, cell lysis and release by zooplankton grazing (Carlson et al., 1998; Nagata et al., 2000; McKnight et al., 2001). Most of this newly produced DOM is biologically labile and consumed and respired rapidly by heterotrophic bacteria (Hansell et al., 2009). A small fraction of that DOM escapes rapid remineralization and is transformed into refractory material by abiotic and biotic processes and accumulates in the surface layer for eventual export to the deep ocean by bottom water formation (Hansell et al., 2009). Polar waters in the Arctic Ocean have lower bacterial growth rates and lower bacterial production compared to lower-latitude waters (Kirchman et al., 2009). Terrestrial DOC is mineralized with a half-life approximately seven years in the Arctic Ocean (Hansell et al., 2004). This implies that even the high terrestrial DOC in the TPD influenced regions, probably did not contribute substantially to bacterial production, which is in agreement with our fairly constant BIX values in the Amundsen Basin among different seasons (Figure 7c).

The primary production in the Arctic Ocean is affected by a complex interaction between different abiotic and biotic drivers, with light and nutrient availability being considered the most important ones (Popova et al., 2012). Light availability is strongly influenced by the presence of sea ice since penetration of solar radiation into the ocean depends on surface albedo, snow depth, and ice thickness. High concentration of tCDOM delivered to the CAO by the TPD also affects the light budget in surface waters: The presence of CDOM is known to attenuate light penetration into the ocean, which can reduce light availability for primary production (Granskog et al., 2007; Lund-Hansen et al., 2015). Nutrient availability is not only affected by horizontal advection of nutrient-rich waters, in the Eurasian Basin most prominently via the Atlantic inflow, but also affected by nutrient supply from upwelling (Carmack et al., 2006). High loads of riverine freshwater transported by the TPD results in low salinity SML creating a strong stratification, separating the surface layer from the deeper layer (Rudels et al., 1991; Gonçalves-Araujo et al., 2015; Nummelin et al., 2016). High-salinity lead water samples from the Amundsen Basin in summer were dominated by tCDOM (Figure 8), showing similar characteristics to the regular Polar Water in the Amundsen Basin. In contrast, low-salinity lead water samples in summer with a larger meltwater contribution and high proportions of freshly produced DOM showed a significant positive correlation between salinity and tCDOM (Figure 8), indicating the meltwater contributed to the low salinity in the surface, which could enhance the stratification in summer. Thus, the pronounced stratification in summer could reduce the availability of upwelled nutrients (Rudels et al., 1991), which may affect the primary production. At the same time, labile DOM may represent a source of energy and matter to the nutrient and light limited ecosystem, especially in winter.

In contrast, the “Atlantification” in the western Nansen Basin and Yermak Plateau resulting from the pronounced northward advection of AW, associated with a reduction in stratification and an increase in nutrient supply, causes an alleviation of both, light and nutrient limitations, and hereby potentially increases the primary productivity in surface waters (Polyakov et al., 2017; Randelhoff et al., 2018). Nitrate concentrations in surface waters, which decrease with an increasing meteoric water fraction (Charette et al., 2020), are lower in the Amundsen Basin than in the Nansen Basin (Slagter et al., 2017; Liguori et al., 2021). This is in good agreement with our

TDN concentrations in the SML of the western Nansen Basin which were higher compared to the Amundsen Basin (Figure 4e).

### *4.5.3. Potential impact of the tCDOM-rich surface waters on the sea ice melt and formation*

High tCDOM in the TPD-influenced regions during the MOSAiC expedition may have a potential influence on the sea ice melt and formation. Sea ice in winter was thinner and the sea-ice concentration in summer was lower in Arctic compared to earlier years (Krumpen et al., 2021). Most of the sea ice mass loss observed in recent years is due to summer solar heating of the SML through ice cracks and open water and subsequent melting of the bottom of the ice (Perovich et al., 2011; Perovich and Richter-Menge, 2015; Polyakov et al., 2017). Light absorption by CDOM can play an important role in the heat budget of Arctic surface waters. It has been shown that the presence of CDOM results in an increased absorption of solar radiation, providing additional heat to enhance the melting of sea ice in the western Arctic Ocean and in the western Fram Strait (Pegau, 2002; Hill, 2008; Granskog et al., 2015). Hence, the observed tCDOM-rich surface waters in the Amundsen Basin potentially contributed to the enhanced sea ice melting. It would be particularly interesting to study if this influence varies with changes in the flow pattern of the TPD.

In the Amundsen Basin, the temperature of AW1 was slightly higher in summer 2020 (mean value of $1.30 \pm 0.20$ °C) than in winter 2019/2020 (mean value of $1.16 \pm 0.04$ °C). During the sea ice formation, CDOM can be removed from the ice during brine rejection (Belzile et al., 2002; Matsuoka et al., 2012; Hölemann et al., 2021). Brine rejection increases the density of the surface waters (Rudels, 1989; Rudels et al., 2004), leading to a reduction in the stability of the water column and allowing more heat from the AW layer to be transferred upwards to the surface, which could inhibit the sea ice formation during winter (Polyakov et al., 2012, 2013). The increased heat transfer from the AW to the SML in winter is not only caused by brine-driven convection, but also affected by the vertical velocity shear below the SML, which is strengthened by strong storms in winter (Polyakov et al., 2013). In the Amundsen Basin at 200 m water depth, a stronger terrestrial signal was observed during storm events than during regular wind conditions (Figure 4). During the storm

events the temperature at 200 m was 0.38 °C, indicating that the vertical mixing induced by the storms caused an increased transfer of heat into the winter SML. Hence, these processes in winter could have potential negative feedback on sea ice formation.

The tCDOM-poor surface waters were dominant in the western Nansen Basin and Yermak Plateau, where stratification is significantly lower than in the TPD-influenced regions. The AW entering the Arctic through the Fram Strait and propagating into these regions contributes to increased melting of sea ice in summer (Polyakov et al., 2020). Furthermore, weakened stratification in winter in these regions allows for enhanced upward heat transfer from the AW, leading to the reduction of the sea ice thickness (Onarheim et al., 2014; Ivanov et al., 2016).

## 4.6. Conclusions

CDOM quantity and quality in surface waters during the year-round MOSAiC expedition were strongly affected by regional differences, with seasonal changes to an extent modifying spatial patterns. Most of the observed differences in CDOM characteristics in surface waters depended on whether the samples were taken inside or outside the TPD. The surface waters in the Amundsen Basin were largely dominated by tCDOM due to the influence of the TPD. In contrast, outside the TPD-influenced regions (i.e., western Nansen Basin and Yermak Plateau), water masses in the SML were characterized by a much greater proportion of freshly generated autochthonous CDOM. The SML in the Fram Strait not only presented a high tCDOM but also a high proportion of newly generated DOM. The summer SML exhibited higher phytoplankton biomass and autochthonous DOM on the Yermak Plateau compared to the Amundsen Basin. The winter AW1 in the Amundsen Basin exhibited lower temperature compared to summer. The differences of CDOM characteristics in the surface waters could have potentially impact on the primary production and sea ice melt and formation. Additionally, these findings have potential implications for studies that take into account the chemical composition of sea ice DOM and aerosols, which both are connected to surface DOM.

## 5. Manuscript III

# Quantitative characterization of dissolved organic matter in original Central Arctic seawater using liquid chromatography FT-ICR mass spectrometry

Xianyu Kong[1]*, Oliver J. Lechtenfeld[2], Boris P. Koch[1,3]*

[1] *Alfred Wegner Institute Helmholtz Centre for Polar and Marine Research, Am Handelshafen 12, 27570 Bremerhaven, Germany*

[2] *Helmholtz Centre for Environmental Research, Permoserstrasse 15, 04318 Leipzig, Germany*

[3] *University of Applied Sciences, An der Karlstadt 8, 27568 Bremerhaven, Germany*

* Corresponding author: Email: Xianyu.Kong@awi.de

Email: Boris.Koch@awi.de

## 5.1. Abstract

The large discharge of freshwater and associated terrigenous materials have a major impact on the physical features and biogeochemical cycles in the Arctic Ocean. The quantitative changes in the terrestrial contribution of dissolved organic matter (DOM) in the eastern Arctic has not been well defined. In this study, we combined Fourier Transform Ion Cyclotron Resonance mass spectrometry hyphenated with liquid chromatography (LC-FTMS) and optical spectroscopy to analyze original filtered seawater for DOM characterization in the Central Arctic Ocean (CAO) based on the year round (Nov 2019–Sept 2020) expedition "Multidisciplinary Drifting Observatory for the Study of Arctic Climate". We aimed to quantify the changes of DOM with different sources (terrestrial versus marine) and their relative distribution at different depths and characterize DOM composition derived from melting sea ice. We observed that DOM in the Central Arctic waters can be quantified by the LC-FTMS measurement as indicative of a good linear correlation between the DOC concentration and the summed mass peak magnitudes for each sample ($int_{sum}$). We used fluorescence excitation-emission matrices (EEMs) and parallel factor analysis (PARAFAC) and identified three terrestrial humic-like fluorescent compounds. These compounds and salinity were used as terrigenous proxies to isolate molecular formulas that represented terrestrially-derived DOM (tDOM) and marine DOM (mDOM), respectively. Up to 83% of the summed mass peak magnitudes were identified as either tDOM or mDOM. The tDOM was characterized by higher degree of unsaturation (as indicated by the mean of intensity weighted average aromaticity index ($AI_{wa}$) that varied from -0.27 for mDOM to -0.12 for tDOM) compared to mDOM. Assuming that the peak magnitudes of tDOM formulas were also correlated with DOC, we estimated that the terrestrially-derived DOC (tDOC; calculated by multiplying the DOC concentration by the proportion of tDOM) in the surface water (i.e., upper 20 m) in the TPD-influenced regions was average 49% higher compared to the regions out of TPD influence. Also, it was estimated that ~17% (or 8 μmol $kg^{-1}$) of the deep DOC (~2000 m) was derived from terrestrial sources and at least ~57% (or 27 μmol $kg^{-1}$) from marine sources in the eastern Arctic. Sea ice meltwater showed a unique molecular DOM composition and was predominated by N-depleted, saturated, low

oxidized and low degraded DOM during August and September in the Amundsen Basin. Our study provides the first extensive DOM dataset that is derived from original water mass spectrometry and allows reasonable quantitative carbon estimates that were not possible beforehand. It is also a unique view on molecular changes in the DOM composition of the CAO over the course of an entire year, and it enabled the identification of new molecular formula proxies that are suitable to identify organic matter derived from sea ice and terrestrial sources. The new technique also supports chemical characterization beyond the molecular formula level.

**Keywords:** Dissolved organic matter; Terrestrially-derived DOM; Marine DOM; High resolution mass spectrometry; Polarity; Optical spectroscopy.

## 5.2. Introduction

Dissolved organic matter (DOM) in the ocean, derived from the autochthonous (marine) or allochthonous (terrestrial) origins, represents the largest active pool of organic carbon in the global carbon cycle. DOM plays a key role in marine biogeochemical cycles by attenuating light (e.g., Morris et al., 1995), regulating the UV and visible light absorption (e.g., Osburn et al., 2001), serving as an energy and nutrient source for heterotrophic communities (e.g., Wetzel, 1984), and acting as a trace metal ligand (e.g., Zhang et al., 2019). The major discharge of Arctic Rivers and associated terrigenous materials large quantities of DOM into the Arctic Ocean and, as a consequence, significant amounts of DOM are exported to the North Atlantic Ocean (Benner et al., 2005; Carmack et al., 2016). The transpolar drift (TPD) is the major surface current that transports sea ice, shelf surface waters and terrestrial DOM from the Laptev and East Siberian Seas across the Arctic Basin towards the Fram Strait and East Greenland Current (Slagter et al., 2017; Charette et al., 2020). During periods of a low Arctic Oscillation (AO) index, the TPD is typically located along the Lomonosov Ridge, whereas it extending more towards the Chukchi shelf during periods of a high AO index (Morison et al., 2012). The TPD largely affects the water properties in the Amundsen Basin and Makarov Basin, which are separated by the Lomonosov ridge, while the Nansen Basin, which is separated from the Amundsen Basin by the Gakkel Ridge, is largely unaffected by the TPD (Slagter et al., 2017). The terrigenous organic matter flowing into rivers is highly colored, aromatic and dominated by complex humic-rich constituents (Dittmar and Stubbins, 2014). Hence, the Arctic Ocean is largely affected by the input of terrigenous organic matter via high fluvial fluxes, which supply high concentrations of dissolved organic carbon (DOC) and chromophoric dissolved organic matter (CDOM) in polar waters (Benner et al., 2005; Slagter et al., 2017).

CDOM is the fraction of DOM that the ultraviolet and visible light (Guéguen et al., 2005), and the part of CDOM that emits a fraction of the absorbed energy as fluorescence, is called fluorescent dissolved organic matter (FDOM). CDOM can be quantified in original water rapidly in the laboratory, in situ, and by remotely sensing (Spencer et al., 2009b; Zielinski et al., 2018; Glukhovets et al., 2020; Lewis and

Arrigo, 2020). Optical spectroscopy (targeting CDOM and FDOM) is widely used to investigate DOM dynamics and distributions in aquatic system due to its simplicity, high sensitivity and cost-effectiveness (Parlanti et al., 2000; Baker and Spencer, 2004; Yamashita and Jaff , 2008). The most comprehensive measurement of fluorescence is the detection of the entire fluorescence emission at different excitation wavelengths, an excitation-emission matrix spectrum (EEMs; Perdue and Benner, 2009). EEMs can be decomposed into the underlying independently fluorescing components using parallel factor analysis (PARAFAC), which is an effective tool to track the sources and composition of DOM (Stedmon et al., 2003; Murphy et al., 2008). Marine DOM is a heterogeneous and highly complex mixture of compounds. DOM in the ocean using conventional analytical techniques, only a small fraction can be chemically characterized and quantified, e.g., monomers of sugars, amino acids, lipids, and lignin. The largest fraction of DOM remains molecularly uncharacterized (Kaiser and Benner, 2009, 2012a, 2012b), which limits the options to use chemical information, for example, to distinguish terrestrial and marine DOM sources. Ultrahigh resolution Fourier-transform ion cyclotron resonance (FT-ICR) mass spectrometry (MS) associated with direct infusion (DI) electrospray ionization (ESI) has emerged as an important analytical technique to resolve the molecular complexity of marine and terrigenous DOM on a molecular mass level (Koch et al., 2005, 2007; Flerus et al., 2012). A subfraction of DOM isolated by solid-phase extraction (SPE-DOM), has been widely used for characterization via FT-ICR MS, resulting in a chemical fingerprint of thousands of molecular formulas (Hertkorn et al., 2007; Koch et al., 2007; Mopper et al., 2007; Capley et al., 2010; Sleighter et al., 2012; Kellerman et al., 2014). However, DOC loading during solid-phase extraction affects extraction efficiency and chemical composition of SPE-DOM (Li et al., 2016b; Kong et al., 2021). Therefore, comparing chemical DOM characteristics in original water (as acquired by e.g., fluorescence) and solid-phase extracted DOM (e.g., via FT-ICR MS; Stubbins et al., 2014) has important limitations (Wünsch et al., 2018b). Chemical fractionation due to solid-phase extraction and matrix effects in DI-ESI FT-ICR MS (Lechtenfeld et al., 2015; Zark and Dittmar, 2018), also strongly limit quantitative interpretations.

High performance liquid chromatography (HPLC) separation offers a promising alternative for DI analysis since it further separates DOM based on, for example, polarity prior to detection (Reemtsma, 2001; Dittmar et al., 2007; Mopper et al., 2007; Brown et al., 2016; Petras et al., 2017; Lu et al., 2018; Lu and Liu, 2019). Some studies utilize offline HPLC separation for FT-ICR MS for SPE-DOM (Koch et al., 2008; Spranger et al., 2019), which is laborious and time-consuming. Few recent studies combined online HPLC separation with FT-ICR MS for original waters (Hawkes et al., 2018b; Kim et al., 2019), which introduces a new fractionation effect in ESI due to a changing solvent matrix along the HPLC gradient. Han et al. 2021 utilizes the FT-ICR MS hyphenated with HPLC using a counter gradient to stabilize the solvent matrix for transient ESI-MS signals and successfully detects more polar compounds using original the Suwannee River Fulvic Acid (SRFA) and peat pore water compared to DI SPE-DOM measurement.

In this study, we combined FT-ICR MS hyphenated with an ultra-high performance liquid chromatography (UPLC) system (referred in the paper as LC-FTMS) and optical spectroscopy to analyze original water for DOM characterization in the Central Arctic Ocean (CAO) during the year-round (November 2019–September 2020) expedition “Multidisciplinary Drifting Observatory for the Study of Arctic Climate” (MOSAiC; Rabe et al., 2022). Our aim was to distinguish DOM from different origins (terrigenous, marine, sea ice), and investigate the source distribution throughout the water column. Two main research hypotheses were tested: (i) DOM sources from original Central Arctic water samples can be quantified using the LC-FTMS analyses; ii) DOM derived from sea ice production can be tracked by LC-FTMS analyses; iii) The chemical features of DOM from different sources can be compared by the optical spectroscopy and LC-FTMS analyses.

## 5.3. Materials and Methods

### *5.3.1. Study area*

The Central Arctic samples were collected on RV Polarstern (Knust, 2017) during the Arctic drift expedition MOSAiC (Multidisciplinary drifting Observatory for the Study of Arctic Climate; PS122). The drift with the sea ice floe started at the Amundsen Basin, via the western Nansen Basin and Yermak Plateau, towards the Fram Strait from October 2019 to July 2020 during legs 1–4, then returning to the Amundsen Basin (near the North Pole) to drift again from August and September 2020 with a new ice floe during leg 5 (Figure 1; Nicolaus et al., 2022).

Samples for ocean waters taken from the CTD/rosette from Polarstern or from the ice station "Ocean City" (sampling depths at approximately 2 m, 10 m, 20 m, 50 m, 100 m, 200 m, 500 m, 1000 m, 2000 m) were filtered through pre-combusted (450 °C, 5 h) glass fiber filters (Whatman; GF/F). Samples from lead waters (from the surface at 0.1 m down to 1 m) during August 25$^{th}$ to September 12$^{th}$ were collected using a peristatic pump (Master flex E/S portable sampler) and filtered through an inline 0.2 µm pore size cartridge filter (Sterivex; polyethersulfone membrane). The filtered samples were stored in acid washed high density polyethylene bottles at −20 °C for dissolved organic matter (DOC) and total dissolved nitrogen (TDN) measurements, as well as LC-FTMS measurement analysis, and stored in pre combusted amber glass vials at 4 °C for absorbance and excitation emission matrices (EEMs) measurements (Kong et al., submitted). Salinity profiles for ocean water samples were acquired with a CTD attached to a rosette system. Salinity for lead water samples was measured with a hand-held multi parameter meter (Cond 340i, WTW).

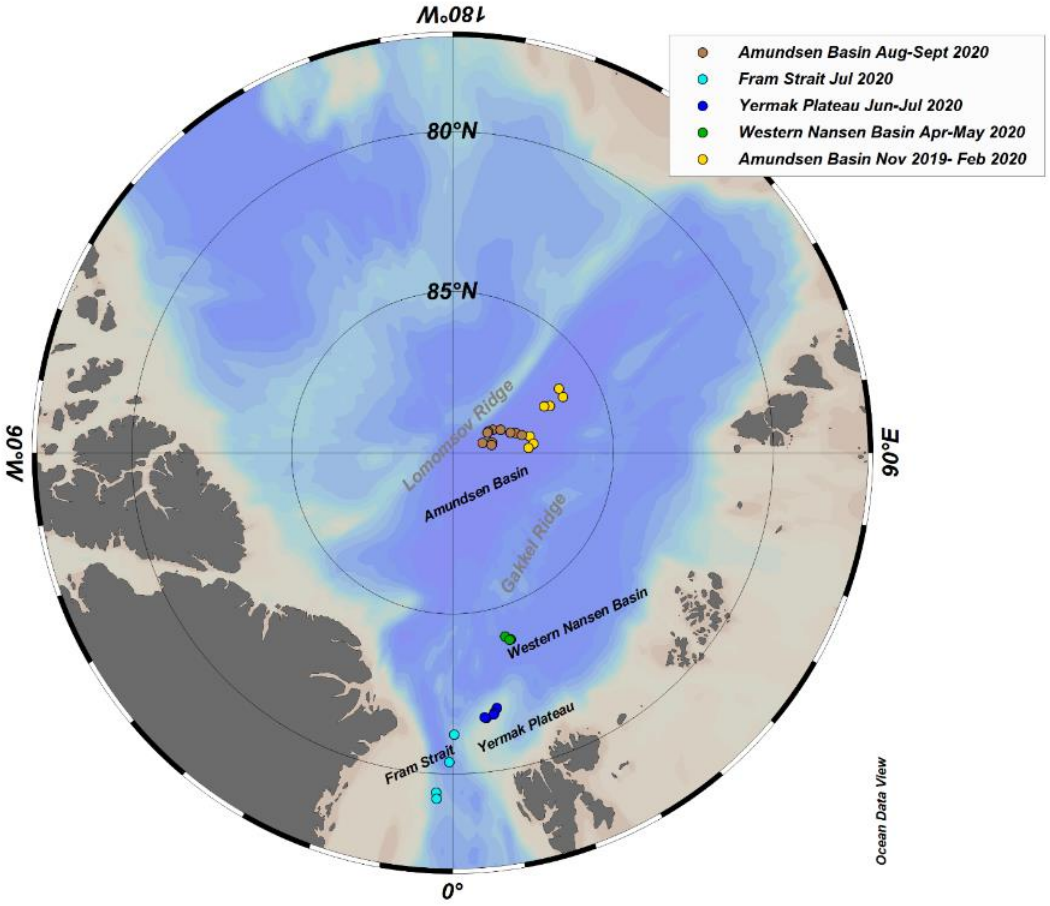


**Figure 1.** Map of the study area.

### *5.3.2. DOC measurement*

DOC and TDN were determined by high temperature catalytic oxidation (HTCO) and non-dispersive infrared spectroscopy and chemiluminescence detection (TOC-VCPN, Shimadzu; for details see Ksionzek et al., 2018). Water samples were directly poured into well-rinsed vials and placed in the autosampler. In the autosampler, the sample was acidified (0.1 M HCl suprapur, Merck) and sparged with oxygen for 5 min to remove inorganic carbon. 50 µL sample volume was injected directly on the catalyst (680 °C). Detection of the generated $CO_2$ was performed with an infrared detector. Total nitrogen was quantified by a chemiluminescence detector.

### *5.3.3. Optical spectroscopy*

FDOM EEMs were measured using a spectrofluorometer (Aqualog, Horiba) equipped with a charge-coupled device (CCD) detector. Excitation wavelengths were performed

from 240 to 600 nm at 3 nm increments, and emission from 220 to 620 nm (~3.3 nm increments). FDOM EEMs and CDOM absorbance spectra were processed by the *staRdom* package in R studio (version 4.1.2; https://www.r-project.org/) (Pucher et al., 2019). The fluorescence spectra were blank corrected using ultrapure water (Whatman, Milli-Q), inner filter effect correction and Raman normalization by dividing by the Raman peak of ultrapure water at an integrated excitation of 350 nm and an emission between 371 and 428 nm (Raman Units (R.U.); Lawaetz and Stedmon, 2009). After that, the total fluorescence intensity ($FDOM_{total}$) was calculated by the sum of all intensity in EEMs. Subsequently, we applied a PARAFAC analysis (Stedmon et al., 2003; Murphy et al., 2013) to decompose EEMs into different underlying fluorescent components (Figure 2). Based on fluorescence maxima, the components C410, C490 and C425 are often assigned as terrestrial derived humic-like FDOM (Coble, 1996; Gonçalves-Araujo et al., 2016; Paulsen et al., 2019; Zabłocka et al., 2020). C340 and C320 are typically attributed to protein-like FDOM (tryptophan-like for C340 and tyrosine-like for C6; Coble, 1996; Grunert et al., 2021; Paulsen et al., 2019). An additional qualitative measure of CDOM is the specific UV absorbance at 254 nm ($SUVA_{254}$ in L $mg^{-1}$ $m^{-1}$), which was calculated by the UV absorbance at 254 nm (given in $m^{-1}$) divided by the DOC concentration in mg $L^{-1}$ (Weishaar et al., 2003). $SUVA_{254}$ has been previously used as a proxy for aromaticity of aquatic humic substances and is positively correlated with molecular weight (Weishaar et al., 2003). The absorption coefficient at λ nm ($a_{CDOM}(\lambda)$ in $m^{-1}$) was calculated by the following equation:

$$a_{CDOM}(\lambda) = 2.303A(\lambda)/l$$

where the factor 2.303 is the natural logarithm of 10, A(λ) is the absorbance at wavelength λ in nm, and *l* is the optical path length in meters (Stedmon and Markager, 2001). The absorption coefficient $a_{CDOM}(350)$ has been suggested as a proxy for CDOM concentration, and used to estimate the inputs of terrigenous DOM and lignin phenol concentrations in the Arctic (Spencer et al., 2009a; Walker et al., 2013; Fichot et al., 2016).

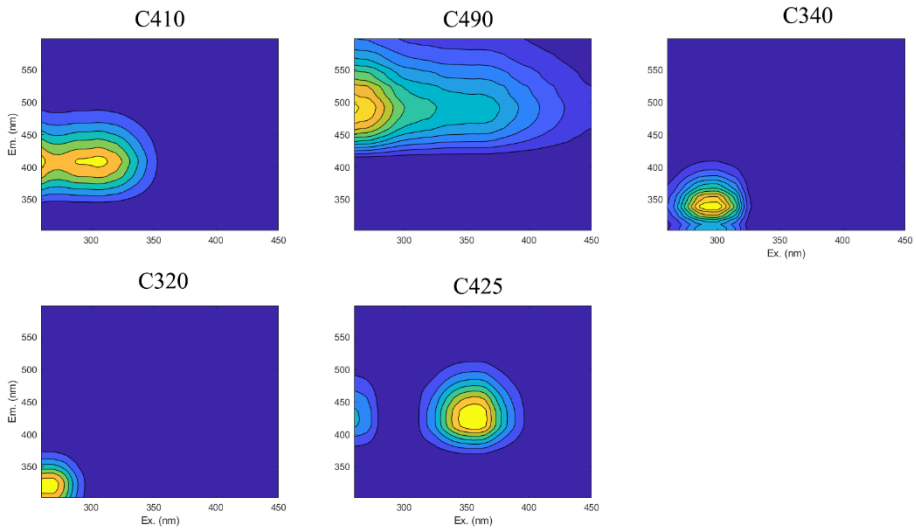


**Figure 2.** Contour plots of the five-component PARAFAC model developed from Fluorescence excitation-emission matrices (EEMs) recorded for all Central Arctic samples.

### *5.3.4. FT-ICR MS measurement hyphenated to UPLC*

**LC-FTMS measurements.** Molecular signatures were analyzed by a 12 T FT-ICR MS (solariX XR, Bruker Daltonics, Billerica, MA) hyphenated with a reversed phase ultra-high performance liquid chromatography (UPLC) system based on a previous method (Han et al., 2021). The chromatographic separation of DOM was carried out using an UPLC system (UltiMate 3000RS, Thermo Fisher Scientific, Waltham, MA USA) equipped with an auto sampler (WPS-3000TRS), column oven (TCC-3000RS), binary pump (HPG-3200RS), and diode array detector (DAD-3000RS). In each analysis, 100 µL of original water was injected and separated according to polarity using a reversed-phase C18 column (ACQUITY UPLC HSS T3, 100 Å, 1.8 µm, 3 × 150 mm, Waters, Milford, MA). Similarly, at the beginning, every 10 samples or at the end, 100 µL of blank (ultrapure water), SRFA standard and pooled samples (mixture of 10 MOSAiC samples) were measured. The compounds (D-glucuronic acid, Vanillic acid, fraxin, isoferulic acid 3-O-ß-D-glucuronide and 2-(4-(2,2-dicarboxy-ethyl)-2,5-dimethoxy-benzyl)-malonic acid; with a concentration range of 40–4700 ng $mL^{-1}$) that we spiked to the SRFA reproducibility control standard, referred to in the paper as model compounds. The mobile phase A and B were ultrapure water ($H_2O$; Milli-Q, Merck, Darmstadt) and methanol (LC-MS

grade, Biosolve), respectively, which were used in a gradient program for the C18 column with a flow rate of 0.2 mL $min^{-1}$ controlled by the first HPLC pump (Table 1). 0.05% formic acid was added to both eluents. A pH of 3 in the aqueous eluent was adjusted by the ammonium hydroxide and the same volume of ammonium hydroxide was added to eluent B. Different from Han et al. (2021), the eluent gradient started at 3.5 min and linearly increased to 100% methanol within 14 min the first HPLC pump. The adjustment of the gradient improved the separation of sea salt that eluted between 8.8 and 13.3 min. A second HPLC pump was applied to be a post column with a counter gradient using the same mobile phases but without buffer addition (Table 2). The time difference between first and second pumps was determined to be 4.5 min. The dead volume of the chromatographic system was determined as 5.3 min via monitoring 210 nm absorption after injection of methanol. The flows (50% ultrapure water and 50% methanol) were combined at the column outlet to ensure a stable solvent condition for further electrospray ionization, and then were split into flows. One was monitoring by DAD (210 nm) in the HPLC system and another was infused into the FT-ICR-MS by electrospray ionization in negative mode (capillary voltage: 4300 V; nebulizer gas pressure: 1.0 bar; dry gas temperature: 200 °C, dry gas flow rate: 3.0 L $min^{-1}$). Ions were accumulated in the hexapole collision cell for 1.6 s prior to being transferred into the ICR cell. Ion accumulation time was set to 1.6 s for each scan. Mass spectra for LC-FTMS measurements were acquired at 4 Mega words in the broadband mode from 147.4 to 1000 m/z.

**Table 1.** Gradient setup of the first pump for C18 column.

| Time (mins) | Ultrapure water (%) | Methanol (%) | Flow rate (mL $min^{-1}$) |
|---|---|---|---|
| 0 | 100 | 0 | 0.2 |
| 3.5 | 100 | 0 | 0.2 |
| 17.5 | 0 | 100 | 0.2 |
| 25.5 | 0 | 100 | 0.2 |
| 28.5 | 0 | 100 | 0.2 |
| 31.5 | 100 | 0 | 0.2 |
| 36.5 | 100 | 0 | 0.2 |
| 41 | 100 | 0 | 0.2 |

**Table 2.** Gradient setup of the second pump for post column.

| Time (mins) | Ultrapure water (%) | Methanol (%) | Flow rate (mL $min^{-1}$) |
|---|---|---|---|
| 0 | 0 | 100 | 0.2 |
| 8 | 0 | 100 | 0.2 |
| 22 | 100 | 0 | 0.2 |
| 30 | 100 | 0 | 0.2 |
| 33 | 100 | 0 | 0.2 |
| 36 | 0 | 100 | 0.2 |
| 41 | 0 | 100 | 0.2 |
| 46.5 | 0 | 100 | 0.2 |

**Data processing.** Due to the dimension of the column and low flow rate, the first methanol from the solvent gradient reached the detector at around 13.3 min. The total ion current (TIC) peaked at 41% methanol (19 min), followed by a drop until 71% methanol (23.3 min). The LC-FTMS data for the first 13.3 min was removed due to the influence of the salt matrix and the LC-FTMS data after 23.3 min was removed due to contaminants. LC-FTMS data was divided into ten retention time segments (one-minute intervals) between 13.3 min and 23.3 min (gray bars; Figure 3). Each retention time segment was internally recalibrated with a list of peaks commonly present in DOM (150–1000 m/z), and the root mean square error was determined with ± 0.4 ppm after calibration. The retention time segment separations and calibration were performed in Compass Data Analysis 5.1 software (Bruker Daltonik GmbH, Germany). Mass peak lists were generated based on a signal to noise ratio of S/N ≥4. Using the open-access software UltraMassExplorer (UME; Leefmann et al., 2019), Molecular formulas (MFs) were assigned to peaks in the mass range of m/z 150–700 with elemental ranges of $C_{1-\infty}H_{1-\infty}O_{0-\infty}N_{0-2}S_{0-1}$ within a mass error of ± 0.5 ppm. Additional filters were applied to the assigned MFs: $0.3 \leq H/C \leq 2.0$ , $0 \leq O/C \leq 1.2$, $0 \leq N/C \leq 1.3$ (Kind and Fiehn, 2007), $H/C \leq 2C + 2 + N$ (“nitrogen-rule”; Koch et al., 2007). The double bond equivalent (DBE) and the number of oxygen atoms (O) were used according to Herzsprung et al., (2014) to further filter the dataset having: $0 <$ DBE $< 25$, $-10 <$ DBE-O $< 10$ (DBE-O: DBE minus O atoms; Herzsprung et al., 2014).

All MFs present in the surfactants (Lechtenfeld et al., 2013) or blank samples were removed from the respective retention time segments. Isotopologue formulas ($^{13}C$) were used to verify the parent formulas for quality control but removed from the final data set. The molecular assignments and filters were performed using R 4.1.2 software (https://www.r-project.org/).

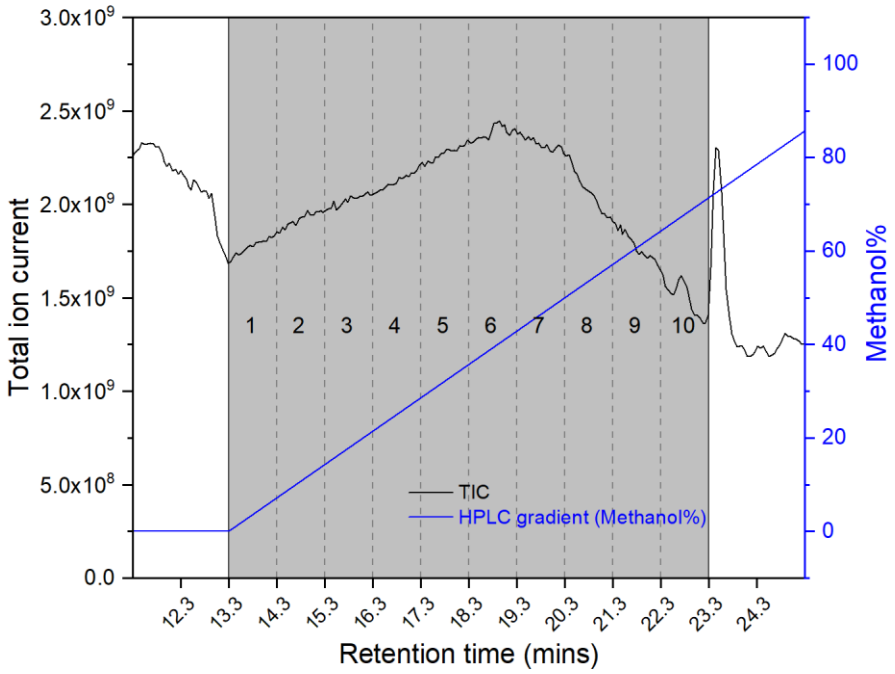


**Figure 3.** Total ion current (TIC) chromatogram from a MOSAiC sample (black curve); and methanol percentage (Methanol%) used in the solvent gradient (blue curve). The selected LC-FT MS data for DOM fingerprints were divided into ten retention time segments (black number) marked by gray bars.

To identify the difference only by the multiples of methylene unit $CH_2$ (i.e., members of $CH_2$ homologous series), the Kendrick mass (KM) for $CH_2$-units (14.000 00 Kendrick mass units) is converted from the measured IUPAC mass scale (14.015 65 Da) by being multiplied by 14.0000/14.01565. The Kendrick mass defect (KMD) is the difference between the nominal IUPAC mass (NM) and KM using the equation: $KMD = NM - KM$ (Hughey et al., 2002; Stenson et al., 2003). The members of a homologous series have the identical KMD (Stenson et al., 2003).

Double bond equivalent (DBE) values (Koch and Dittmar, 2006) were calculated using the equation:

$$DBE = C - \frac{H + N}{2} + 1$$

where C, H and N refer to the number of carbon, hydrogen and nitrogen atoms in a molecular formula (MF), respectively. DBE-O (DBE minus O) indicates the DBE minus O atom (Herzsprung et al., 2014).

The average aromaticity index (AI; Koch and Dittmar, 2006, 2016) was calculated for each samples as:

$$AI = \frac{1 + C - O - S - 0.5(N + P + H)}{C - O - N - S - P}$$

where C, H, N, O and S refer to the peak magnitude weighted average number of carbon, hydrogen, nitrogen, oxygen and sulphur atoms in each sample.

The nominal oxidation state of carbon (NOSC; LaRowe and Van Cappellen, 2011) was calculated as follows:

$$NOSC = 4 - \frac{4C + H - 3N - 2O - 2S}{C}$$

where C, H, N, O and S refer to the number of carbon, hydrogen, nitrogen, oxygen and sulphur atoms in a MF, respectively. The higher NOSC values indicates that molecules are oxidized (LaRowe and Van Cappellen, 2011).

The degradation index $I_{DEG}$ were calculated according to Flerus et al. (2012) as follows:

$$I_{DEG} = \frac{\sum(magnitudesNEG_{Ideg})}{\sum(magnitudesNEG_{Ideg} + magnitudesPOS_{Ideg})}$$

where $magnitudesNEG_{Ideg}$ was raw peak magnitudes of five negative correlating compounds with $\Delta C^{14}$ ($NEG_{Ideg}$: $C_{17}H_{20}O_9$, $C_{19}H_{22}O_{10}$, $C_{20}H_{22}O_{10}$, $C_{20}H_{24}O_{11}$, $C_{21}H_{26}O_{11}$), and $magnitudesPOS_{Ideg}$ was raw peak magnitudes of five positive correlating compounds with $\Delta C^{14}$ ($POS_{Ideg}$: $C_{13}H_{18}O_7$, $C_{14}H_{20}O_7$, $C_{15}H_{22}O_7$, $C_{15}H_{22}O_8$,

$C_{16}H_{24}O_8$). Higher $I_{DEG}$ values generally correspond to a higher degree of degradation (Flerus et al., 2012).

The index $I_{Terr}$ was introduced by the Medeiros et al., (2016). The authors selected 40 MFs from the pool of 184 t-Peaks (indicators of riverine input) with the highest negative correlation with $\delta^{13}C$ values (as terrestrial sources: Terr) and the 40 MFs from the "island of stability" (Lechtenfeld et al., 2014) with the highest positive correlation with $\delta^{13}C$ values (as marine sources: Mar). We modified $I_{Terr}$ by selecting those 10 formulas of $I_{Terr}$ that occurred in a maximum of samples in our database in order to avoid that the ratio is skewed by the absence of some formulas. This resulted in the modified index ($I_{Terr2}$) that calculated as:

$$I_{Terr2} = \frac{\sum(magnitudesTerr2)}{\sum(magnitudesTerr2 + magnitudesMar2)}$$

where Terr2 formulas were: $C_{17}H_{18}O_7$, $C_{18}H_{18}O_7$, $C_{17}H_{16}O_7$, $C_{17}H_{16}O_8$, $C_{15}H_{16}O_6$ and Mar2 formulas were: $C_{20}H_{24}O_9$, $C_{20}H_{24}O_{10}$, $C_{19}H_{22}O_{10}$, $C_{17}H_{21}O_8N_1$, $C_{20}H_{26}O_9$. Higher $I_{terr2}$ values indicate a higher contribution of terrigenous material in the sample (Medeiros et al., 2016).

Intensity weighted average (wa) parameters were abbreviated as $NOSC_{wa}$, $AI_{wa}$, $DBE_{wa}$, $H/C_{wa}$, $O/C_{wa}$, $C/N_{wa}$, $C/S_{wa}$, $N/C_{wa}$, $S/C_{wa}$, and $m/z_{wa}$. The molecular assignments and filters were performed using R (version 4.1.2; https://www.r-project.org/) via the UltraMassExplorer package (Leefmann et al., 2019).

### *5.3.5. Statistical analysis*

From the total set of formulas, we first calculated aggregated formula sets for each sample, by calculating the sum of peak magnitudes for identical formulas that occurred in different retention time segments. For the aggregated sets, we also calculated normalized peak magnitudes to explore qualitative differences between samples. Normalized intensities were calculated based on the summed magnitudes of those formulas that occurred in all aggregated formula sets. The Spearman rank correlation was carried out at the 99% confidence limit ($p<0.01$) between normalized mass peak intensities and terrigenous proxies (salinity and terrestrial humic-like

FDOM C490, C425 and C410) based on 93 samples. The Spearman's r > 0 at the 99% confidence limit were defined significant correlations. Correlations were performed using R 4.1.2 software and the package "corrplot".

## 5.4. Results

### *5.4.1. DOM quantification in original seawater using LC-FTMS*

The summed peak magnitudes for each LC-FTMS run ($int_{sum}$) was significantly correlated with the DOC concentration (R = 0.88; Figure 4a), $a_{CDOM}(350)$ (R = 0.85; Figure 4b), and $FDOM_{total}$ (R= 0.85; Figure 4c), independent of sample type (ocean or lead water samples). For $I_{Terr2}$ and $AI_{wa}$, it significantly correlated with DOC concentration, $FDOM_{total}$ and $SUVA_{254}$ (Figure 4d–i). For ocean water samples, $I_{DEG}$ correlated negatively with DOC concentration (Figure 4j; R = −0.94), $FDOM_{total}$ (Figure 4k; R = −0.90), and $SUVA_{254}$ (Figure 4l; R = −0.92) whereas $C/N_{wa}$ correlated positively with DOC concentration (Figure 4m; R = 0.83), $FDOM_{total}$ (Figure 4n; R = 0.92), and $SUVA_{254}$ (Figure 4o; R = 0.87). In contrast, for the lead water samples with low DOC concentration (< 70 µmol $kg^{-1}$; Figures 4j–o), DOC, $FDOM_{total}$ and $SUVA_{254}$ positively correlated with $I_{DEG}$ at R values of 0.97, 0.92 and 0.86, respectively, but correlated negatively with $C/N_{wa}$ with R values of −0.95, −0.94 and −0.88, respectively. In conclusion, sea ice meltwater showed relatively low $I_{DEG,}$ and $I_{Terr2}$ but high $C/N_{wa}$ compared to seawater.

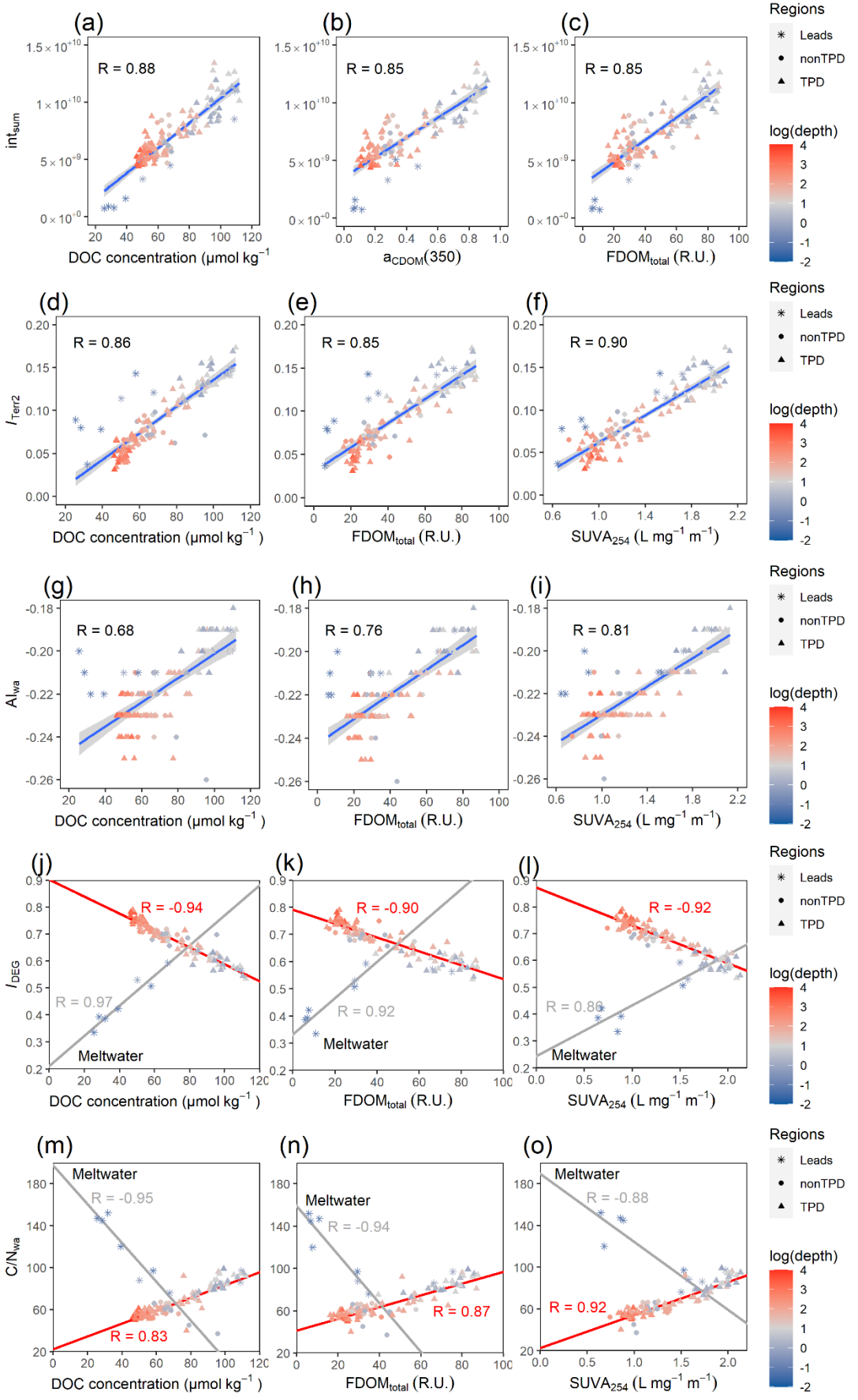
(a)
(b)
(c)
(d)
(e)
(f)
(g)
(h)
(i)
(j)
(k)
(l)
(m)
(n)
(o)
R = 0.88
R = 0.85
R = 0.85
R = 0.86
R = 0.85
R = 0.90
R = 0.68
R = 0.76
R = 0.81
R = -0.94
R = 0.97
R = -0.90
R = 0.92
R = -0.92
R = 0.86
R = -0.95
R = 0.83
R = -0.94
R = 0.87
R = -0.88
R = 0.92
Meltwater
intsum
DOC concentration (μmol kg−1)
aCDOM(350)
FDOMtotal (R.U.)
ITerr2
SUVA254 (L mg−1 m−1)
AIwa
IDEG
C/Nwa
Regions
Leads
nonTPD
TPD
log(depth)

**Figure 4.** Chemical characterization of original water DOM collected from the Central Arctic in lead water samples of the Amundsen Basin (asterisk), and in ocean water samples inside the influence of the transpolar drift (TPD) (triangles; Amundsen Basin, and Fram Strait) and outside the TPD (dots; western Nansen Basin and Yermak Plateau). 1st row: correlation of $int_{sum}$ and (a) DOC concentration, (b) $a_{CDOM}(350)$ and (c) $FDOM_{total}$; 2nd row: correlation of $I_{Terr2}$ and (d) DOC concentration, (e) $FDOM_{total}$ and (f) $SUV_{254}$; 3rd row: correlation of $AI_{wa}$ and (g) DOC concentration, (h) $FDOM_{total}$ and (i) $SUV_{254}$; 4th row: correlation of $I_{DEG}$ and (j) DOC concentration, (k) $FDOM_{total}$ and (l) $SUV_{254}$; 5th row: correlation of $C/N_{wa}$ and (m) DOC concentration, (n) $FDOM_{total}$ and (o) $SUV_{254}$ for all Central Arctic samples (n = 118). log(depth) represents the $log_{10}$-transformed water depth in meters. The blue line indicated the linear regression for all samples. The red line indicated the linear regression for ocean water samples. The gray line indicated the linear regression for lead water samples.

### *5.4.2. Relationship between MFs and terrigenous proxies*

Spearman rank correlations between normalized intensities of MFs and terrigenous proxies were carried out to distinguish groups of MFs associated with different sources. Applying Spearman rank correlations at the 99% confidence limit ($p < 0.01$; Figure 5), MFs (9.2% of total MFs; 35.9% of total intensity for all samples) that were not only significantly positively correlated with terrigenous proxies terrestrial FDOM component C490, C425 and C410, but also significantly negatively correlated with salinity, were categorized as terrestrial-derived peaks (t peaks). MFs, that were the inversely correlated with these terrigenous proxies (9.5% of total MFs; 47.0% of total intensity for all samples), were categorized as marine-derived peaks (m peaks), and the remaining MFs were categorized as non-correlated peaks (n peaks; n = 81.3% of total MFs; 17.0% of total intensity for all samples; Table 3). The numbers of MFs of t, m, and n peaks identified for each terrigenous proxy are displayed in Table 3.

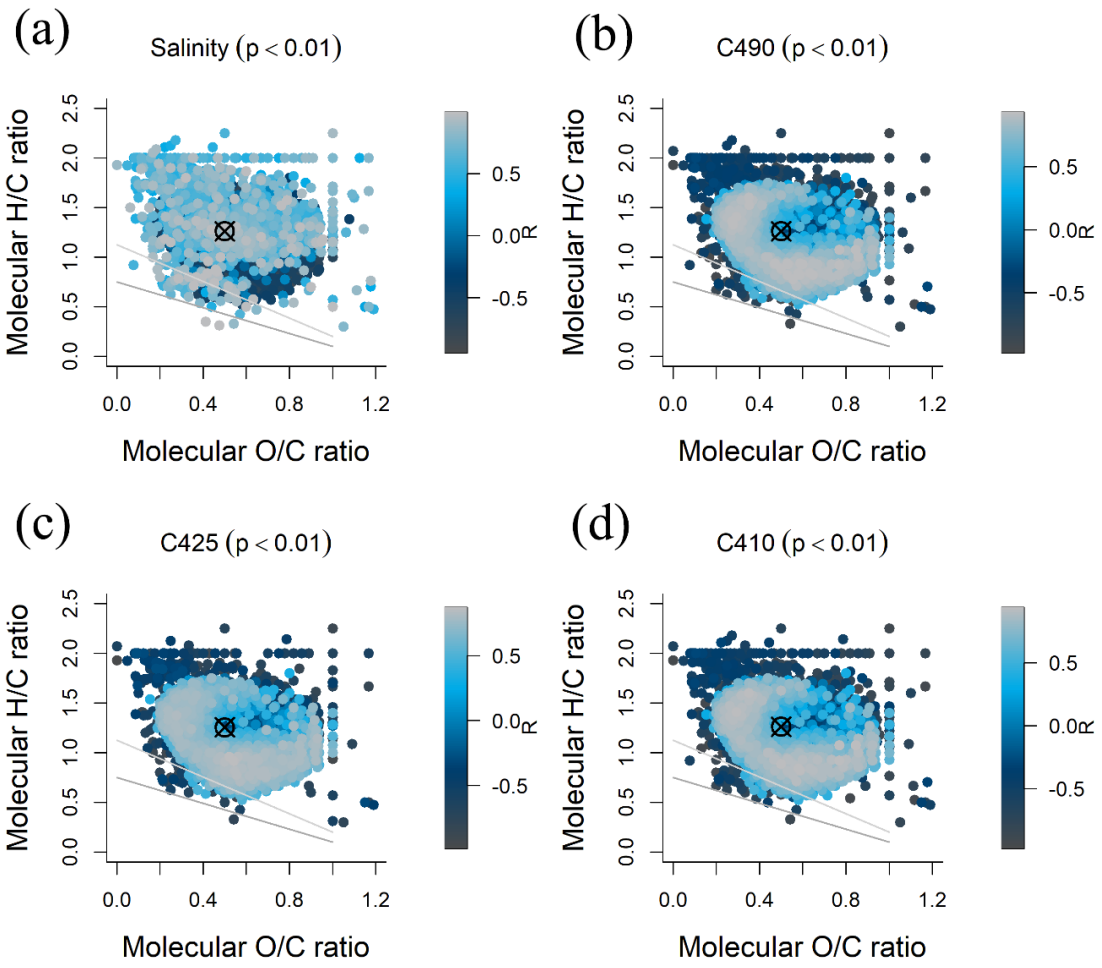


**Figure 5**. Van Krevelen diagrams for MFs that were significantly ($p < 0.01$) correlated with (a) salinity, (b) terrestrial humic-like component C490, (c) C425, (d) and C410. The color scale indicates Spearman correlation coefficient R ($p < 0.01$) between normalized intensities of MFs and terrigenous parameters.

**Table 3.** Numbers of MFs of t, m and n peaks associated with salinity and three terrigenous components derived from PARAFAC analysis.

| Terrigenous proxies | t peaks | m peaks | n peaks |
|---|---|---|---|
| C490 | 1651 | 2256 | 12803 |
| C410 | 1662 | 2249 | 12799 |
| C425 | 1593 | 1843 | 13274 |
| Salinity | 1678 | 2374 | 12658 |
| Unique | 1544 | 1587 | / |

The intensities of t, m, and n peaks were summed up separately for each sample, resulting in three classes of DOM (terrestrially-derived DOM (tDOM), marine DOM (mDOM) and non-correlated DOM (nDOM), respectively). The relative proportions of tDOM, mDOM and nDOM were calculated by the intensities of tDOM, mDOM and nDOM, divided by the $int_{sum}$ in the corresponding sample, referred to as $int_{sum}$%. With increasing water depths, $int_{sum}$% for tDOM decreased, whereas $int_{sum}$% for mDOM increased (Figure 6b). The $int_{sum}$% was higher for tDOM but lower for mDOM in the TPD-influenced regions compared to the regions out of TPD influence (Figure 6b). Based on the good linear correlation between $int_{sum}$ and DOC concentrations and under the assumption that the tDOM, mDOM and nDOM subfractions also correlate with DOC, we calculated the DOC-yield for each fraction by multiplying the DOC concentration by the proportion of each fraction in the corresponding sample. The DOC-yield for tDOM (i.e., terrestrially-derived DOC (tDOC)) and mDOM (i.e., marine DOC (mDOC)) decreased with the increasing water depths, and the mDOC was higher than the tDOC throughout the water column (Figure 6c). In deep water (~2000 m depth), the tDOC accounted for ~26% of $int_{sum}$ equivalent to ~12 μmol $kg^{-1}$ and mDOC accounted for ~57% of $int_{sum}$ equivalent to ~27 μmol $kg^{-1}$. The tDOM formulas were characterized by lower $m/z_{wa}$, $H/C_{wa}$, $N/C_{wa}$, and $S/C_{wa}$ (Figure 6d–f), but higher $AI_{wa}$ (Figure 6a) compared to mDOM.

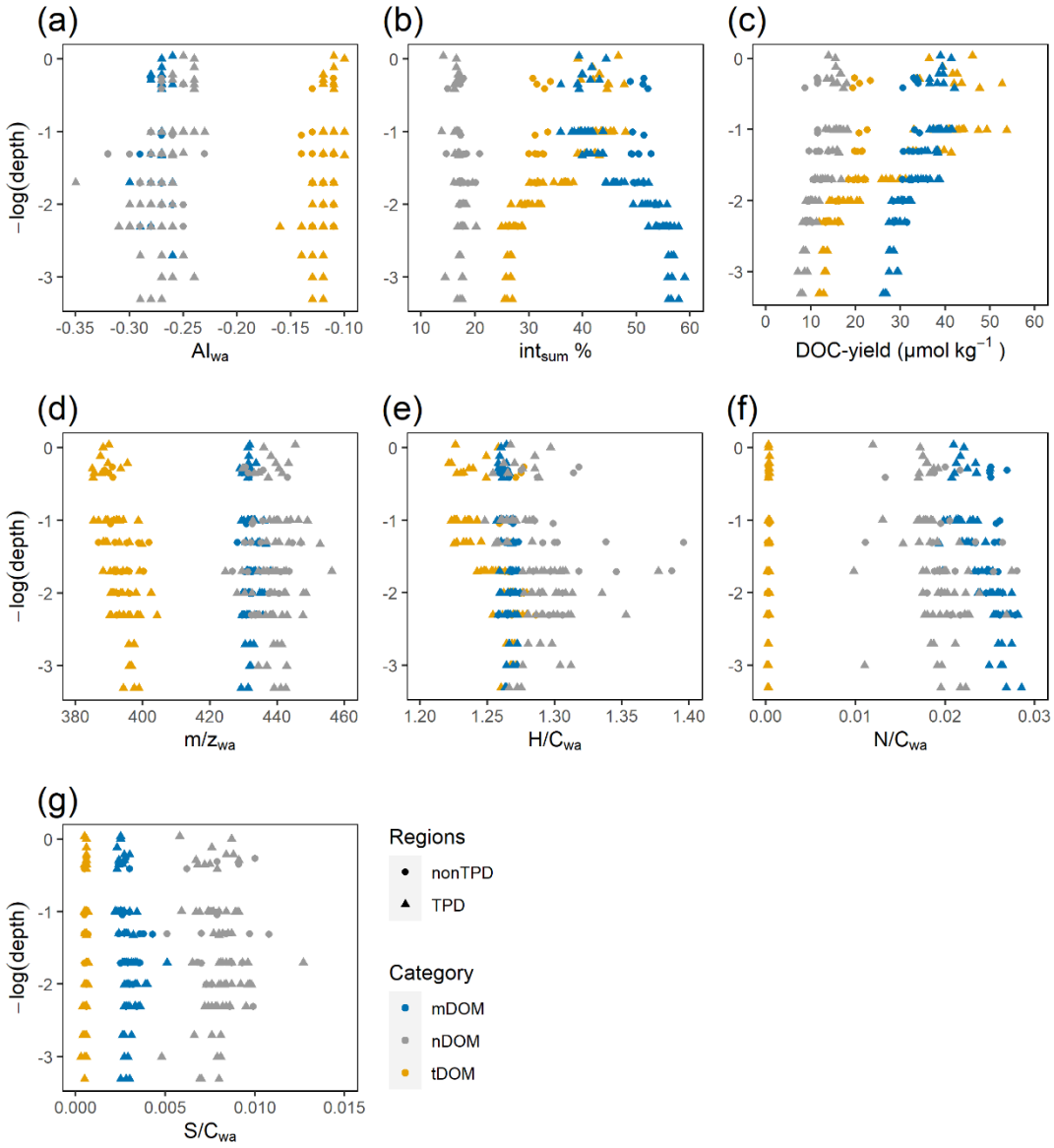


**Figure 6.** Changes in quantity and chemical quality of DOM with water depths inside the influence of the transpolar drift (TPD) (triangles; Amundsen Basin, and Fram Strait) and outside the TPD (dots; western Nansen Basin and Yermak Plateau) and for DOM categories: (a) $AI_{wa}$, (b) the relative contribution of tDOM and mDOM, (c) the corresponding DOC-yield, (d) $m/z_{wa}$, (e) $H/C_{wa}$, (f) $N/C_{wa}$, (g) $S/C_{wa}$, and over the water column for ocean water samples (n = 93). The −log(depth) indicates the negative $\log_{10}$-transformed water depth in meters.

### *5.4.3. Polarity-based separation*

Differences between the retention time segments are described using different mass parameters including summed peak magnitudes in each retention time segment for each LC-FTMS run ($int_{sum, RT}$), $m/z_{wa}$, $DBE_{wa}$, $AI_{wa}$, $H/C_{wa}$, $O/C_{wa}$, $NOSC_{wa}$, $N/C_{wa}$, and $S/C_{wa}$ (Figure 7). During the chromatographic separation, the $int_{sum, RT}$ increased appreciably from retention time segments 1 to 6, and decreased afterwards (Figure 7a). The $DBE_{wa}$, and $m/z_{wa}$ did not change appreciably from retention time segments 1 to 10 (Figure 7b and c). We also observed a continuous increase in $AI_{wa}$ and $H/C_{wa}$ (Figure 7d and e), but a continuous decrease in $O/C_{wa}$ and $NOSC_{wa}$ (Figure 7f and g). For the ease of readability and different from the official definition, we will call hydrophilic molecular formulas with an O/C ratio greater than 0.5 "polar" and more hydrophobic formulas with an O/C ratio <0.5 "nonpolar". Most of the polar formulas could be detected in the first five retention time segments and most of the nonpolar formulas were detected in the last five retention time segments. The $N/C_{wa}$ decreased from retention time segments 1 to 6, and slightly increased afterwards (Figure 7h). The $S/C_{wa}$ showed a decreasing trend except the last two retention time segments (Figure i). In conclusion, and as expected by the solvent gradient, the separation mechanism was related to polarity, independent of DBE, m/z and $int_{sum}$. We also evaluated the "peak width" (i.e., the number of retention time segments in which a MF occurred) and compared it to the peak width of model compounds that we spiked to the SRFA control standard. The average peak width of a MF in all Central Arctic samples was 3.8 min, ranging from 1 to 10 min. This was a considerably wider peak width compared to the model compounds that eluted in a 0.5–1 min retention time window.

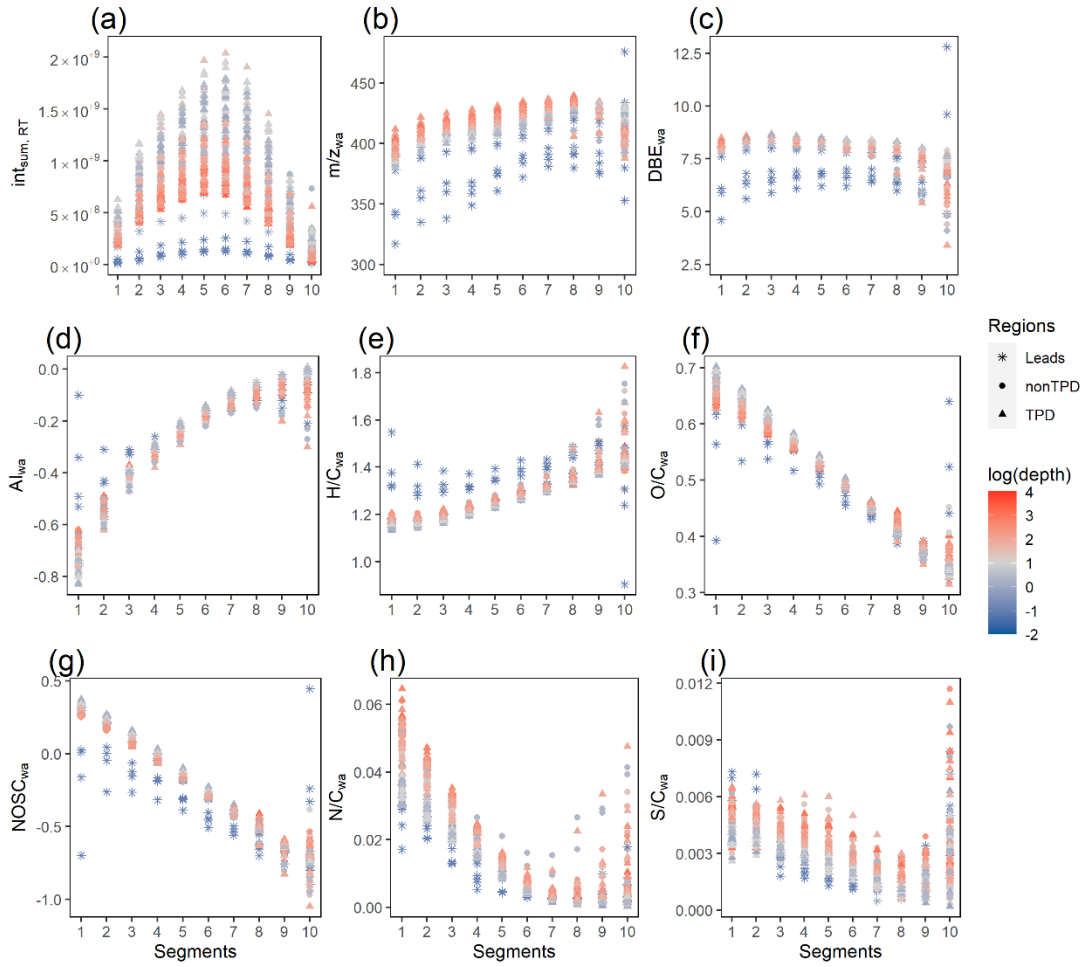


**Figure 7.** The molecular parameters of (a) $int_{sum,\ RT}$, (b) $m/z_{wa}$, (c) $DBE_{wa}$, (d) $AI_{wa}$, (e) $H/C_{wa}$, (f) $O/C_{wa}$, (g) $NOSC_{wa}$, (h) $N/C_{wa}$, and (i) $S/C_{wa}$ from online LC-FTMS measurements for all Central Arctic water samples (n = 118) in lead water samples of the Amundsen Basin (asterisk), and in ocean water samples inside the influence of the transpolar drift (TPD) (triangles; Amundsen Basin, and Fram Strait) and outside the TPD (dots; western Nansen Basin and Yermak Plateau). The log(depth) indicates the $log_{10}$-transformed water depth in meters.

Considering the elution profile of all Central Arctic samples (n = 118; retention time from 13.3–23.3 min for LC-FTMS), we identified a total of 68596 MFs and 18237 unique MFs, with an average of 766 unique MFs in each retention time segment (Table 4). On average, nitrogen and sulfur free MFs (CHO) accounted for 28.6% of all MFs and 78.7% of total mass peak intensity (Table 4). Only nitrogen-containing heteroatom compounds (CHON) accounted for 37.1% of the peaks and 16.2% of total

mass peak intensities. The 6267 MFs containing S (CHOS and CHONS) represented 34.4% of formulas and 5.1% of total mass peak intensity. During the chromatographic separation, there was a continuous increase in the relative contribution of CHO formulas and a decrease in CHON and CHONS formulas (Table 4).

**Table 4.** Summary of MC-FTMS retention time segments: Comparison of the numbers of CHO, CHON, CHOS, and CHONS molecular formulas (MFs) for each retention time segment, numbers of unique MFs (Unique MFs) for each retention time segment, the proportion of number of each heteroatom compound accounting for total number of MFs (CHO (%), CHON (%), CHOS (%) and CHONS (%)), weighted averaged m/z ($m/z_{wa}$), and relative contribution of the summed peak magnitudes in each retention time segment to the summed peak magnitudes (Intensity (%)) magnitudes for all samples (n = 118).

| Segments | MFs | Unique MFs | CHO (%) | CHON (%) | CHOS (%) | CHONS (%) | $m/z_{wa}$ | Intensity (%) |
|---|---|---|---|---|---|---|---|---|
| 1 | 5883 | 1130 | 31.3 | 36.6 | 14.3 | 17.8 | 395.1 | 4.4 |
| 2 | 6949 | 779 | 32.1 | 35.7 | 14.6 | 17.6 | 407.2 | 9.1 |
| 3 | 7333 | 633 | 34.0 | 35.0 | 15.0 | 16.0 | 412.0 | 11.7 |
| 4 | 7605 | 546 | 36.0 | 34.7 | 15.2 | 14.2 | 414.0 | 13.5 |
| 5 | 7715 | 528 | 37.3 | 35.4 | 15.0 | 12.3 | 417.9 | 15.1 |
| 6 | 7625 | 541 | 40.1 | 35.2 | 14.7 | 9.9 | 423.0 | 15.4 |
| 7 | 7378 | 614 | 42.4 | 34.4 | 14.6 | 8.6 | 427.1 | 13.6 |
| 8 | 6940 | 684 | 44.7 | 33.6 | 14.3 | 7.3 | 430.0 | 9.8 |
| 9 | 6123 | 876 | 47.1 | 31.5 | 14.4 | 7.0 | 428.0 | 5.6 |
| 10 | 5018 | 1332 | 46.6 | 30.1 | 13.5 | 9.9 | 415.6 | 1.8 |

To further identify and illustrate compositional differences in different retention times, a van Krevelen diagram (Kim et al., 2003) was displayed for all retention time segments and all samples (Figure 8a). We observed a remarkable separation of the retention time segments 1–5 and 6–10 for polar and nonpolar MFs (divided at an O/C of ~0.5). To further discriminate MFs according to their masses, the Kendrick mass defect (Hughey et al., 2002; Stenson et al., 2003) was plotted for all retention time

segments (Figure 8b). All MFs, which only differed in the number of $CH_2$ groups, have an identical KMD and thus can be regarded as "pseudo" homologous series. The same homologous series in the Kendrick mass defect revealed a gradually shift to the right from early to late retention time segments (Figure 8b). Additionally, nonpolar segments (6–10) were shifted towards lower Kendrick mass defects compared to early retention time segments (1–5). As a consequence of this gradual change in the molecular composition with retention time and the presence of structural isomers, MFs were spread over several adjacent retention time segments (average peak width = 3.8 min).

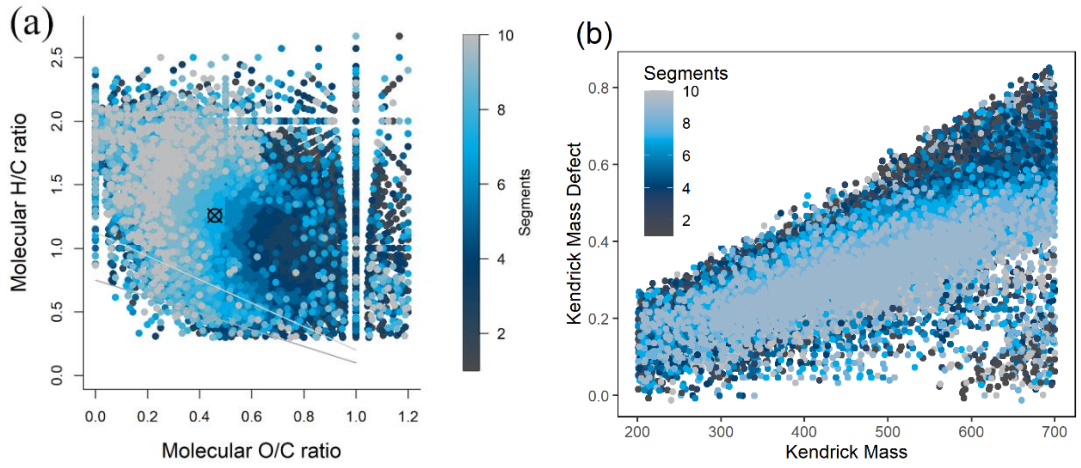


**Figure 8**. The van Krevelen diagram (a), and Kendrick mass defect (KMD) plot (b) for all ten retention time segments (color scale) for all Central Arctic samples (n = 118).

Based on the LC-FTMS information, we compared chemical differences in DOM derived from different Arctic regions. The $int_{sum,\ RT}$ and $C/N_{wa}$ showed a decreasing trend with increasing depth. Based on $C/N_{wa}$, samples from Amundsen Basin and Fram Strait showed an overall higher terrestrial contribution compared to the western Nansen Basin and Yermak Plateau in the upper 200 m (Figure 9).

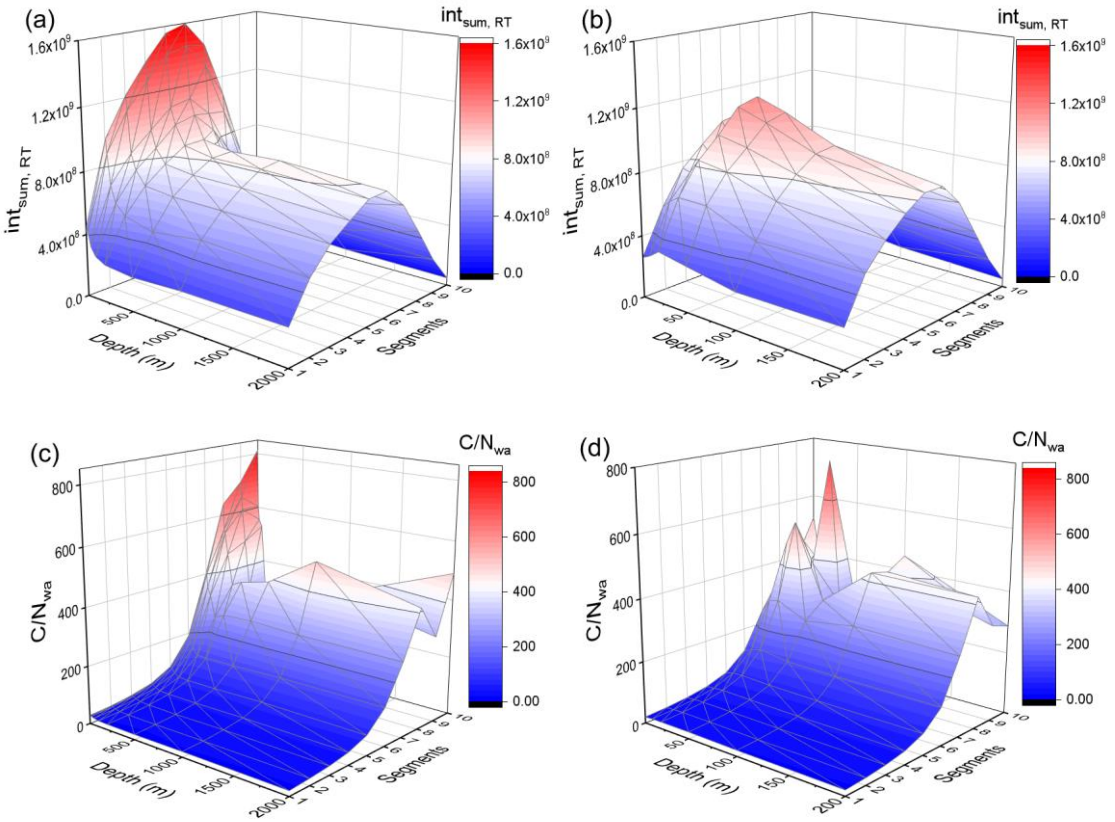


**Figure 9.** Changes in summed peak magnitudes in each retention time segment for each LC-FTMS run ($int_{sum,\ RT}$; top panels), and $C/N_{wa}$ (lower panels) based on different retention time segments in Amundsen Basin and Fram Strait (~2 m to ~2000 m; left panels), and western Nansen Basin and Yermak Plateau (~2m to ~200 m; right panels) at water depths (n = 109).

## 5.5. Discussion

### *5.5.1. DOM quantification in the Central Arctic*

Two major chemical fractionation effects so far challenged the representative and quantitative characterization of DOM: (i) desalting and pre-concentration via SPE (cf. Kong et al., 2021) and (ii) selective ionization of molecules in the ionization process of the mass spectrometer (Kiontke et al., 2016). With our new method, we were able to measure original seawater at concentrations as low as 26 µmol DOC $kg^{-1}$ and eliminate fractionation effects introduced by SPE. We found that the summed peak magnitudes for each sample ($int_{sum}$) correlated extraordinarily well with DOC concentration of a sample (Figure 4a). This was despite the fact that some highly polar compounds were hidden in the neglected part of the chromatogram in which the sea salt eluted (retention time between 8.8–13.3 min). However, it has been previously reported that the number of detected highly polar MFs were much higher for LC-FTMS measurement as compared to DI analyses (Han et al., 2021). Of course, an ideal ionization source for the quantitative characterization of DOM by FT-ICR-MS should be non-selective (Mopper et al., 2007). However, molecules with e.g. varying basicity, polarity, volatility and molecular size vary in their ionization efficiencies on ESI-MS response (Oss et al., 2010; Kiontke et al., 2016). Therefore, without a full separation and structure elucidation, a traditional calibration with known standards is impossible. The ionization efficiency for analytes is affected by the ionic contaminants (matrix effects) or multiple analytes (ionization suppression; Tang et al., 2004; Ghosh et al., 2012). The LC method applied, prevents additional solvent matrix-related ionization changes by using a counter gradient that creates constant solvent conditions (50% ultrapure water and 50% methanol) and minimizes matrix effects. DI-ESI analysis suffers from vast structural complexity of DOM, thus compounds with the same chemical formula but different chemical structures overlap in the mass spectrum. The ionization of the lower efficiency compound is suppressed by the higher efficiency compounds (Tang et al., 2004; Ohno et al., 2016). The ionization of high m/z compounds is suppressed due to the presence of low m/z compounds (Reemtsma and These, 2003; Rowland et al., 2014). HPLC separation prior to ionization can reduce DOM complexity and ion suppression effects to a certain degree, and lead to a

separation of isomeric compounds, thereby increasing the number of compounds detected and improving quantification. The LC method also has the advantage that sulfur and nitrogen-containing MFs are better represented in LC-FTMS compared to DI measurements, especially for terrestrial samples with low nitrogen content (Han et al., 2021). Due to the large terrestrial contribution of terrestrial organic matter in the Arctic Ocean via the Arctic rivers (e.g., Hansell et al., 2004), we observed significant correlations between indicators derived by mass spectrometry ($I_{Terr2}$, $I_{DEG}$, $AI_{wa}$ and $C/N_{wa}$) and parameters such as DOC concentration, $FDOM_{total}$ and $SUVA_{254}$ (Figure 4). This is in agreement with previous studies demonstrating that the Amundsen Basin and Fram Strait are influenced by high loads of terrestrial DOM from the Laptev Sea and the East Siberian Sea into the Central Arctic (Stedmon et al., 2011; Charette et al., 2020). It has been shown that in addition to the solution basicity of compounds, the polarity and vaporability of compounds have important effects on the ionization efficiency under acidic solvent conditions (Kiontke et al., 2016). We found that the summed peak magnitudes for each retention time segment (i.e., polarity) in each sample ($int_{sum, RT}$) significantly correlated with DOC concentration and terrestrial humic-like components. Thus, we assumed that MFs correlating with terrestrial proxies show a similar ionization as the average molecular formula. If this assumption is true, we can estimate their quantitative contribution to bulk DOC concentration.

### *5.5.2. Identification and quantification of DOM subfractions in the Central Arctic*

The analysis of lead water samples and the correlation of FTMS-derived peak-magnitudes with salinity and parameters derived from optical analyses identified characteristic MFs representing three DOM end-members for different organic matter sources: (i) DOM from sea ice meltwater, most likely containing a large fraction of labile fresh material due to production of sea ice algae (Thomas et al., 2010), (ii) tDOM that was mainly transported from Arctic rivers to the Central Arctic, originating from decomposition and leaching of plant materials and soil organic matter (Raymond et al., 2007), (iii) mDOM, originating from processes such as the extracellular release by phytoplankton (Lancelot, 1979; Lignell, 1990; Marañón et al., 2005), release by zooplankton grazing (excretion, sloppy feeding, egestion, and dissolution of fecal material; Strom et al., 1997), cell lysis from viral infection (Proctor and Fuhrman,

1990) and solubilization of particles (mostly from detritus or marine snow; Smith et al., 1992, 1995).

With increasing DOC concentration and salinity, we observed an increase in $I_{DEG}$, $I_{Terr2}$ and $AI_{wa}$, but a decrease of $C/N_{wa}$ for lead water samples (Figure 4), suggesting a dilution of tDOM by sea ice meltwater. In addition, lead water samples with low salinity and low DOC concentration showed lower $O/C_{wa}$ and $NOSC_{wa}$ but higher $H/C_{wa}$ than ocean water samples. In summary, sea ice meltwater was predominated by N-depleted, saturated, low oxidized and low degraded DOM during August and September in the Amundsen Basin. In a previous study, we also found relatively high proportions of freshly produced DOM in low-salinity lead water using fluorescence detection (Kong et al., submitted). Other previous studies have also shown that fresh algal-derived DOM from sea ice meltwater is bioavailable, and substantial DOM depletion in the sea ice is due to a loss of combined neutral sugars and amino acids (Kähler et al., 1997; Amon et al., 2001; Jørgensen et al., 2015). Sea ice meltwater is dominated by a large fraction of labile organic matter since the melting of sea ice could lead to lysis of cells and consequently to a release of fresh DOM (Thomas et al., 2010). This is consistent with our observation of a predominance of N-depleted, low oxidized and low degraded DOM in the meltwater.

Based on the Spearman rank correlations between normalized intensities of MFs and four terrigenous proxies (Figure 5), MFs representing tDOM and mDOM were identified (Figure 6). The tDOC in the surface water (i.e., upper 20 m) in the TPD-influenced regions was 49% higher compared to the regions outside of the TPD influence. This is consistent with our CDOM observation (Kong et al., submitted) that the surface mixed layer (SML) in the TPD-influenced regions was largely characterized by a high contribution of terrestrially-derived CDOM compared to the western Nansen Basin and Yermak Plateau. In addition, the tDOM showed lower $H/C_{wa}$, but higher $AI_{wa}$ compared to mDOM (Figure 6a, e). $AI_{wa}$ correlated well with $SUVA_{254}$ (Figure 4i), thus, the $AI_{wa}$ value was a lot higher and in conjunction with the relatively lower $H/C_{wa}$ in tDOM compared to mDOM, which was indicative of the much more unsaturated and aromatic nature of tDOM. We also found t peaks that showed higher O/C and lower H/C ratios (Figure 5). This is consistent with results for

DOM derived from plant and soil organic matter, that typically shows a higher aromaticity than marine DOM (Weishaar et al., 2003; Koch et al., 2005). In addition, the tDOM showed higher $C/N_{wa}$ compared to mDOM (Figure 6f), consistent with many previous studies that highlighted higher C/N ratios in terrestrial compared to marine DOM (Hopkinson et al., 1997; Amon and Meon, 2004). C/N ratios in DOM in the Arctic rivers typically reach values around 40 (Lara et al., 1998; Lobbes et al., 2000; Holmes et al., 2012) compared to marine DOM with C/N values of about 20 (Hopkinson et al., 1997; Benner et al., 2005).

Although the bulk DOC concentration decreased with water depth, the relative contribution of mDOM increased in the Central Arctic (Figure 6b, c). Apart from a decreasing contribution of terrestrial organic matter, in terms of volume, approximately 70% of the prokaryotic oceanic biomass is situated below a depth of 200 m, and decreases exponentially from ~10 m to ~5000 m in all oceanic basins (Herndl et al., 2023). DOM is mostly derived from processes such as extracellular release and leachate of algae and bacteria. Most labile DOM is consumed and respired rapidly by heterotrophic bacteria into DIC, and a small fraction of that DOM escapes rapid remineralization and eventually is exported to greater depths by the thermohaline circulation (Hansell et al., 2009). mDOM in our study showed higher $S/C_{wa}$ compared to tDOM (Figure 6g). It is well known that dimethylsulfoniopropionate (DMSP) is an important labile component of the marine dissolved organic sulfur (DOS) pool that is produced by the phytoplankton and heterotrophic bacteria (McParland and Levine, 2019). The estimated minimum global inventory of marine DOS is 6.7 Pg (1 Pg = $10^{15}$ g) of sulfur based on stoichiometric estimates (Ksionzek et al., 2016). In addition, sulfur-driven chemolithoautotrophy is prevalent in the oxygenated deep ocean (Swan et al., 2011).

Furthermore, tDOM formulas showed lower $m/z_{wa}$ (i.e., lower molecular weight) compared to mDOM (Figure 6d). A size-reactivity continuum model proposed by Amon and Benner, (1994, 1996) suggests that the bioreactivity of organic matter decreases continuously with the size from larger to smaller. Several studies showed a largely conservative mixing of terrigenous DOM along a salinity gradient across the Arctic shelves, suggesting a relatively refractory character of terrestrial DOM (Guay et

al., 1999; Kattner et al., 1999; Dittmar and Kattner, 2003; Kohler et al., 2003; Hölemann et al., 2021). The phytoplankton-derived DOM is more abundant in the higher molecular weight fractions whereas tDOM is dominated the lower molecular weight fraction in the Arctic Ocean (Amon and Meon, 2004). However, Cooper et al. (2005) estimated that ~30% of tDOC is initially removed over the shelves before entering the Eurasian Arctic. Kaiser et al. (2017) showed ~50% of the annual discharge of tDOC from Siberian rivers is mineralized on the Eurasian shelves. Holmes et al. (2008) pointed out that the degree of bioavailability of terrestrial DOC transported by Alaska rivers to the Arctic Ocean has large seasonal variation. 20–40% of the tDOM during the spring freshet in Alaskan rivers is labile on the timescale of months, while tDOM is more resistant to degradation during summer periods. Raymond et al. (2007) showed that the radiocarbon age of terrestrial DOC transported during spring floods is young and likely consists of recently fixed carbon in leaf litter and soil, with about 50% being 1–5 years old and about 35% being 6–20 years old. River runoff has an average residence time of 3.5 ± 2.0 years on the Eurasian shelves before passing offshore to join the TPD (Schlosser et al., 1994). The subsequent transport time from Eurasian shelves to reach the Fram Strait is about three years (Jahn et al., 2010). Hence, the most labile tDOM may be removed on the Eurasian shelves before being transported to the Central Arctic. The analysis of stable carbon isotopes indicate that 25–33% of the terrestrial DOC discharged by rivers to the Arctic Ocean is exported to the North Atlantic via the East Greenland Current (Benner et al., 2005), or 20%–50% as estimated using DOM fluorescence (Amon et al., 2003), or 12%–41% as estimated using the lignin content (Opsahl et al., 1999). Therefore, after the removal of the most labile tDOM fraction on the continental shelves, the remainder of tDOM can be removed on longer timescales within the Arctic Ocean due to microbial or photochemical mineralization processes (Hansell et al., 2004). Kuliński et al. (2016) showed that the higher contribution of refectory fraction in tDOM compared to that in mDOM based an incubation experiment of 188 days. In addition, it is reported that up to 30% of the deep DOC reservoirs is modern ($\delta^{14}C \geq -50‰$; Follett et al., 2014), thus, the mixture of the “modern” and “old” mDOM may result in higher average molecular weight than tDOM. We also observed that the relative contribution of tDOM and tDOC concentration decreased with increasing water depth

in the Central Arctic (Figure 6b, c). The terrigenous DOC is estimated to be mineralized with a half-life of 7.1 ± 3.2 years in the western Arctic Ocean (Hansell et al., 2004). Letscher et al. (2011) suggested that the relatively labile tDOC is removed over the Eurasian shelves in <5 years, and more refractory tDOC is removed over longer timescales in the halocline and deep waters. This is in line with our observation that changes in tDOC concentration in polar surface waters were relatively high, while changes in tDOC concentration in deep water were relatively low (Figure 6c).

Up to 26% (or 12 μmol $kg^{-1}$) of deep DOC (~2000 m depth) in the Eurasian Basin water was derived from terrestrial sources based on the identified t peaks (Table 3 and Figure 6 b, c). It is reported that 30% of deep DOC in Canada Basin could be terrestrially derived based on carbon isotope data suggesting that significant quantities of tDOM can be transported to deep Arctic, presumably from terrestrial POC sources (Griffith et al., 2012). It should be emphasized that each MF can cover a large number of structural isomers. During the chromatographic separation, we observed continuous increases in $AI_{wa}$, $H/C_{wa}$, $O/C_{wa}$ and $NOSC_{wa}$ (Figure 7d–g). This is not unexpected because oxygen-rich and unsaturated compounds elute first, in the part of the solvent gradient with greater polarity. In addition, the same homologous series in the Kendrick mass defect indicated a gradually shift to the right from early to late retention time (Figure 8b). The average peak width of a MF in all samples was 3.8 min and ranged from 1 to 10 min. In comparison, the model compounds that we spiked to the SRFA controls showed elution times of 0.5–1 min. Hence, each MF that had peak widths of more than two minutes represented different isomers. 81.3% of all MFs, accounting for an average of 17% of the total intensity for all samples, were not correlated with terrigenous proxies. On the one hand, there may be substantial specific MFs in the single sample due to the complexity and heterogeneity of DOM. On the other hand, the different DOM isomers exist in different sources of DOM (marine versus terrestrial) which may bias the correlation with terrigenous proxies. These nDOM formulas represented properties that were more similar to mDOM than to tDOM (Figure 6). The relationship between DOC and salinity is commonly used to study the mixing of different end members across the estuaries and ocean margins and to calculate DOC end-member concentrations (Amon et al., 2003; Dittmar and Kattner, 2003; Hansell et al., 2004). In the same way, a plot of $int_{sum}$% for tDOM versus DOC

(Figure 10) provided insights on the relationship between bulk DOC concentration and the relative proportions of tDOM, which demonstrated linear mixing between terrestrial, high-DOC water and marine, low-DOC water.

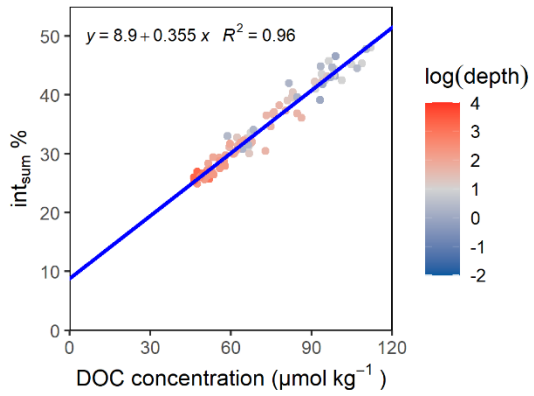


**Figure 10**. Linear regression between DOC concentration and $int_{sum}$% for tDOM formulas. The log(depth) indicates the log-transformed depth based on 10.

The assignment of tDOM MFs is biased by the fact that many of the tDOM formulas are also present in mDOM but do not contribute much to the magnitude-based correlation. The zero-DOC intercept of the y-axis (i.e., 8.9%) indicated the relative proportion of these mDOM MFs (i.e., marine end member). We can subtract this value to correct the tDOM contribution and estimate that 17% (or 8 μmol $kg^{-1}$) of the deep DOC (~2000 m depth) in the eastern Arctic was derived from terrestrial sources. If we perform a similar regression between $FDOM_{total}$ versus $int_{sum}$% for tDOM, the zero-$FDOM_{total}$ intercept of the y-axis was 21%, thus, the terrestrial FDOM contribution could be estimated as ~5% of the DOC in the deep water (~2,000 m depth). If we use tDOC concentration in the deep ocean as the average tDOC concentration and assume that tDOC in the eastern Arctic was are representative for the entire Arctic, we can roughly calculate the total tDOC inventory in the Arctic by multiplying the tDOC concentration by the volume of the entire Arctic, eventually got a tDOC inventory of value of ~1–2 Pg C. Of course, this approach could be applied to the western Arctic in the future, allowing for a more accurate estimate of tDOC inventory in the Arctic. In conclusion, quantification of DOM can be achieved by FT-LC MS, which can improve our mechanistic understanding of the origin of DOM, further possibly involving its formation, transport and transformation processes, and its contribution to the cycle of marine elements.

# 6. Conclusions and perspective

In this thesis, we found that chemical fractionation during SPE is caused by the adsorption mechanism shifting from DOM-PPL physisorption to increased DOM self-assembly. DOM self-assembly during the SPE can decrease carbon extraction efficiency, increase DOM molecular weight through non-covalent bonds, and alter molecular composition and optical properties. The study suggested that PPL preferentially extracts relatively nonpolar and terrestrial-derived, while self-assembly may increase the relative recovery of polar and microbially derived compounds. Moreover, the targeted quantification of single compounds extracted from SPE in aquatic water samples can be affected by the loading-dependent chemical fractionation induced by the unequal contributions of PPL physisorption and DOM self-assembly. The relative DOC loading weight on the column ($DOC_{load}$) is recommended to facilitate comparisons between SPE with different sorbents, sample concentrations and volumes. If samples with similar origins but very different organic carbon concentrations are analyzed to compare molecular properties, it is crucial to keep $DOC_{load}$ similar to minimize variances. This can be achieved by coordinating $DOC_{load}$ by measuring the DOC concentration first and adjusting the loading volume accordingly to keep the $DOC_{load}$ similar for all samples. If the SPE procedure is performed in the field, DOC concentration can be estimated by the fluorescence or absorption, which has been widely preformed in situ for original water measurement. The comparison between DOM samples from different sources may be affected by different adsorption affinity to the sorbent and self-assembly. In addition, the online fluorescence monitoring of the permeate is a simple and alternately way to track the chemical change during the SPE. Online fluorescence modeling enables to assess the degree of variability as a function of $DOC_{load}$, optimizes the $DOC_{load}$ for SPE procedure and allows more reliable interpretations of SPE-based analytical DOM data.

The seasonal and spatial variability of terrestrial and autochthonous DOM in the CAO during the MOSAiC was estimated by CDOM and FDOM data. Significant spatial differences were observed in the surface waters due to the varying influence of the TPD, with seasonal changes slightly modifying spatial patterns. Regions largely affected by tDOM were Amundsen Basin and Fram Strait, whereas the western

Nansen Basin and Yermak Plateau were dominated by the autochthonous CDOM. Although EEMs data can be decomposed into different individual fluorescent components, it is not suitable for estimating the relative contribution of each component because different fluorophores may have different abilities to absorb incident radiation and convert it to fluorescence.

To overcome chemical fractionation effects via SPE, we applied a new LC-FTMS method for DOM characterization that does not require SPE anymore. The technique provided major advantages for the field of DOM research: (i) highly sensitive to acquire mass spectra for samples with DOC concentrations as low as 26 µmol $kg^{-1}$ DOC, (ii) quantitative representation of bulk DOC concentration, (iii) quantification of sub-fractions of DOM (e.g. terrestrial contribution), (iv) enabling direct comparison to techniques that also can be applied for original water, and (v) separation of DOM into 10 different polarity fraction supporting structure elucidation and reducing the ionization suppression effects. Although the new technique avoids chemical fractionation induced by SPE, the neglected part of the chromatogram eluted by sea salt still hides some highly polar compounds that are not detected. Nevertheless, higher numbers of highly polar DOM MFs and higher numbers of heteroatoms of MFs were detected by LC-FTMS as compared to DI analyses (Han et al., 2021). Our estimates on the marine and terrestrial DOC proportion were based on the assumption that the respective MFs show a similar ionization behavior as the average molecular formula. It is still important studying how reliable a quantification of sub-fractions is and if this concept can be applied to other quantitative estimates in the future. The new approach also proved the existence of structural isomers. It is important to investigate the relationship between isomeric DOM compounds and DOM sources in the future. Also, it would be interesting to use other terrestrial proxies, such as $\delta^{13}C$, to isolate MFs into different sources and compare them with the current results.

This study provides a guideline and molecular formula targets that are suitable to be isolated in chromatographic sub-fractions. Isolated fractions can be analyzed with additional analytical techniques such as NMR, which help to make progress in the field of true structure elucidation. This would help immensely to improve our mechanistic and quantitative understanding on how DOM in the CAO is formed, transported and transformed and how it contributes to marine element cycles.

## 7. References


Aferni, A. E., Guettari, M., and Tajouri, T. (2021). Mathematical model of Boltzmann's sigmoidal equation applicable to the spreading of the coronavirus (Covid-19) waves. *Environ. Sci. Pollut. Res.* 28, 40400–40408. doi: 10.1007/s11356-020-11188-y.

Amon, R. M. W., and Benner, R. (1994). Rapid cycling of high-molecular-weight dissolved organic matter in the ocean. *Nature* 369, 549–552. doi: 10.1038/369549a0.

Amon, R. M. W., and Benner, R. (1996). Bacterial utilization of different size classes of dissolved organic matter. *Limnol. Oceanogr.* 41, 41–51. doi: 10.4319/lo.1996.41.1.0041.

Amon, R. M. W., Budéus, G., and Meon, B. (2003). Dissolved organic carbon distribution and origin in the Nordic Seas: Exchanges with the Arctic Ocean and the North Atlantic. *J. Geophys. Res.* 108, 3221. doi: 10.1029/2002JC001594.

Amon, R. M. W., Fitznar, H.-P., and Benner, R. (2001). Linkages among the bioreactivity, chemical composition, and diagenetic state of marine dissolved organic matter. *Limnol. Oceanogr.* 46, 287–297. doi: 10.4319/lo.2001.46.2.0287.

Amon, R. M. W., and Meon, B. (2004). The biogeochemistry of dissolved organic matter and nutrients in two large Arctic estuaries and potential implications for our understanding of the Arctic Ocean system. *Mar. Chem.* 92, 311–330. doi: 10.1016/j.marchem.2004.06.034.

Amon, R. M. W., Rinehart, A. J., Duan, S., Louchouarn, P., Prokushkin, A., Guggenberger, G., et al. (2012). Dissolved organic matter sources in large Arctic rivers. *Geochim. Cosmochim. Acta* 94, 217–237. doi: 10.1016/j.gca.2012.07.015.

Anderson, L. A. (1995). On the hydrogen and oxygen content of marine phytoplankton. *Deep Sea Res. Part I Oceanogr. Res. Pap.* 42, 1675–1680. doi: 10.1016/0967-0637(95)00072-E.

Anderson, L. G., and Amon, R. M. W. (2015). "DOM in the Arctic Ocean," in *Biogeochemistry of Marine Dissolved Organic Matter* (Elsevier), 609–633. doi: 10.1016/B978-0-12-405940-5.00014-5.

Arakawa, N., Aluwihare, L. I., Simpson, A. J., Soong, R., Stephens, B. M., and Lane-

Coplen, D. (2017). Carotenoids are the likely precursor of a significant fraction of marine dissolved organic matter. *Sci. Adv.* 3, e1602976. doi: 10.1126/sciadv.1602976.

Arrigo, K., and Brown, C. (1996). Impact of chromophoric dissolved organic matter on UV inhibition of primary productivity in the sea. *Mar. Ecol. Prog. Ser.* 140, 207–216. doi: 10.3354/meps140207.

Asmala, E., Bowers, D. G., Autio, R., Kaartokallio, H., and Thomas, D. N. (2014). Qualitative changes of riverine dissolved organic matter at low salinities due to flocculation. *J. Geophys. Res. Biogeosciences* 119, 1919–1933. doi: 10.1002/2014JG002722.

Azam, F., Fenchel, T., Field, J., Gray, J., Meyer-Reil, L., and Thingstad, F. (1983). The Ecological Role of Water-Column Microbes in the Sea. *Mar. Ecol. Prog. Ser.* 10, 257–263. doi: 10.3354/meps010257.

Baghoth, S. A., Sharma, S. K., and Amy, G. L. (2011). Tracking natural organic matter (NOM) in a drinking water treatment plant using fluorescence excitation–emission matrices and PARAFAC. *Water Res.* 45, 797–809. doi: 10.1016/j.watres.2010.09.005.

Baker, A., and Spencer, R. G. M. (2004). Characterization of dissolved organic matter from source to sea using fluorescence and absorbance spectroscopy. *Sci. Total Environ.* 333, 217–232. doi: 10.1016/j.scitotenv.2004.04.013.

Baltar, F., Alvarez-Salgado, X. A., Arístegui, J., Benner, R., Hansell, D. A., Herndl, G. J., et al. (2021). What Is Refractory Organic Matter in the Ocean? *Front. Mar. Sci.* 8, 642637. doi: 10.3389/fmars.2021.642637.

Bates, N. R., and Mathis, J. T. (2009). The Arctic Ocean marine carbon cycle: evaluation of air-sea CO2 exchanges, ocean acidification impacts and potential feedbacks. *Biogeosciences* 6, 2433–2459. doi: 10.5194/bg-6-2433-2009.

Battin, T. J., Luyssaert, S., Kaplan, L. A., Aufdenkampe, A. K., Richter, A., and Tranvik, L. J. (2009). The boundless carbon cycle. *Nat. Geosci.* 2, 598–600. doi: 10.1038/ngeo618.

Bauer, J. E., Williams, P. M., and Druffel, E. R. M. (1992). 14C activity of dissolved organic carbon fractions in the north-central Pacific and Sargasso Sea. *Nature* 357, 667–670. doi: 10.1038/357667a0.

Becker, S., Tebben, J., Coffinet, S., Wiltshire, K., Iversen, M. H., Harder, T., et al. (2020). Laminarin is a major molecule in the marine carbon cycle. *Proc. Natl. Acad. Sci.* 117, 6599–6607. doi: 10.1073/pnas.1917001117.

Behrenfeld, M. J., and Falkowski, P. G. (1997). Photosynthetic rates derived from satellite-based chlorophyll concentration. *Limnol. Oceanogr.* 42, 1–20. doi: 10.4319/lo.1997.42.1.0001.

Behrenfeld, M. J., O'Malley, R. T., Siegel, D. A., McClain, C. R., Sarmiento, J. L., Feldman, G. C., et al. (2006). Climate-driven trends in contemporary ocean productivity. *Nature* 444, 752–755. doi: 10.1038/nature05317.

Bélanger, S., Xie, H., Krotkov, N., Larouche, P., Vincent, W. F., and Babin, M. (2006). Photomineralization of terrigenous dissolved organic matter in Arctic coastal waters from 1979 to 2003: Interannual variability and implications of climate change. *Global Biogeochem. Cycles* 20, GB4005. doi: 10.1029/2006GB002708.

Belzile, C., Gibson, J. A. E., and Vincent, W. F. (2002). Colored dissolved organic matter and dissolved organic carbon exclusion from lake ice: Implications for irradiance transmission and carbon cycling. *Limnol. Oceanogr.* 47, 1283–1293. doi: 10.4319/lo.2002.47.5.1283.

Benner, R., and Amon, R. M. W. (2015). The Size-Reactivity Continuum of Major Bioelements in the Ocean. *Ann. Rev. Mar. Sci.* 7, 185–205. doi: 10.1146/annurev-marine-010213-135126.

Benner, R., Benitez-Nelson, B., Kaiser, K., and Amon, R. M. W. (2004). Export of young terrigenous dissolved organic carbon from rivers to the Arctic Ocean. *Geophys. Res. Lett.* 31, L05305. doi: 10.1029/2003GL019251.

Benner, R., Louchouarn, P., and Amon, R. M. W. (2005). Terrigenous dissolved organic matter in the Arctic Ocean and its transport to surface and deep waters of the North Atlantic. *Global Biogeochem. Cycles* 19, GB2025. doi: 10.1029/2004GB002398.

Benner, R., Pakulski, J. D., McCarthy, M., Hedges, J. I., and Hatcher, P. G. (1992). Bulk Chemical Characteristics of Dissolved Organic Matter in the Ocean. *Science.* 255, 1561–1564. doi: 10.1126/science.255.5051.1561.

Benner, R., and Ziegler, S. (1999). "Do Photochemical Transformations of Dissolved Organic Matter Produce Biorefractory as well as Bioreactive Substrates?," in

*Proceedinsgs of the 8th International Symposium on MIcrobial Ecology*, eds. C. R. Bell, M. Brylinsky, and P. Johnson-Green.

Beszczynska-Möller, A., Fahrbach, E., Schauer, U., and Hansen, E. (2012). Variability in Atlantic water temperature and transport at the entrance to the Arctic Ocean, 1997–2010. *ICES J. Mar. Sci.* 69, 852–863. doi: 10.1093/icesjms/fss056.

Bianchi, T. S. (2011). The role of terrestrially derived organic carbon in the coastal ocean: A changing paradigm and the priming effect. *Proc. Natl. Acad. Sci.* 108, 19473–19481. doi: 10.1073/pnas.1017982108.

Bielicka-Daszkiewicz, K., and Voelkel, A. (2009). Theoretical and experimental methods of determination of the breakthrough volume of SPE sorbents. *Talanta* 80, 614–621. doi: 10.1016/j.talanta.2009.07.037.

Biersmith, A., and Benner, R. (1998). Carbohydrates in phytoplankton and freshly produced dissolved organic matter. *Mar. Chem.* 63, 131–144. doi: 10.1016/S0304-4203(98)00057-7.

Bolan, N. S., Adriano, D. C., Kunhikrishnan, A., James, T., McDowell, R., and Senesi, N. (2011). "Dissolved organic matter: biogeochemistry, dynamics, and environmental significance in soils," in *Advances in Agronomy* (Elsevier Inc.), 1–75. doi: 10.1016/B978-0-12-385531-2.00001-3.

Boles, E., Provost, C., Garçon, V., Bertosio, C., Athanase, M., Koenig, Z., et al. (2020). Under-Ice Phytoplankton Blooms in the Central Arctic Ocean: Insights From the First Biogeochemical IAOOS Platform Drift in 2017. *J. Geophys. Res. Ocean.* 125, e2019JC015608. doi: 10.1029/2019JC015608.

Bönisch, G., and Schlosser, P. (1995). Deep water formation and exchange rates in the Greenland/Norwegian Seas and the Eurasian Basin of the Arctic Ocean derived from tracer balances. *Prog. Oceanogr.* 35, 29–52. doi: 10.1016/0079-6611(95)00004-Z.

Broek, T. A. B., Walker, B. D., Guilderson, T. P., and McCarthy, M. D. (2017). Coupled ultrafiltration and solid phase extraction approach for the targeted study of semi-labile high molecular weight and refractory low molecular weight dissolved organic matter. *Mar. Chem.* 194, 146–157. doi: 10.1016/j.marchem.2017.06.007.

Brogi, S. R., Derrien, M., and Hur, J. (2019). In-Depth assessment of the effect of

sodium azide on the optical properties of dissolved organic matter. *J. Fluoresc.* 29, 877–885. doi: 10.1007/s10895-019-02398-w.

Brown, T. A., Jackson, B. A., Bythell, B. J., and Stenson, A. C. (2016). Benefits of multidimensional fractionation for the study and characterization of natural organic matter. *J. Chromatogr. A* 1470, 84–96. doi: 10.1016/j.chroma.2016.10.005.

Cao, F., Zhu, Y., Kieber, D. J., and Miller, W. L. (2020). Distribution and photo-reactivity of chromophoric and fluorescent dissolved organic matter in the Northeastern North Pacific Ocean. *Deep Sea Res. Part I Oceanogr. Res. Pap.* 155, 103168. doi: 10.1016/j.dsr.2019.103168.

Capelle, D. W., Kuzyk, Z. Z. A., Papakyriakou, T., Guéguen, C., Miller, L. A., and Macdonald, R. W. (2020). Effect of terrestrial organic matter on ocean acidification and CO2 flux in an Arctic shelf sea. *Prog. Oceanogr.* 185, 102319. doi: 10.1016/j.pocean.2020.102319.

Capley, E. N., Tipton, J. D., Marshall, A. G., and Stenson, A. C. (2010). Chromatographic reduction of isobaric and isomeric complexity of fulvic acids To enable multistage tandem mass spectral characterization. *Anal. Chem.* 82, 8194–8202. doi: 10.1021/ac1016216.

Carlson, C. A., and Ducklow, H. W. (1995). Dissolved organic carbon in the upper ocean of the central equatorial Pacific Ocean, 1992: Daily and finescale vertical variations. *Deep Sea Res. Part II Top. Stud. Oceanogr.* 42, 639–656. doi: 10.1016/0967-0645(95)00023-J.

Carlson, C. A., Ducklow, H. W., Hansell, D. A., and Smith Jr, W. O. (1998). Organic carbon partitioning during spring phytoplankton blooms in the Ross Sea polynya and the Sargasso Sea. *Limnol. Oceanogr.* 43, 375–386. doi: 10.4319/lo.1998.43.3.0375.

Carmack, E., Barber, D., Christensen, J., Macdonald, R., Rudels, B., and Sakshaug, E. (2006). Climate variability and physical forcing of the food webs and the carbon budget on panarctic shelves. *Prog. Oceanogr.* 71, 145–181. doi: 10.1016/j.pocean.2006.10.005.

Carmack, E. C., Yamamoto-Kawai, M., Haine, T. W. N., Bacon, S., Bluhm, B. A., Lique, C., et al. (2016). Freshwater and its role in the Arctic Marine System:

Sources, disposition, storage, export, and physical and biogeochemical consequences in the Arctic and global oceans. *J. Geophys. Res. Biogeosciences* 121, 675–717. doi: 10.1002/2015JG003140.

Carr, M.-E., Friedrichs, M. A. M., Schmeltz, M., Noguchi Aita, M., Antoine, D., Arrigo, K. R., et al. (2006). A comparison of global estimates of marine primary production from ocean color. *Deep Sea Res. Part II Top. Stud. Oceanogr.* 53, 741–770. doi: 10.1016/j.dsr2.2006.01.028.

Carr, N., Davis, C. E., Blackbird, S., Daniels, L. R., Preece, C., Woodward, M., et al. (2019). Seasonal and spatial variability in the optical characteristics of DOM in a temperate shelf sea. *Prog. Oceanogr.* 177, 101929. doi: 10.1016/j.pocean.2018.02.025.

Charette, M. A., Kipp, L. E., Jensen, L. T., Dabrowski, J. S., Whitmore, L. M., Fitzsimmons, J. N., et al. (2020). The transpolar drift as a source of riverine and shelf-derived trace elements to the Central Arctic Ocean. *J. Geophys. Res. Ocean.* 125, e2019JC015920. doi: 10.1029/2019JC015920.

Chen, H., Stubbins, A., and Hatcher, P. G. (2011). A mini-electrodialysis system for desalting small volume saline samples for Fourier transform ion cyclotron resonance mass spectrometry. *Limnol. Oceanogr. Methods* 9, 582–592. doi: 10.4319/lom.2011.9.582.

Chen, M., Kim, S., Park, J.-E., Jung, H.-J., and Hur, J. (2016a). Structural and compositional changes of dissolved organic matter upon solid-phase extraction tracked by multiple analytical tools. *Anal. Bioanal. Chem.* 408, 6249–6258. doi: 10.1007/s00216-016-9728-0.

Chen, M., Kim, S., Park, J.-E., Kim, H. S., and Hur, J. (2016b). Effects of dissolved organic matter (DOM) sources and nature of solid extraction sorbent on recoverable DOM composition: Implication into potential lability of different compound groups. *Anal. Bioanal. Chem.* 408, 4809–4819. doi: 10.1007/s00216-016-9569-x.

Chin, W.-C., Orellana, M. V., and Verdugo, P. (1998). Spontaneous assembly of marine dissolved organic matter into polymer gels. *Nature* 391, 568–572. doi: 10.1038/35345.

Chin, Y.-P., Aiken, G., and O'Loughlin, E. (1994). Molecular weight, polydispersity,

and spectroscopic properties of aquatic humic substances. *Environ. Sci. Technol.* 28, 1853–1858. doi: 10.1021/es00060a015.

Coble, P. G. (1996). Characterization of marine and terrestrial DOM in seawater using excitation-emission matrix spectroscopy. *Mar. Chem.* 51, 325–346. doi: 10.1016/0304-4203(95)00062-3.

Coble, P. G. (2007). Marine optical biogeochemistry: The chemistry of ocean color. *Chem. Rev.* 107, 402–418. doi: 10.1021/cr050350+.

Coble, P. G., Lead, J., Baker, A., Reynolds, D. M., and Spencer, R. G. (2014). *Aquatic organic matter fluorescence*. doi: 10.1017/CBO9781139045452.010.

Cooper, L. W., Benner, R., McClelland, J. W., Peterson, B. J., Holmes, R. M., Raymond, P. A., et al. (2005). Linkages among runoff, dissolved organic carbon, and the stable oxygen isotope composition of seawater and other water mass indicators in the Arctic Ocean. *J. Geophys. Res. Biogeosciences* 110, G02013. doi: 10.1029/2005JG000031.

D'Andrilli, J., Cooper, W. T., Foreman, C. M., and Marshall, A. G. (2015). An ultrahigh-resolution mass spectrometry index to estimate natural organic matter lability. *Rapid Commun. Mass Spectrom.* 29, 2385–2401. doi: 10.1002/rcm.7400.

Determann, S., Lobbes, J. M., Reuter, R., and Rullkötter, J. (1998). Ultraviolet fluorescence excitation and emission spectroscopy of marine algae and bacteria. *Mar. Chem.* 62, 137–156. doi: 10.1016/S0304-4203(98)00026-7.

Dittmar, T. (2008). The molecular level determination of black carbon in marine dissolved organic matter. *Org. Geochem.* 39, 396–407. doi: 10.1016/j.orggeochem.2008.01.015.

Dittmar, T., and Kattner, G. (2003). The biogeochemistry of the river and shelf ecosystem of the Arctic Ocean: a review. *Mar. Chem.* 83, 103–120. doi: 10.1016/S0304-4203(03)00105-1.

Dittmar, T., Koch, B., Hertkorn, N., and Kattner, G. (2008). A simple and efficient method for the solid-phase extraction of dissolved organic matter (SPE-DOM) from seawater. *Limnol. Oceanogr. Methods* 6, 230–235. doi: 10.4319/lom.2008.6.230.

Dittmar, T., and Koch, B. P. (2006). Thermogenic organic matter dissolved in the abyssal ocean. *Mar. Chem.* 102, 208–217. doi: 10.1016/j.marchem.2006.04.003.

Dittmar, T., and Stubbins, A. (2014). “Dissolved organic matter in aquatic systems,” in *Treatise on Geochemistry* (Elsevier), 125–156. doi: 10.1016/B978-0-08-095975-7.01010-X.

Dittmar, T., Whitehead, K., Minor, E. C., and Koch, B. P. (2007). Tracing terrigenous dissolved organic matter and its photochemical decay in the ocean by using liquid chromatography/mass spectrometry. *Mar. Chem.* 107, 378–387. doi: 10.1016/j.marchem.2007.04.006.

Ducklow, H., Steinberg, D., and Buesseler, K. (2001). Upper ocean carbon export and the biological pump. *Oceanography* 14, 50–58. doi: 10.5670/oceanog.2001.06.

Ducklow, H. W. (1999). The bacterial component of the oceanic euphotic zone. *FEMS Microbiol. Ecol.* 30, 1–10. doi: 10.1111/j.1574-6941.1999.tb00630.x.

Edet, U. A., and Ifelebuegu, A. O. (2020). Kinetics, isotherms, and thermodynamic modeling of the adsorption of phosphates from model wastewater using recycled brick waste. *Processes* 8, 665. doi: 10.3390/pr8060665.

Fichot, C. G., Benner, R., Kaiser, K., Shen, Y., Amon, R. M. W., Ogawa, H., et al. (2016). Predicting dissolved lignin phenol concentrations in the coastal ocean from chromophoric dissolved organic matter (CDOM) absorption coefficients. *Front. Mar. Sci.* 3, 7. doi: 10.3389/fmars.2016.00007.

Fichot, C. G., Kaiser, K., Hooker, S. B., Amon, R. M. W., Babin, M., Bélanger, S., et al. (2013). Pan-Arctic distributions of continental runoff in the Arctic Ocean. *Sci. Rep.* 3, 1053. doi: 10.1038/srep01053.

Field, C. B., Behrenfeld, M. J., Randerson, J. T., and Falkowski, P. (1998). Primary production of the biosphere: integrating terrestrial and oceanic components. *Science.* 281, 237–240. doi: 10.1126/science.281.5374.237.

Fitznar, H. P., Lobbes, J. M., and Kattner, G. (1999). Determination of enantiomeric amino acids with high-performance liquid chromatography and pre-column derivatisation with o-phthaldialdehyde and N-isobutyrylcysteine in seawater and fossil samples (mollusks). *J. Chromatogr. A* 832, 123–132. doi: 10.1016/S0021-9673(98)01000-0.

Flerus, R., Koch, B. P., Schmitt-Kopplin, P., Witt, M., and Kattner, G. (2011). Molecular level investigation of reactions between dissolved organic matter and extraction solvents using FT-ICR MS. *Mar. Chem.* 124, 100–107. doi:

10.1016/j.marchem.2010.12.006.

Flerus, R., Lechtenfeld, O. J., Koch, B. P., McCallister, S. L., Schmitt-Kopplin, P., Benner, R., et al. (2012). A molecular perspective on the ageing of marine dissolved organic matter. *Biogeosciences* 9, 1935–1955. doi: 10.5194/bg-9-1935-2012.

Follett, C. L., Repeta, D. J., Rothman, D. H., Xu, L., and Santinelli, C. (2014). Hidden cycle of dissolved organic carbon in the deep ocean. *Proc. Natl. Acad. Sci.* 111, 16706–16711. doi: 10.1073/pnas.1407445111.

Fraga, F., Ríos, A. F., Pérez, F. F., and Figueiras, F. G. (1998). Theoretical limits of oxygen:carbon and oxygen:nitrogen ratios during photosynthesis and mineralisation of organic matter in the sea. *Sci. Mar.* 62, 161–168. doi: 10.3989/scimar.1998.62n1-2161.

Frey, K. E., and Smith, L. C. (2005). Amplified carbon release from vast West Siberian peatlands by 2100. *Geophys. Res. Lett.* 32, L09401. doi: 10.1029/2004GL022025.

Galy, V., France-Lanord, C., Beyssac, O., Faure, P., Kudrass, H., and Palhol, F. (2007). Efficient organic carbon burial in the Bengal fan sustained by the Himalayan erosional system. *Nature* 450, 407–410. doi: 10.1038/nature06273.

Ghosh, C., Shinde, C. P., and Chakraborty, B. S. (2012). Influence of ionization source design on matrix effects during LC–ESI-MS/MS analysis. *J. Chromatogr. B* 893–894, 193–200. doi: 10.1016/j.jchromb.2012.03.012.

Glukhovets, D., Kopelevich, O., Yushmanova, A., Vazyulya, S., Sheberstov, S., Karalli, P., et al. (2020). Evaluation of the CDOM Absorption Coefficient in the Arctic Seas Based on Sentinel-3 OLCI Data. *Remote Sens.* 12, 3210. doi: 10.3390/rs12193210.

Gonçalves-Araujo, R., Granskog, M. A., Bracher, A., Azetsu-Scott, K., Dodd, P. A., and Stedmon, C. A. (2016). Using fluorescent dissolved organic matter to trace and distinguish the origin of Arctic surface waters. *Sci. Rep.* 6, 33978. doi: 10.1038/srep33978.

Gonçalves-Araujo, R., Rabe, B., Peeken, I., and Bracher, A. (2018). High colored dissolved organic matter (CDOM) absorption in surface waters of the central-eastern Arctic Ocean: Implications for biogeochemistry and ocean color

algorithms. *PLoS One* 13, e0190838. doi: 10.1371/journal.pone.0190838.

Gonçalves-Araujo, R., Stedmon, C. A., Heim, B., Dubinenkov, I., Kraberg, A., Moiseev, D., et al. (2015). From fresh to marine waters: Characterization and fate of dissolved organic matter in the Lena River Delta Region, Siberia. *Front. Mar. Sci.* 2, 108. doi: 10.3389/fmars.2015.00108.

Gonsior, M., Schmitt-Kopplin, P., and Bastviken, D. (2013). Depth-dependent molecular composition and photo-reactivity of dissolved organic matter in a boreal lake under winter and summer conditions. *Biogeosciences* 10, 6945–6956. doi: 10.5194/bg-10-6945-2013.

Granskog, M. A., Fer, I., Rinke, A., and Steen, H. (2018). Atmosphere-ice-ocean-ecosystem processes in a thinner Arctic sea ice regime: The Norwegian young sea ICE (N-ICE2015) expedition. *J. Geophys. Res. Ocean.* 123, 1586–1594. doi: 10.1002/2017JC013328.

Granskog, M. A., Macdonald, R. W., Mundy, C.-J., and Barber, D. G. (2007). Distribution, characteristics and potential impacts of chromophoric dissolved organic matter (CDOM) in Hudson Strait and Hudson Bay, Canada. *Cont. Shelf Res.* 27, 2032–2050. doi: 10.1016/j.csr.2007.05.001.

Granskog, M. A., Pavlov, A. K., Sagan, S., Kowalczuk, P., Raczkowska, A., and Stedmon, C. A. (2015). Effect of sea-ice melt on inherent optical properties and vertical distribution of solar radiant heating in Arctic surface waters. *J. Geophys. Res. Ocean.* 120, 7028–7039. doi: 10.1002/2015JC011087.

Granskog, M. A., Stedmon, C. A., Dodd, P. A., Amon, R. M. W., Pavlov, A. K., De Steur, L., et al. (2012). Characteristics of colored dissolved organic matter (CDOM) in the Arctic outflow in the Fram Strait: Assessing the changes and fate of terrigenous CDOM in the Arctic Ocean. *J. Geophys. Res. Ocean.* 117, C12021. doi: 10.1029/2012JC008075.

Green, N. W., Perdue, E. M., Aiken, G. R., Butler, K. D., Chen, H., Dittmar, T., et al. (2014). An intercomparison of three methods for the large-scale isolation of oceanic dissolved organic matter. *Mar. Chem.* 161, 14–19. doi: 10.1016/j.marchem.2014.01.012.

Griffith, D. R., McNichol, A. P., Xu, L., McLaughlin, F. A., Macdonald, R. W., Brown, K. A., et al. (2012). Carbon dynamics in the western Arctic Ocean:

insights from full-depth carbon isotope profiles of DIC, DOC, and POC. *Biogeosciences* 9, 1217–1224. doi: 10.5194/bg-9-1217-2012.

Grunert, B. K., Tzortziou, M., Neale, P., Menendez, A., and Hernes, P. (2021). DOM degradation by light and microbes along the Yukon River-coastal ocean continuum. *Sci. Rep.* 11, 10236. doi: 10.1038/s41598-021-89327-9.

Guay, C. K., Klinkhammer, G. P., Falkner, K. K., Benner, R., Coble, P. G., Whitledge, T. E., et al. (1999). High-resolution measurements of dissolved organic carbon in the Arctic Ocean by in situ fiber-optic spectrometry. *Geophys. Res. Lett.* 26, 1007–1010. doi: 10.1029/1999GL900130.

Guéguen, C., Guo, L., and Tanaka, N. (2005). Distributions and characteristics of colored dissolved organic matter in the Western Arctic Ocean. *Cont. Shelf Res.* 25, 1195–1207. doi: 10.1016/j.csr.2005.01.005.

Haine, T. W. N., Curry, B., Gerdes, R., Hansen, E., Karcher, M., Lee, C., et al. (2015). Arctic freshwater export: Status, mechanisms, and prospects. *Glob. Planet. Change* 125, 13–35. doi: 10.1016/j.gloplacha.2014.11.013.

Han, L., Kaesler, J., Peng, C., Reemtsma, T., and Lechtenfeld, O. J. (2021). Online counter gradient LC-FT-ICR-MS enables detection of highly polar natural organic matter fractions. *Anal. Chem.* 93, 1740–1748. doi: 10.1021/acs.analchem.0c04426.

Hansell, D. A. (2013). Recalcitrant dissolved organic carbon fractions. *Ann. Rev. Mar. Sci.* 5, 421–445. doi: 10.1146/annurev-marine-120710-100757.

Hansell, D. A., Carlson, C. A., and Schlitzer, R. (2012). Net removal of major marine dissolved organic carbon fractions in the subsurface ocean. *Global Biogeochem. Cycles* 26. doi: 10.1029/2011GB004069.

Hansell, D. A., Kadko, D., and Bates, N. R. (2004). Degradation of terrigenous dissolved organic carbon in the western Arctic Ocean. *Science.* 304, 858–861. doi: 10.1126/science.1096175.

Hansell, D., Carlson, C., Repeta, D., and Schlitzer, R. (2009). Dissolved organic matter in the ocean: A controversy stimulates new insights. *Oceanography* 22, 202–211. doi: 10.5670/oceanog.2009.109.

Hansen, A. M., Kraus, T. E. C., Pellerin, B. A., Fleck, J. A., Downing, B. D., and Bergamaschi, B. A. (2016). Optical properties of dissolved organic matter

(DOM): Effects of biological and photolytic degradation. *Limnol. Oceanogr.* 61, 1015–1032. doi: 10.1002/lno.10270.

Hawkes, J. A., Dittmar, T., Patriarca, C., Tranvik, L., and Bergquist, J. (2016). Evaluation of the Orbitrap mass spectrometer for the molecular fingerprinting analysis of natural dissolved organic matter. *Anal. Chem.* 88, 7698–7704. doi: 10.1021/acs.analchem.6b01624.

Hawkes, J. A., Patriarca, C., Sjöberg, P. J. R., Tranvik, L. J., and Bergquist, J. (2018a). Extreme isomeric complexity of dissolved organic matter found across aquatic environments. *Limnol. Oceanogr. Lett.* 3, 21–30. doi: 10.1002/lol2.10064.

Hawkes, J. A., Radoman, N., Bergquist, J., Wallin, M. B., Tranvik, L. J., and Löfgren, S. (2018b). Regional diversity of complex dissolved organic matter across forested hemiboreal headwater streams. *Sci. Rep.* 8, 16060. doi: 10.1038/s41598-018-34272-3.

Hedges, J. ., Eglinton, G., Hatcher, P. ., Kirchman, D. ., Arnosti, C., Derenne, S., et al. (2000). The molecularly-uncharacterized component of nonliving organic matter in natural environments. *Org. Geochem.* 31, 945–958. doi: 10.1016/S0146-6380(00)00096-6.

Hedges, J. I. (1992). Global biogeochemical cycles: progress and problems. *Mar. Chem.* 39, 67–93. doi: 10.1016/0304-4203(92)90096-S.

Hedges, J. I. (2002). "Why dissolved organics matter," in *Biogeochemistry of Marine Dissolved Organic Matter*, eds. D. A. Hansell and C. A. Carlson (Elsevier Science, San Diego, CA.). Available at: https://www.researchgate.net/publication/269107473_What_is_governance/link/548173090cf22525dcb61443/download%0Ahttp://www.econ.upf.edu/~reynal/Civil wars_12December2010.pdf%0Ahttps://think-asia.org/handle/11540/8282%0Ahttps://www.jstor.org/stable/41857625.

Hedges, J. I., Keil, R. G., and Benner, R. (1997). What happens to terrestrial organic matter in the ocean? *Org. Geochem.* 27, 195–212. doi: 10.1016/S0146-6380(97)00066-1.

Helms, J. R., Stubbins, A., Ritchie, J. D., Minor, E. C., Kieber, D. J., and Mopper, K. (2008). Absorption spectral slopes and slope ratios as indicators of molecular weight, source, and photobleaching of chromophoric dissolved organic matter.

*Limnol. Oceanogr.* 53, 955–969. doi: 10.4319/lo.2008.53.3.0955.

Herndl, G. J., Bayer, B., Baltar, F., and Reinthaler, T. (2023). Prokaryotic life in the deep ocean's water column. *Ann. Rev. Mar. Sci.* 15. doi: 10.1146/annurev-marine-032122-115655.

Hernes, P. J., and Benner, R. (2006). Terrigenous organic matter sources and reactivity in the North Atlantic Ocean and a comparison to the Arctic and Pacific oceans. *Mar. Chem.* 100, 66–79. doi: 10.1016/j.marchem.2005.11.003.

Hertkorn, N., Benner, R., Frommberger, M., Schmitt-Kopplin, P., Witt, M., Kaiser, K., et al. (2006). Characterization of a major refractory component of marine dissolved organic matter. *Geochim. Cosmochim. Acta* 70, 2990–3010. doi: 10.1016/j.gca.2006.03.021.

Hertkorn, N., Harir, M., Cawley, K. M., Schmitt-Kopplin, P., and Jaffé, R. (2016). Molecular characterization of dissolved organic matter from subtropical wetlands: a comparative study through the analysis of optical properties, NMR and FTICR/MS. *Biogeosciences* 13, 2257–2277. doi: 10.5194/bg-13-2257-2016.

Hertkorn, N., Ruecker, C., Meringer, M., Gugisch, R., Frommberger, M., Perdue, E. M., et al. (2007). High-precision frequency measurements: indispensable tools at the core of the molecular-level analysis of complex systems. *Anal. Bioanal. Chem.* 389, 1311–1327. doi: 10.1007/s00216-007-1577-4.

Herzsprung, P., Hertkorn, N., von Tümpling, W., Harir, M., Friese, K., and Schmitt-Kopplin, P. (2014). Understanding molecular formula assignment of Fourier transform ion cyclotron resonance mass spectrometry data of natural organic matter from a chemical point of view. *Anal. Bioanal. Chem.* 406, 7977–7987. doi: 10.1007/s00216-014-8249-y.

Herzsprung, P., von Tümpling, W., Hertkorn, N., Harir, M., Büttner, O., Bravidor, J., et al. (2012). Variations of DOM Quality in Inflows of a Drinking Water Reservoir: Linking of van Krevelen Diagrams with EEMF Spectra by Rank Correlation. *Environ. Sci. Technol.* 46, 5511–5518. doi: 10.1021/es300345c.

Hill, V. J. (2008). Impacts of chromophoric dissolved organic material on surface ocean heating in the Chukchi Sea. *J. Geophys. Res.* 113, C07024. doi: 10.1029/2007JC004119.

Hirose, K. (2007). Metal–organic matter interaction: Ecological roles of ligands in

oceanic DOM. *Appl. Geochemistry* 22, 1636–1645. doi: 10.1016/j.apgeochem.2007.03.042.

Hockaday, W. C., Purcell, J. M., Marshall, A. G., Baldock, J. A., and Hatcher, P. G. (2009). Electrospray and photoionization mass spectrometry for the characterization of organic matter in natural waters: a qualitative assessment. *Limnol. Oceanogr. Methods* 7, 81–95. doi: 10.4319/lom.2009.7.81.

Hölemann, J. A., Juhls, B., Bauch, D., Janout, M., Koch, B. P., and Heim, B. (2021). The impact of the freeze–melt cycle of land-fast ice on the distribution of dissolved organic matter in the Laptev and East Siberian seas (Siberian Arctic). *Biogeosciences* 18, 3637–3655. doi: 10.5194/bg-18-3637-2021.

Holmes, R. M., McClelland, J. W., Peterson, B. J., Tank, S. E., Bulygina, E., Eglinton, T. I., et al. (2012). Seasonal and annual fluxes of nutrients and organic matter from large rivers to the Arctic Ocean and surrounding seas. *Estuaries and Coasts* 35, 369–382. doi: 10.1007/s12237-011-9386-6.

Holmes, R. M., McClelland, J. W., Raymond, P. A., Frazer, B. B., Peterson, B. J., and Stieglitz, M. (2008). Lability of DOC transported by Alaskan rivers to the Arctic Ocean. *Geophys. Res. Lett.* 35, L03402. doi: 10.1029/2007GL032837.

Hopkinson, C. S., Fry, B., and Nolin, A. L. (1997). Stoichiometry of dissolved organic matter dynamics on the continental shelf of the northeastern U.S.A. *Cont. Shelf Res.* 17, 473–489. doi: 10.1016/S0278-4343(96)00046-5.

Hopkinson, C. S., and Vallino, J. J. (2005). Efficient export of carbon to the deep ocean through dissolved organic matter. *Nature* 433, 142–145. doi: 10.1038/nature03191.

Hu, X., Myers, P. G., and Lu, Y. (2019). Pacific water pathway in the Arctic Ocean and Beaufort Gyre in two simulations with different horizontal resolutions. *J. Geophys. Res. Ocean.* 124, 6414–6432. doi: 10.1029/2019JC015111.

Hugelius, G., Strauss, J., Zubrzycki, S., Harden, J. W., Schuur, E. A. G., Ping, C.-L., et al. (2014). Estimated stocks of circumpolar permafrost carbon with quantified uncertainty ranges and identified data gaps. *Biogeosciences* 11, 6573–6593. doi: 10.5194/bg-11-6573-2014.

Hughey, C. A., Rodgers, R. P., and Marshall, A. G. (2002). Resolution of 11 000 compositionally distinct components in a single electrospray ionization Fourier

transform ion cyclotron resonance mass spectrum of crude oil. *Anal. Chem.* 74, 4145–4149. doi: 10.1021/ac020146b.

Huguet, A., Vacher, L., Relexans, S., Saubusse, S., Froidefond, J. M., and Parlanti, E. (2009). Properties of fluorescent dissolved organic matter in the Gironde Estuary. *Org. Geochem.* 40, 706–719. doi: 10.1016/j.orggeochem.2009.03.002.

Hülse, D., Arndt, S., Wilson, J. D., Munhoven, G., and Ridgwell, A. (2017). Understanding the causes and consequences of past marine carbon cycling variability through models. *Earth-Science Rev.* 171, 349–382. doi: 10.1016/j.earscirev.2017.06.004.

Ishii, S. K. L., and Boyer, T. H. (2012). Behavior of reoccurring PARAFAC components in fluorescent dissolved organic matter in natural and engineered systems: A critical review. *Environ. Sci. Technol.* 46, 2006–2017. doi: 10.1021/es2043504.

Ivanov, V., Alexeev, V., Koldunov, N. V., Repina, I., Sandø, A. B., Smedsrud, L. H., et al. (2016). Arctic Ocean heat impact on regional ice decay: A suggested positive feedback. *J. Phys. Oceanogr.* 46, 1437–1456. doi: 10.1175/JPO-D-15-0144.1.

Jahn, A., Tremblay, L. B., Newton, R., Holland, M. M., Mysak, L. A., and Dmitrenko, I. A. (2010). A tracer study of the Arctic Ocean's liquid freshwater export variability. *J. Geophys. Res. Ocean.* 115, C07015. doi: 10.1029/2009JC005873.

Jiao, N., Herndl, G. J., Hansell, D. A., Benner, R., Kattner, G., Wilhelm, S. W., et al. (2010). Microbial production of recalcitrant dissolved organic matter: long-term carbon storage in the global ocean. *Nat. Rev. Microbiol.* 8, 593–599. doi: 10.1038/nrmicro2386.

Johnson, M. S., Couto, E. G., Abdo, M., and Lehmann, J. (2011). Fluorescence index as an indicator of dissolved organic carbon quality in hydrologic flowpaths of forested tropical watersheds. *Biogeochemistry* 105, 149–157. doi: 10.1007/s10533-011-9595-x.

Johnson, W. M., Kido Soule, M. C., and Kujawinski, E. B. (2017). Extraction efficiency and quantification of dissolved metabolites in targeted marine metabolomics. *Limnol. Oceanogr. Methods* 15, 417–428. doi: 10.1002/lom3.10181.

Jones, E. P., Anderson, L. G., Jutterström, S., Mintrop, L., and Swift, J. H. (2008). Pacific freshwater, river water and sea ice meltwater across Arctic Ocean basins: Results from the 2005 Beringia Expedition. *J. Geophys. Res.* 113, C08012. doi: 10.1029/2007JC004124.

Jørgensen, L., Stedmon, C. A., Kaartokallio, H., Middelboe, M., and Thomas, D. N. (2015). Changes in the composition and bioavailability of dissolved organic matter during sea ice formation. *Limnol. Oceanogr.* 60, 817–830. doi: 10.1002/lno.10058.

Kähler, P., BjØrnsen, P. K., Lochte, K., and Antia, A. (1997). Dissolved organic matter and its utilization by bacteria during spring in the Southern Ocean. *Deep. Res. Part II Top. Stud. Oceanogr.* 44, 341–353. doi: 10.1016/S0967-0645(96)00071-9.

Kaiser, K., and Benner, R. (2009). Biochemical composition and size distribution of organic matter at the Pacific and Atlantic time-series stations. *Mar. Chem.* 113, 63–77. doi: 10.1016/j.marchem.2008.12.004.

Kaiser, K., and Benner, R. (2012a). Characterization of lignin by gas chromatography and mass spectrometry using a simplified CuO oxidation method. *Anal. Chem.* 84, 459–464. doi: 10.1021/ac202004r.

Kaiser, K., and Benner, R. (2012b). Organic matter transformations in the upper mesopelagic zone of the North Pacific: Chemical composition and linkages to microbial community structure. *J. Geophys. Res. Ocean.* 117, C01023. doi: 10.1029/2011JC007141.

Kaiser, K., Benner, R., and Amon, R. M. W. (2017). The fate of terrigenous dissolved organic carbon on the Eurasian shelves and export to the North Atlantic. *J. Geophys. Res. Ocean.* 122, 4–22. doi: 10.1002/2016JC012380.

Kandasamy, S., and Nath, B. N. (2016). Perspectives on the terrestrial organic matter transport and burial along the land-deep sea continuum: caveats in our understanding of biogeochemical processes and future needs. *Front. Mar. Sci.* 3, 259. doi: 10.3389/fmars.2016.00259.

Karcher, M., Smith, J. N., Kauker, F., Gerdes, R., and Smethie Jr, W. M. (2012). Recent changes in Arctic Ocean circulation revealed by iodine-129 observations and modeling. *J. Geophys. Res. Ocean.* 117, C08007. doi:

10.1029/2011JC007513.

Kattner, G., Lobbes, J. ., Fitznar, H. ., Engbrodt, R., Nöthig, E.-M., and Lara, R. . (1999). Tracing dissolved organic substances and nutrients from the Lena River through Laptev Sea (Arctic). *Mar. Chem.* 65, 25–39. doi: 10.1016/S0304-4203(99)00008-0.

Keiluweit, M., Wanzek, T., Kleber, M., Nico, P., and Fendorf, S. (2017). Anaerobic microsites have an unaccounted role in soil carbon stabilization. *Nat. Commun.* 8, 1771. doi: 10.1038/s41467-017-01406-6.

Kellerman, A. M., Dittmar, T., Kothawala, D. N., and Tranvik, L. J. (2014). Chemodiversity of dissolved organic matter in lakes driven by climate and hydrology. *Nat. Commun.* 5, 3804. doi: 10.1038/ncomms4804.

Kellerman, A. M., Kothawala, D. N., Dittmar, T., and Tranvik, L. J. (2015). Persistence of dissolved organic matter in lakes related to its molecular characteristics. *Nat. Geosci.* 8, 454–457. doi: 10.1038/ngeo2440.

Kerner, M., Hohenberg, H., Ertl, S., Reckermann, M., and Spitzy, A. (2003). Self-organization of dissolved organic matter to micelle-like microparticles in river water. *Nature* 422, 150–154. doi: 10.1038/nature01469.

Kharbush, J. J., Close, H. G., Van Mooy, B. A. S., Arnosti, C., Smittenberg, R. H., Le Moigne, F. A. C., et al. (2020). Particulate organic carbon deconstructed: molecular and chemical composition of particulate organic carbon in the Ocean. *Front. Mar. Sci.* 7, 518. doi: 10.3389/fmars.2020.00518.

Kikuchi, T., Hatakeyama, K., and Morison, J. H. (2004). Distribution of convective Lower Halocline Water in the eastern Arctic Ocean. *J. Geophys. Res.* 109, C12030. doi: 10.1029/2003JC002223.

Kim, D., Kim, S., Son, S., Jung, M.-J., and Kim, S. (2019). Application of online liquid chromatography 7 T FT-ICR mass spectrometer equipped with quadrupolar detection for analysis of natural organic matter. *Anal. Chem.* 91, 7690–7697. doi: 10.1021/acs.analchem.9b00689.

Kim, J., Kim, Y., Kang, H.-W., Kim, S. H., Rho, T., and Kang, D.-J. (2020). Tracing water mass fractions in the deep western Indian Ocean using fluorescent dissolved organic matter. *Mar. Chem.* 218, 103720. doi: 10.1016/j.marchem.2019.103720.

Kim, S., Kaplan, L. A., Benner, R., and Hatcher, P. G. (2004). Hydrogen-deficient molecules in natural riverine water samples—evidence for the existence of black carbon in DOM. *Mar. Chem.* 92, 225–234. doi: 10.1016/j.marchem.2004.06.042.

Kim, S., Kramer, R. W., and Hatcher, P. G. (2003). Graphical method for analysis of ultrahigh-resolution broadband mass spectra of natural organic matter, the Van Krevelen Diagram. *Anal. Chem.* 75, 5336–5344. doi: 10.1021/ac034415p.

Kind, T., and Fiehn, O. (2007). Seven Golden Rules for heuristic filtering of molecular formulas obtained by accurate mass spectrometry. *BMC Bioinformatics* 8, 105. doi: 10.1186/1471-2105-8-105.

Kiontke, A., Oliveira-Birkmeier, A., Opitz, A., and Birkemeyer, C. (2016). Electrospray ionization efficiency is dependent on different molecular descriptors with respect to solvent pH and instrumental configuration. *PLoS One* 11, e0167502. doi: 10.1371/journal.pone.0167502.

Kipp, L., and Charette, M. (2022). The Arctic radium isotope observing network (ARION): tracking climate-driven changes in Arctic Ocean chemistry. *Oceanography*. doi: 10.5670/oceanog.2022.105.

Kirchman, D. L., Morán, X. A. G., and Ducklow, H. (2009). Microbial growth in the polar oceans — role of temperature and potential impact of climate change. *Nat. Rev. Microbiol.* 7, 451–459. doi: 10.1038/nrmicro2115.

Knap, A. H., Michaels, A., Close, A., Ducklow, H., and Dickson, A. (1996). *Protocols for the Joint Global Ocean Flux Study ( JGOFS ) Core Measurements*.

Knust, R. (2017). Polar Research and Supply Vessel POLARSTERN operated by the Alfred-Wegener-Institute. *J. large-scale Res. Facil. JLSRF* 3, A119. doi: 10.17815/jlsrf-3-163.

Koch, B. P., and Dittmar, T. (2006). From mass to structure: an aromaticity index for high-resolution mass data of natural organic matter. *Rapid Commun. Mass Spectrom.* 20, 926–932. doi: 10.1002/rcm.2386.

Koch, B. P., and Dittmar, T. (2016). From mass to structure: an aromaticity index for high-resolution mass data of natural organic matter. *Rapid Commun. Mass Spectrom.* 30, 250. doi: 10.1002/rcm.7433.

Koch, B. P., Dittmar, T., Witt, M., and Kattner, G. (2007). Fundamentals of molecular formula assignment to ultrahigh resolution mass data of natural organic matter.

*Anal. Chem.* 79, 1758–1763. doi: 10.1021/ac061949s.

Koch, B. P., Ludwichowski, K.-U., Kattner, G., Dittmar, T., and Witt, M. (2008). Advanced characterization of marine dissolved organic matter by combining reversed-phase liquid chromatography and FT-ICR-MS. *Mar. Chem.* 111, 233–241. doi: 10.1016/j.marchem.2008.05.008.

Koch, B. P., Witt, M., Engbrodt, R., Dittmar, T., and Kattner, G. (2005). Molecular formulae of marine and terrigenous dissolved organic matter detected by electrospray ionization Fourier transform ion cyclotron resonance mass spectrometry. *Geochim. Cosmochim. Acta* 69, 3299–3308. doi: 10.1016/j.gca.2005.02.027.

Kohler, H., Meon, B., Gordeev, V. V, Spitzy, A., and Amon, R. M. W. (2003). Dissolved organic matter (DOM) in the estuaries of Ob and Yenisei and the adjacent Kara Sea, Russia. *Sib. river run-off Kara Sea*, 281–308. Available at: http://www.google.co.uk/search?aq=f&sourceid=chrome&ie=UTF-8&q=Dissolved+organic+matter+(DOM)+in+the+estuaries+of+Ob+and+Yenisei+and+the+adjacent+Kara+Sea,+Russia%5Cnpapers2://publication/uuid/A5538302-5ADC-49B4-BF05-66F857556756.

Kong, X., Jendrossek, T., Ludwichowski, K.-U., Marx, U., and Koch, B. P. (2021). Solid-phase extraction of aquatic organic matter: loading-dependent chemical fractionation and self-assembly. *Environ. Sci. Technol.* 55, 15495–15504. doi: 10.1021/acs.est.1c04535.

Kong, X., Sun, Y., Su, R., and Shi, X. (2017). Real-time eutrophication status evaluation of coastal waters using support vector machine with grid search algorithm. *Mar. Pollut. Bull.* 119, 307–319. doi: 10.1016/j.marpolbul.2017.04.022.

Koprivnjak, J.-F., Pfromm, P. H., Ingall, E., Vetter, T. A., Schmitt-Kopplin, P., Hertkorn, N., et al. (2009). Chemical and spectroscopic characterization of marine dissolved organic matter isolated using coupled reverse osmosis–electrodialysis. *Geochim. Cosmochim. Acta* 73, 4215–4231. doi: 10.1016/j.gca.2009.04.010.

Korhonen, M., Rudels, B., Marnela, M., Wisotzki, A., and Zhao, J. (2013). Time and space variability of freshwater content, heat content and seasonal ice melt in the

Arctic Ocean from 1991 to 2011. *Ocean Sci.* 9, 1015–1055. doi: 10.5194/os-9-1015-2013.

Kruger, B. R., Dalzell, B. J., and Minor, E. C. (2011). Effect of organic matter source and salinity on dissolved organic matter isolation via ultrafiltration and solid phase extraction. *Aquat. Sci.* 73, 405–417. doi: 10.1007/s00027-011-0189-4.

Ksionzek, K. B., Lechtenfeld, O. J., McCallister, S. L., Schmitt-Kopplin, P., Geuer, J. K., Geibert, W., et al. (2016). Dissolved organic sulfur in the ocean: Biogeochemistry of a petagram inventory. *Science.* 354, 456–459. doi: 10.1126/science.aaf7796.

Ksionzek, K. B., Zhang, J., Ludwichowski, K.-U., Wilhelms-Dick, D., Trimborn, S., Jendrossek, T., et al. (2018). Stoichiometry, polarity, and organometallics in solid-phase extracted dissolved organic matter of the Elbe-Weser estuary. *PLoS One* 13, e0203260. doi: 10.1371/journal.pone.0203260.

Kuliński, K., Hammer, K., Schneider, B., and Schulz-Bull, D. (2016). Remineralization of terrestrial dissolved organic carbon in the Baltic Sea. *Mar. Chem.* 181, 10–17. doi: 10.1016/j.marchem.2016.03.002.

Laane, R. W. P. M., and Koole, L. (1982). The relation between fluorescence and dissolved organic carbon in the Ems-Dollart estuary and the Western Wadden Sea. *Netherlands J. Sea Res.* 15, 217–227. doi: 10.1016/0077-7579(82)90005-9.

Lancelot, C. (1979). Gross Excretion Rates of Natural Marine Phytoplankton and Heterotrophic Uptake of Excreted Products in the Southern North Sea, as Determined by Short-Term Kinetics. *Mar. Ecol. Prog. Ser.* 1, 179–186. doi: 10.3354/meps001179.

Lara, R. J., Rachold, V., Kattner, G., Hubberten, H. W., Guggenberger, G., Skoog, A., et al. (1998). Dissolved organic matter and nutrients in the Lena River, Siberian Arctic: Characteristics and distribution. *Mar. Chem.* 59, 301–309. doi: 10.1016/S0304-4203(97)00076-5.

Lara, R. J., and Thomas, D. N. (1994). Isolation of Marine Dissolved Organic Matter: Evaluation of Sequential Combinations of XAD Resins 2, 4, and 7. *Anal. Chem.* 66, 2417–2419. doi: 10.1021/ac00086a032.

LaRowe, D. E., and Van Cappellen, P. (2011). Degradation of natural organic matter: A thermodynamic analysis. *Geochim. Cosmochim. Acta* 75, 2030–2042. doi:

10.1016/j.gca.2011.01.020.

Lavonen, E. E., Kothawala, D. N., Tranvik, L. J., Gonsior, M., Schmitt-Kopplin, P., and Köhler, S. J. (2015). Tracking changes in the optical properties and molecular composition of dissolved organic matter during drinking water production. *Water Res.* 85, 286–294. doi: 10.1016/j.watres.2015.08.024.

Lawaetz, A. J., and Stedmon, C. A. (2009). Fluorescence Intensity Calibration Using the Raman Scatter Peak of Water. *Appl. Spectrosc.* 63, 936–940. doi: 10.1366/000370209788964548.

Lechtenfeld, O. J. (2012). Biogeochemistry of marine dissolved organic matter: Molecular composition, reactivity and new methods. *Ph.D. Thesis*.

Lechtenfeld, O. J., Hertkorn, N., Shen, Y., Witt, M., and Benner, R. (2015). Marine sequestration of carbon in bacterial metabolites. *Nat. Commun.* 6, 6711. doi: 10.1038/ncomms7711.

Lechtenfeld, O. J., Kattner, G., Flerus, R., McCallister, S. L., Schmitt-Kopplin, P., and Koch, B. P. (2014). Molecular transformation and degradation of refractory dissolved organic matter in the Atlantic and Southern Ocean. *Geochim. Cosmochim. Acta* 126, 321–337. doi: 10.1016/j.gca.2013.11.009.

Lechtenfeld, O. J., Koch, B. P., Gašparović, B., Frka, S., Witt, M., and Kattner, G. (2013). The influence of salinity on the molecular and optical properties of surface microlayers in a karstic estuary. *Mar. Chem.* 150, 25–38. doi: 10.1016/j.marchem.2013.01.006.

Lechtenfeld, O. J., Koch, B. P., Geibert, W., Ludwichowski, K. U., and Kattner, G. (2011). Inorganics in organics: Quantification of organic phosphorus and sulfur and trace element speciation in natural organic matter using HPLC-ICPMS. *Anal. Chem.* 83, 8968–8974. doi: 10.1021/ac201765a.

Lee, C., Wakeham, S., and Arnosti, C. (2004). Particulate Organic Matter in the Sea: The Composition Conundrum. *AMBIO A J. Hum. Environ.* 33, 565–575. doi: 10.1579/0044-7447-33.8.565.

Leefmann, T., Frickenhaus, S., and Koch, B. P. (2019). UltraMassExplorer: a browser-based application for the evaluation of high-resolution mass spectrometric data. *Rapid Commun. Mass Spectrom.* 33, 193–202. doi: 10.1002/rcm.8315.

Letscher, R. T., Hansell, D. A., and Kadko, D. (2011). Rapid removal of terrigenous dissolved organic carbon over the Eurasian shelves of the Arctic Ocean. *Mar. Chem.* 123, 78–87. doi: 10.1016/j.marchem.2010.10.002.

Lewis, C. B., Walker, B. D., and Druffel, E. R. M. (2020). Isotopic and optical heterogeneity of solid phase extracted marine dissolved organic carbon. *Mar. Chem.* 219, 103752. doi: 10.1016/j.marchem.2020.103752.

Lewis, K. M., and Arrigo, K. R. (2020). Ocean Color Algorithms for Estimating Chlorophyll a , CDOM Absorption, and Particle Backscattering in the Arctic Ocean. *J. Geophys. Res. Ocean.* 125, e2019JC015706. doi: 10.1029/2019JC015706.

Li, Y., Harir, M., Lucio, M., Gonsior, M., Koch, B. P., Schmitt-Kopplin, P., et al. (2016a). Comprehensive structure-selective characterization of dissolved organic matter by reducing molecular complexity and increasing analytical dimensions. *Water Res.* 106, 477–487. doi: 10.1016/j.watres.2016.10.034.

Li, Y., Harir, M., Lucio, M., Kanawati, B., Smirnov, K., Flerus, R., et al. (2016b). Proposed Guidelines for Solid Phase Extraction of Suwannee River Dissolved Organic Matter. *Anal. Chem.* 88, 6680–6688. doi: 10.1021/acs.analchem.5b04501.

Li, Y., Harir, M., Uhl, J., Kanawati, B., Lucio, M., Smirnov, K. S., et al. (2017). How representative are dissolved organic matter (DOM) extracts? A comprehensive study of sorbent selectivity for DOM isolation. *Water Res.* 116, 316–323. doi: 10.1016/j.watres.2017.03.038.

Lignell, R. (1990). Excretion of organic carbon by phytoplankton:its relation to algal biomass, primary productivity and bacterial secondary productivity in the Baltic Sea. *Mar. Ecol. Prog. Ser.* 68, 85–99. doi: 10.3354/meps068085.

Liguori, B. T. P., Ehlert, C., Nöthig, E., Ooijen, J. C., and Pahnke, K. (2021). The Transpolar Drift Influence on the Arctic Ocean Silicon Cycle. *J. Geophys. Res. Ocean.* 126, e2021JC017352. doi: 10.1029/2021JC017352.

Lin, H., and Guo, L. (2020). Variations in Colloidal DOM Composition with Molecular Weight within Individual Water Samples as Characterized by Flow Field-Flow Fractionation and EEM-PARAFAC Analysis. *Environ. Sci. Technol.* 54, 1657–1667. doi: 10.1021/acs.est.9b07123.

Lobbes, J. M., Fitznar, H. P., and Kattner, G. (2000). Biogeochemical characteristics

of dissolved and particulate organic matter in Russian rivers entering the Arctic Ocean. *Geochim. Cosmochim. Acta* 64, 2973–2983. doi: 10.1016/S0016-7037(00)00409-9.

Lu, K., Gardner, W. S., and Liu, Z. (2018). Molecular Structure Characterization of Riverine and Coastal Dissolved Organic Matter with Ion Mobility Quadrupole Time-of-Flight LCMS (IM Q-TOF LCMS). *Environ. Sci. Technol.* 52, 7182–7191. doi: 10.1021/acs.est.8b00999.

Lu, K., and Liu, Z. (2019). Molecular Level Analysis Reveals Changes in Chemical Composition of Dissolved Organic Matter From South Texas Rivers After High Flow Events. *Front. Mar. Sci.* 6, 673. doi: 10.3389/fmars.2019.00673.

Lund-Hansen, L. C., Markager, S., Hancke, K., Stratmann, T., Rysgaard, S., Ramløv, H., et al. (2015). Effects of sea-ice light attenuation and CDOM absorption in the water below the Eurasian sector of central Arctic Ocean (>88°N). *Polar Res.* 34, 23978. doi: 10.3402/polar.v34.23978.

Macdonald, R. W., Harner, T., and Fyfe, J. (2005). Recent climate change in the Arctic and its impact on contaminant pathways and interpretation of temporal trend data. *Sci. Total Environ.* 342, 5–86. doi: 10.1016/j.scitotenv.2004.12.059.

MacGilchrist, G. A., Garabato, A. C. N., Tsubouchi, T., Bacon, S., Torres-Valdés, S., and Azetsu-Scott, K. (2014). The Arctic Ocean carbon sink. *Deep Sea Res. Part I Oceanogr. Res. Pap.* 86, 39–55. doi: 10.1016/j.dsr.2014.01.002.

Madonia, A., Caruso, G., Piazzolla, D., Bonamano, S., Piermattei, V., Zappalà, G., et al. (2020). Chromophoric Dissolved Organic Matter as a Tracer of Fecal Contamination for Bathing Water Quality Monitoring in the Northern Tyrrhenian Sea (Latium, Italy). *J. Mar. Sci. Eng.* 8, 430. doi: 10.3390/jmse8060430.

Mahmoud, M. A. (2016). Kinetics studies of uranium sorption by powdered corn cob in batch and fixed bed system. *J. Adv. Res.* 7, 79–87. doi: 10.1016/j.jare.2015.02.004.

Mann, P. J., Spencer, R. G. M., Hernes, P. J., Six, J., Aiken, G. R., Tank, S. E., et al. (2016). Pan-Arctic Trends in Terrestrial Dissolved Organic Matter from Optical Measurements. *Front. Earth Sci.* 4, 25. doi: 10.3389/feart.2016.00025.

Mannino, A., and Rodger Harvey, H. (2004). Black carbon in estuarine and coastal ocean dissolved organic matter. *Limnol. Oceanogr.* 49, 735–740. doi:

10.4319/lo.2004.49.3.0735.

Marañón, E., Cermeño, P., and Pérez, V. (2005). Continuity in the photosynthetic production of dissolved organic carbon from eutrophic to oligotrophic waters. *Mar. Ecol. Prog. Ser.* 299, 7–17. doi: 10.3354/meps299007.

Martias, C., Tedetti, M., Lantoine, F., Jamet, L., and Dupouy, C. (2018). Characterization and sources of colored dissolved organic matter in a coral reef ecosystem subject to ultramafic erosion pressure (New Caledonia, Southwest Pacific). *Sci. Total Environ.* 616–617, 438–452. doi: 10.1016/j.scitotenv.2017.10.261.

Martínez-Pérez, A. M., Nieto-Cid, M., Osterholz, H., Catalá, T. S., Reche, I., Dittmar, T., et al. (2017). Linking optical and molecular signatures of dissolved organic matter in the Mediterranean Sea. *Sci. Rep.* 7, 3436. doi: 10.1038/s41598-017-03735-4.

Masiello, C. A., and Druffel, E. R. M. (1998). Black Carbon in Deep-Sea Sediments. *Science.* 280, 1911–1913. doi: 10.1126/science.280.5371.1911.

Mathew, K. A., Van Ardelan, M., Villa Gonzalez, S., Vadstein, O., Vezhapparambu, V. S., Leiknes, Ø., et al. (2021). Temporal dynamics of carbon sequestration in coastal North Atlantic fjord system as seen through dissolved organic matter characterisation. *Sci. Total Environ.* 782, 146402. doi: 10.1016/j.scitotenv.2021.146402.

Mathis, J. T., Hansell, D. A., Kadko, D., Bates, N. R., and Cooper, L. W. (2007). Determining net dissolved organic carbon production in the hydrographically complex western Arctic Ocean. *Limnol. Oceanogr.* 52, 1789–1799. doi: 10.4319/lo.2007.52.5.1789.

Matsuoka, A., Bricaud, A., Benner, R., Para, J., Sempéré, R., Prieur, L., et al. (2012). Tracing the transport of colored dissolved organic matter in water masses of the Southern Beaufort Sea: relationship with hydrographic characteristics. *Biogeosciences* 9, 925–940. doi: 10.5194/bg-9-925-2012.

Matsuoka, A., Hill, V., Huot, Y., Babin, M., and Bricaud, A. (2011). Seasonal variability in the light absorption properties of western Arctic waters: Parameterization of the individual components of absorption for ocean color applications. *J. Geophys. Res.* 116, C02007. doi: 10.1029/2009JC005594.

McClelland, J. W., Holmes, R. M., Dunton, K. H., and Macdonald, R. W. (2012). The Arctic Ocean Estuary. *Estuaries and Coasts* 35, 353–368. doi: 10.1007/s12237-010-9357-3.

McKay, G., Korak, J. A., Erickson, P. R., Latch, D. E., McNeill, K., and Rosario-Ortiz, F. L. (2018). The Case Against Charge Transfer Interactions in Dissolved Organic Matter Photophysics. *Environ. Sci. Technol.* 52, 406–414. doi: 10.1021/acs.est.7b03589.

McKnight, D. M., Boyer, E. W., Westerhoff, P. K., Doran, P. T., Kulbe, T., and Andersen, D. T. (2001). Spectrofluorometric characterization of dissolved organic matter for indication of precursor organic material and aromaticity. *Limnol. Oceanogr.* 46, 38–48. doi: 10.4319/lo.2001.46.1.0038.

McParland, E. L., and Levine, N. M. (2019). The role of differential DMSP production and community composition in predicting variability of global surface DMSP concentrations. *Limnol. Oceanogr.* 64, 757–773. doi: 10.1002/lno.11076.

Medeiros, P. M., Seidel, M., Niggemann, J., Spencer, R. G. M., Hernes, P. J., Yager, P. L., et al. (2016). A novel molecular approach for tracing terrigenous dissolved organic matter into the deep ocean. *Global Biogeochem. Cycles* 30, 689–699. doi: 10.1002/2015GB005320.

Meincke, J., Rudels, B., and Friedrich, H. J. (1997). The Arctic Ocean–Nordic Seas thermohaline system. *ICES J. Mar. Sci.* 54, 283–299. doi: 1054–3139/97/040283.

Miller, W. L., and Zepp, R. G. (1995). Photochemical production of dissolved inorganic carbon from terrestrial organic matter: Significance to the oceanic organic carbon cycle. *Geophys. Res. Lett.* 22, 417–420. doi: 10.1029/94GL03344.

Moody, C. S., and Worrall, F. (2017). Modeling rates of DOC degradation using DOM composition and hydroclimatic variables. *J. Geophys. Res. Biogeosciences* 122, 1175–1191. doi: 10.1002/2016JG003493.

Mopper, K., Stubbins, A., Ritchie, J. D., Bialk, H. M., and Hatcher, P. G. (2007). Advanced Instrumental Approaches for Characterization of Marine Dissolved Organic Matter: Extraction Techniques, Mass Spectrometry, and Nuclear Magnetic Resonance Spectroscopy. *Chem. Rev.* 107, 419–442. doi: 10.1021/cr050359b.

Moran, M. A., and Zepp, R. G. (1997). Role of photoreactions in the formation of

biologically labile compounds from dissolved organic matter. *Limnol. Oceanogr.* 42, 1307–1316. doi: 10.4319/lo.1997.42.6.1307.

Morison, J., Kwok, R., Peralta-Ferriz, C., Alkire, M., Rigor, I., Andersen, R., et al. (2012). Changing Arctic Ocean freshwater pathways. *Nature* 481, 66–70. doi: 10.1038/nature10705.

Moritz, M., and Geszke-Moritz, M. (2020). Sulfonic Acid Derivative-Modified SBA-15, PHTS and MCM-41 Mesoporous Silicas as Carriers for a New Antiplatelet Drug: Ticagrelor Adsorption and Release Studies. *Materials (Basel).* 13, 2913. doi: 10.3390/ma13132913.

Morris, D. P., Zagarese, H., Williamson, C. E., Balseiro, E. G., Hargreaves, B. R., Modenutti, B., et al. (1995). The attenuation of solar UV radiation in lakes and the role of dissolved organic carbon. *Limnol. Oceanogr.* 40, 1381–1391. doi: 10.4319/lo.1995.40.8.1381.

Murphy, K. R., Hambly, A., Singh, S., Henderson, R. K., Baker, A., Stuetz, R., et al. (2011). Organic Matter Fluorescence in Municipal Water Recycling Schemes: Toward a Unified PARAFAC Model. *Environ. Sci. Technol.* 45, 2909–2916. doi: 10.1021/es103015e.

Murphy, K. R., Stedmon, C. A., Graeber, D., and Bro, R. (2013). Fluorescence spectroscopy and multi-way techniques. PARAFAC. *Anal. Methods* 5, 6557–6566. doi: 10.1039/c3ay41160e.

Murphy, K. R., Stedmon, C. A., Waite, T. D., and Ruiz, G. M. (2008). Distinguishing between terrestrial and autochthonous organic matter sources in marine environments using fluorescence spectroscopy. *Mar. Chem.* 108, 40–58. doi: 10.1016/j.marchem.2007.10.003.

Murphy, K. R., Timko, S. A., Gonsior, M., Powers, L. C., Wünsch, U. J., and Stedmon, C. A. (2018). Photochemistry Illuminates Ubiquitous Organic Matter Fluorescence Spectra. *Environ. Sci. Technol.* 52, 11243–11250. doi: 10.1021/acs.est.8b02648.

Mysak, L. A. (2001). Patterns of Arctic Circulation. *Science.* 293, 1269–1270. doi: 10.1126/science.1064217.

Nagata, T., Fukuda, H., Fukuda, R., and Koike, I. (2000). Bacterioplankton distribution and production in deep Pacific waters: Large-scale geographic

variations and possible coupling with sinking particle fluxes. *Limnol. Oceanogr.* 45, 426–435. doi: 10.4319/lo.2000.45.2.0426.

Nelson, N. B., and Gauglitz, J. M. (2016). Optical Signatures of Dissolved Organic Matter Transformation in the Global Ocean. *Front. Mar. Sci.* 2, 118. doi: 10.3389/fmars.2015.00118.

Nelson, N. B., Siegel, D. A., Carlson, C. A., and Swan, C. M. (2010). Tracing global biogeochemical cycles and meridional overturning circulation using chromophoric dissolved organic matter. *Geophys. Res. Lett.* 37, L03610. doi: 10.1029/2009GL042325.

Nicolaus, M., Perovich, D. K., Spreen, G., Granskog, M. A., von Albedyll, L., Angelopoulos, M., et al. (2022). Overview of the MOSAiC expedition: Snow and sea ice. *Elem. Sci. Anthr.* 10, 000046. doi: 10.1525/elementa.2021.000046.

Nouara, A., Panagiotopoulos, C., Balesdent, J., Violaki, K., Bard, E., Fagault, Y., et al. (2019). Liquid chromatographic isolation of individual carbohydrates from environmental matrices for stable carbon analysis and radiocarbon dating. *Anal. Chim. Acta* 1067, 137–146. doi: 10.1016/j.aca.2019.03.028.

Novotny, N. R., Capley, E. N., and Stenson, A. C. (2014). Fact or artifact: the representativeness of ESI-MS for complex natural organic mixtures. *J. Mass Spectrom.* 49, 316–326. doi: 10.1002/jms.3345.

Nummelin, A., Ilicak, M., Li, C., and Smedsrud, L. H. (2016). Consequences of future increased Arctic runoff on Arctic Ocean stratification, circulation, and sea ice cover. *J. Geophys. Res. Ocean.* 121, 617–637. doi: 10.1002/2015JC011156.

O'Donnell, J. A., Aiken, G. R., Swanson, D. K., Panda, S., Butler, K. D., and Baltensperger, A. P. (2016). Dissolved organic matter composition of Arctic rivers: Linking permafrost and parent material to riverine carbon. *Global Biogeochem. Cycles* 30, 1811–1826. doi: 10.1002/2016GB005482.

Ohno, T. (2002). Fluorescence Inner-Filtering Correction for Determining the Humification Index of Dissolved Organic Matter. *Environ. Sci. Technol.* 36, 742–746. doi: 10.1021/es0155276.

Ohno, T., Sleighter, R. L., and Hatcher, P. G. (2016). Comparative study of organic matter chemical characterization using negative and positive mode electrospray ionization ultrahigh-resolution mass spectrometry. *Anal. Bioanal. Chem.* 408,

2497–2504. doi: 10.1007/s00216-016-9346-x.

Onarheim, I. H., Smedsrud, L. H., Ingvaldsen, R. B., and Nilsen, F. (2014). Loss of sea ice during winter north of Svalbard. *Tellus A Dyn. Meteorol. Oceanogr.* 66, 23933. doi: 10.3402/tellusa.v66.23933.

Opsahl, S., Benner, R., and Amon, R. M. W. (1999). Major flux of terrigenous dissolved organic matter through the Arctic Ocean. *Limnol. Oceanogr.* 44, 2017–2023. doi: 10.4319/lo.1999.44.8.2017.

Osburn, C. L., Retamal, L., and Vincent, W. F. (2009). Photoreactivity of chromophoric dissolved organic matter transported by the Mackenzie River to the Beaufort Sea. *Mar. Chem.* 115, 10–20. doi: 10.1016/j.marchem.2009.05.003.

Osburn, C. L., Zagarese, H. E., Morris, D. P., Hargreaves, B. R., and Cravero, W. E. (2001). Calculation of spectral weighting functions for the solar photobleaching of chromophoric dissolved organic matter in temperate lakes. *Limnol. Oceanogr.* 46, 1455–1467. doi: 10.4319/lo.2001.46.6.1455.

Oss, M., Kruve, A., Herodes, K., and Leito, I. (2010). Electrospray Ionization Efficiency Scale of Organic Compounds. *Anal. Chem.* 82, 2865–2872. doi: 10.1021/ac902856t.

Paffrath, R., Laukert, G., Bauch, D., van der Loeff, M. R., and Pahnke, K. (2021). Separating individual contributions of major Siberian rivers in the Transpolar Drift of the Arctic Ocean. *Sci. Rep.* 11, 8216. doi: 10.1038/s41598-021-86948-y.

Parlanti, E., Wörz, K., Geoffroy, L., and Lamotte, M. (2000). Dissolved organic matter fluorescence spectroscopy as a tool to estimate biological activity in a coastal zone submitted to anthropogenic inputs. *Org. Geochem.* 31, 1765–1781. doi: 10.1016/S0146-6380(00)00124-8.

Parrish, C. C. (2013). Lipids in Marine Ecosystems. *ISRN Oceanogr.* 2013, 1–16. doi: 10.5402/2013/604045.

Passow, U. (2002). Transparent exopolymer particles (TEP) in aquatic environments. *Prog. Oceanogr.* 55, 287–333. doi: 10.1016/S0079-6611(02)00138-6.

Passow, U., Shipe, R. ., Murray, A., Pak, D. ., Brzezinski, M. ., and Alldredge, A. . (2001). The origin of transparent exopolymer particles (TEP) and their role in the sedimentation of particulate matter. *Cont. Shelf Res.* 21, 327–346. doi: 10.1016/S0278-4343(00)00101-1.

Paulsen, M. L., Müller, O., Larsen, A., Møller, E. F., Middelboe, M., Sejr, M. K., et al. (2019). Biological transformation of Arctic dissolved organic matter in a NE Greenland fjord. *Limnol. Oceanogr.* 64, 1014–1033. doi: 10.1002/lno.11091.

Pavlov, A. K., Granskog, M. A., Stedmon, C. A., Ivanov, B. V., Hudson, S. R., and Falk-Petersen, S. (2015). Contrasting optical properties of surface waters across the Fram Strait and its potential biological implications. *J. Mar. Syst.* 143, 62–72. doi: 10.1016/j.jmarsys.2014.11.001.

Pavlov, A. K., Taskjelle, T., Kauko, H. M., Hamre, B., Hudson, S. R., Assmy, P., et al. (2017). Altered inherent optical properties and estimates of the underwater light field during an Arctic under-ice bloom of Phaeocystis pouchetii. *J. Geophys. Res. Ocean.* 122, 4939–4961. doi: 10.1002/2016JC012471.

Pegau, W. S. (2002). Inherent optical properties of the central Arctic surface waters. *J. Geophys. Res.* 107, 8035. doi: 10.1029/2000JC000382.

Perdue, E., and Benner, R. (2009). "Marine organic matter," in *Biophysico-Chemical Processes Involving Natural Nonliving Organic Matter in Environmental Systems*, eds. N. Senesi, B. Xing, and P. M. Huang (John Wiley & Sons), 407–449.

Perminova, I. V., Dubinenkov, I. V., Kononikhin, A. S., Konstantinov, A. I., Zherebker, A. Y., Andzhushev, M. A., et al. (2014). Molecular Mapping of Sorbent Selectivities with Respect to Isolation of Arctic Dissolved Organic Matter as Measured by Fourier Transform Mass Spectrometry. *Environ. Sci. Technol.* 48, 7461–7468. doi: 10.1021/es5015423.

Perovich, D. K., and Richter-Menge, J. A. (2015). Regional variability in sea ice melt in a changing Arctic. *Philos. Trans. R. Soc. A Math. Phys. Eng. Sci.* 373, 20140165. doi: 10.1098/rsta.2014.0165.

Perovich, D. K., Richter-Menge, J. A., Jones, K. F., Light, B., Elder, B. C., Polashenski, C., et al. (2011). Arctic sea-ice melt in 2008 and the role of solar heating. *Ann. Glaciol.* 52, 355–359. doi: 10.3189/172756411795931714.

Petras, D., Koester, I., Da Silva, R., Stephens, B. M., Haas, A. F., Nelson, C. E., et al. (2017). High-Resolution Liquid Chromatography Tandem Mass Spectrometry Enables Large Scale Molecular Characterization of Dissolved Organic Matter. *Front. Mar. Sci.* 4, 405. doi: 10.3389/fmars.2017.00405.

Polimene, L., Torres, R., Powley, H. R., Bedington, M., Juhls, B., Palmtag, J., et al.

(2022). Biological lability of terrestrial DOM increases CO2 outgassing across Arctic shelves. *Biogeochemistry*, 1–12. doi: 10.1007/s10533-022-00961-5.

Polyakov, I. V., Pnyushkov, A. V., Alkire, M. B., Ashik, I. M., Baumann, T. M., Carmack, E. C., et al. (2017). Greater role for Atlantic inflows on sea-ice loss in the Eurasian Basin of the Arctic Ocean. *Science.* 356, 285–291. doi: 10.1126/science.aai8204.

Polyakov, I. V., Pnyushkov, A. V., Rember, R., Ivanov, V. V., Lenn, Y.-D., Padman, L., et al. (2012). Mooring-based observations of double-diffusive staircases over the Laptev Sea slope. *J. Phys. Oceanogr.* 42, 95–109. doi: 10.1175/2011JPO4606.1.

Polyakov, I. V., Pnyushkov, A. V., Rember, R., Padman, L., Carmack, E. C., and Jackson, J. M. (2013). Winter convection transports atlantic water heat to the surface layer in the eastern Arctic Ocean. *J. Phys. Oceanogr.* 43, 2142–2155. doi: 10.1175/JPO-D-12-0169.1.

Polyakov, I. V., Rippeth, T. P., Fer, I., Alkire, M. B., Baumann, T. M., Carmack, E. C., et al. (2020). Weakening of Cold Halocline Layer Exposes Sea Ice to Oceanic Heat in the Eastern Arctic Ocean. *J. Clim.* 33, 8107–8123. doi: 10.1175/JCLI-D-19-0976.1.

Popova, E. E., Yool, A., Coward, A. C., Dupont, F., Deal, C., Elliott, S., et al. (2012). What controls primary production in the Arctic Ocean? Results from an intercomparison of five general circulation models with biogeochemistry. *J. Geophys. Res. Ocean.* 117, C00D12. doi: 10.1029/2011JC007112.

Proctor, L. M., and Fuhrman, J. A. (1990). Viral mortality of marine bacteria and cyanobacteria. *Nature* 343, 60–62. doi: 10.1038/343060a0.

Pucher, M., Wünsch, U., Weigelhofer, G., Murphy, K., Hein, T., and Graeber, D. (2019). staRdom: Versatile Software for Analyzing Spectroscopic Data of Dissolved Organic Matter in R. *Water* 11, 2366. doi: 10.3390/w11112366.

Rabe, B., Heuzé, C., Regnery, J., Aksenov, Y., Allerholt, J., Athanase, M., et al. (2022). Overview of the MOSAiC expedition: Physical oceanography. *Elem. Sci. Anthr.* 10, 00062. doi: 10.1525/elementa.2021.00062.

Raeke, J., Lechtenfeld, O. J., Wagner, M., Herzsprung, P., and Reemtsma, T. (2016). Selectivity of solid phase extraction of freshwater dissolved organic matter and

its effect on ultrahigh resolution mass spectra. *Environ. Sci. Process. Impacts* 18, 918–927. doi: 10.1039/C6EM00200E.

Randelhoff, A., Reigstad, M., Chierici, M., Sundfjord, A., Ivanov, V., Cape, M., et al. (2018). Seasonality of the Physical and Biogeochemical Hydrography in the Inflow to the Arctic Ocean Through Fram Strait. *Front. Mar. Sci.* 5, 224. doi: 10.3389/fmars.2018.00224.

Raymond, P. A., McClelland, J. W., Holmes, R. M., Zhulidov, A. V., Mull, K., Peterson, B. J., et al. (2007). Flux and age of dissolved organic carbon exported to the Arctic Ocean: A carbon isotopic study of the five largest arctic rivers. *Global Biogeochem. Cycles* 21, GB4011. doi: 10.1029/2007GB002934.

Raymond, P. A., and Spencer, R. G. M. (2015). "Riverine DOM," in *Biogeochemistry of Marine Dissolved Organic Matter* (Elsevier), 509–533. doi: 10.1016/B978-0-12-405940-5.00011-X.

Reemtsma, T. (2001). The use of liquid chromatography-atmospheric pressure ionization-mass spectrometry in water analysis – Part II: Obstacles. *TrAC Trends Anal. Chem.* 20, 533–542. doi: 10.1016/S0165-9936(01)00103-0.

Reemtsma, T., and These, A. (2003). On-line coupling of size exclusion chromatography with electrospray ionization-tandem mass spectrometry for the analysis of aquatic fulvic and humic acids. *Anal. Chem.* 75, 1500–1507. doi: 10.1021/ac0261294.

Rho, H., Chon, K., Park, J., and Cho, J. (2019). Rapid and Effective Isolation of Dissolved Organic Matter Using Solid-Phase Extraction Cartridges Packed with Amberlite XAD 8/4 Resins. *Water* 11, 67. doi: 10.3390/w11010067.

Romera-Castillo, C., Chen, M., Yamashita, Y., and Jaf , R. (2014). Fluorescence characteristics of size-fractionated dissolved organic matter: Implications for a molecular assembly based structure? *Water Res.* 55, 40–51. doi: 10.1016/j.watres.2014.02.017.

Romera-Castillo, C., Sarmento, H., Álvarez-Salgado, X. A., Gasol, J. M., and Marrasé, C. (2011). Net Production and Consumption of Fluorescent Colored Dissolved Organic Matter by Natural Bacterial Assemblages Growing on Marine Phytoplankton Exudates. *Appl. Environ. Microbiol.* 77, 7490–7498. doi: 10.1128/AEM.00200-11.

Romera-Castillo, C., Sarmento, H., Álvarez-Salgado, X. A., Gasol, J. M., and Marraséa, C. (2010). Production of chromophoric dissolved organic matter by marine phytoplankton. *Limnol. Oceanogr.* 55, 446–454. doi: 10.4319/lo.2010.55.1.0446.

Rowland, S. M., Robbins, W. K., Corilo, Y. E., Marshall, A. G., and Rodgers, R. P. (2014). Solid-Phase Extraction Fractionation To Extend the Characterization of Naphthenic Acids in Crude Oil by Electrospray Ionization Fourier Transform Ion Cyclotron Resonance Mass Spectrometry. *Energy & Fuels* 28, 5043–5048. doi: 10.1021/ef5015023.

Rudels, B. (1989). The formation of polar surface water, the ice export and the exchanges through the Fram Strait. *Prog. Oceanogr.* 22, 205–248. doi: 10.1016/0079-6611(89)90013-X.

Rudels, B. (1995). The thermohaline circulation of the Arctic Ocean and the Greenland Sea. *Philos. Trans. R. Soc. London. Ser. A Phys. Eng. Sci.* 352, 287–299. doi: 10.1098/rsta.1995.0071.

Rudels, B., Anderson, L. G., and Jones, E. P. (1996). Formation and evolution of the surface mixed layer and halocline of the Arctic Ocean. *J. Geophys. Res. Ocean.* 101, 8807–8821. doi: 10.1029/96JC00143.

Rudels, B., Jones, E. P., Schauer, U., and Eriksson, P. (2004). Atlantic sources of the Arctic Ocean surface and halocline waters. *Polar Res.* 23, 181–208. doi: 10.1111/j.1751-8369.2004.tb00007.x.

Rudels, B., Korhonen, M., Schauer, U., Pisarev, S., Rabe, B., and Wisotzki, A. (2015). Circulation and transformation of Atlantic water in the Eurasian Basin and the contribution of the Fram Strait inflow branch to the Arctic Ocean heat budget. *Prog. Oceanogr.* 132, 128–152. doi: 10.1016/j.pocean.2014.04.003.

Rudels, B., Larsson, A.-M., and Sehlstedt, P.-I. (1991). Stratification and water mass formation in the Arctic Ocean: some implications for the nutrient distribution. *Polar Res.* 10, 19–32. doi: 10.1111/j.1751-8369.1991.tb00631.x.

Schirrmeister, L., Siegert, C., Kuznetsova, T., Kuzmina, S., Andreev, A., Kienast, F., et al. (2002). Paleoenvironmental and paleoclimatic records from permafrost deposits in the Arctic region of Northern Siberia. *Quat. Int.* 89, 97–118. doi: 10.1016/S1040-6182(01)00083-0.

Schittich, A.-R., Wünsch, U. J., Kulkarni, H. V., Battistel, M., Bregnhøj, H., Stedmon, C. A., et al. (2018). Investigating Fluorescent Organic-Matter Composition as a Key Predictor for Arsenic Mobility in Groundwater Aquifers. *Environ. Sci. Technol.* 52, 13027–13036. doi: 10.1021/acs.est.8b04070.

Schlosser, P., Bauch, D., Fairbanks, R., and Bönisch, G. (1994). Arctic river-runoff: mean residence time on the shelves and in the halocline. *Deep Sea Res. Part I Oceanogr. Res. Pap.* 41, 1053–1068. doi: 10.1016/0967-0637(94)90018-3.

Schubert, C. J., and Stein, R. (1997). Lipid distribution in surface sediments from the eastern central Arctic Ocean. *Mar. Geol.* 138, 11–25. doi: 10.1016/S0025-3227(97)00017-0.

Sholkovitz, E. R. (1976). Flocculation of dissolved organic and inorganic matter during the mixing of river water and seawater. *Geochim. Cosmochim. Acta* 40, 831–845. doi: 10.1016/0016-7037(76)90035-1.

Sholkovitz, E. R., Boyle, E. A., and Price, N. B. (1978). The removal of dissolved humic acids and iron during estuarine mixing. *Earth Planet. Sci. Lett.* 40, 130–136. doi: 10.1016/0012-821X(78)90082-1.

Shupe, M. D., Rex, M., Blomquist, B., Persson, P. O. G., Schmale, J., Uttal, T., et al. (2022). Overview of the MOSAiC expedition: Atmosphere. *Elem. Sci. Anthr.* 10, 00060. doi: 10.1525/elementa.2021.00060.

Siegel, D. A., Maritorena, S., Nelson, N. B., Behrenfeld, M. J., and McClain, C. R. (2005). Colored dissolved organic matter and its influence on the satellite-based characterization of the ocean biosphere. *Geophys. Res. Lett.* 32, L20605. doi: 10.1029/2005GL024310.

Singer, G. A., Fasching, C., Wilhelm, L., Niggemann, J., Steier, P., Dittmar, T., et al. (2012). Biogeochemically diverse organic matter in Alpine glaciers and its downstream fate. *Nat. Geosci.* 5, 710–714. doi: 10.1038/ngeo1581.

Skoog, A., and Benner, R. (1997). Aldoses in various size fractions of marine organic matter: Implications for carbon cycling. *Limnol. Oceanogr.* 42, 1803–1813. doi: 10.4319/lo.1997.42.8.1803.

Slagter, H. A., Reader, H. E., Rijkenberg, M. J. A., van der Loeff, M. R., de Baar, H. J. W., and Gerringa, L. J. A. (2017). Organic Fe speciation in the Eurasian Basins of the Arctic Ocean and its relation to terrestrial DOM. *Mar. Chem.* 197, 11–25.

doi: 10.1016/j.marchem.2017.10.005.

Sleighter, R. L., Chen, H., Wozniak, A. S., Willoughby, A. S., Caricasole, P., and Hatcher, P. G. (2012). Establishing a Measure of Reproducibility of Ultrahigh-Resolution Mass Spectra for Complex Mixtures of Natural Organic Matter. *Anal. Chem.* 84, 9184–9191. doi: 10.1021/ac3018026.

Sleighter, R. L., and Hatcher, P. G. (2008). Molecular characterization of dissolved organic matter (DOM) along a river to ocean transect of the lower Chesapeake Bay by ultrahigh resolution electrospray ionization Fourier transform ion cyclotron resonance mass spectrometry. *Mar. Chem.* 110, 140–152. doi: 10.1016/j.marchem.2008.04.008.

Smith, D. C., Simon, M., Alldredge, A. L., and Azam, F. (1992). Intense hydrolytic enzyme activity on marine aggregates and implications for rapid particle dissolution. *Nature* 359, 139–142. doi: 10.1038/359139a0.

Smith, D. C., Steward, G. F., Long, R. A., and Azam, F. (1995). Bacterial mediation of carbon fluxes during a diatom bloom in a mesocosm. *Deep Sea Res. Part II Top. Stud. Oceanogr.* 42, 75–97. doi: 10.1016/0967-0645(95)00005-B.

Smith, J. N., Karcher, M., Casacuberta, N., Williams, W. J., Kenna, T., and Smethie, W. M. (2021). A Changing Arctic Ocean: How Measured and Modeled 129 I Distributions Indicate Fundamental Shifts in Circulation Between 1994 and 2015. *J. Geophys. Res. Ocean.* 126, e2020JC016740. doi: 10.1029/2020JC016740.

Solomon, A., Heuzé, C., Rabe, B., Bacon, S., Bertino, L., Heimbach, P., et al. (2021). Freshwater in the Arctic Ocean 2010–2019. *Ocean Sci.* 17, 1081–1102. doi: 10.5194/os-17-1081-2021.

Spencer, R. G. M., Aiken, G. R., Butler, K. D., Dornblaser, M. M., Striegl, R. G., and Hernes, P. J. (2009a). Utilizing chromophoric dissolved organic matter measurements to derive export and reactivity of dissolved organic carbon exported to the Arctic Ocean: A case study of the Yukon River, Alaska. *Geophys. Res. Lett.* 36, L06401. doi: 10.1029/2008GL036831.

Spencer, R. G. M., Aiken, G. R., Wickland, K. P., Striegl, R. G., and Hernes, P. J. (2008). Seasonal and spatial variability in dissolved organic matter quantity and composition from the Yukon River basin, Alaska. *Global Biogeochem. Cycles* 22, GB4002. doi: 10.1029/2008GB003231.

Spencer, R. G. M., Mann, P. J., Dittmar, T., Eglinton, T. I., McIntyre, C., Holmes, R. M., et al. (2015). Detecting the signature of permafrost thaw in Arctic rivers. *Geophys. Res. Lett.* 42, 2830–2835. doi: 10.1002/2015GL063498.

Spencer, R. G. M., Stubbins, A., Hernes, P. J., Baker, A., Mopper, K., Aufdenkampe, A. K., et al. (2009b). Photochemical degradation of dissolved organic matter and dissolved lignin phenols from the Congo River. *J. Geophys. Res.* 114, G03010. doi: 10.1029/2009JG000968.

Spranger, T., Pinxteren, D. Van, Reemtsma, T., Lechtenfeld, O. J., and Herrmann, H. (2019). 2D Liquid Chromatographic Fractionation with Ultra-high Resolution MS Analysis Resolves a Vast Molecular Diversity of Tropospheric Particle Organics. *Environ. Sci. Technol.* 53, 11353–11363. doi: 10.1021/acs.est.9b03839.

Stedmon, C. A., Amon, R. M. W., Rinehart, A. J., and Walker, S. A. (2011). The supply and characteristics of colored dissolved organic matter (CDOM) in the Arctic Ocean: Pan Arctic trends and differences. *Mar. Chem.* 124, 108–118. doi: 10.1016/j.marchem.2010.12.007.

Stedmon, C. A., and Bro, R. (2008). Characterizing dissolved organic matter fluorescence with parallel factor analysis: a tutorial. *Limnol. Oceanogr. Methods* 6, 572–579. doi: 10.4319/lom.2008.6.572.

Stedmon, C. A., and Markager, S. (2001). The optics of chromophoric dissolved organic matter (CDOM) in the Greenland Sea: An algorithm for differentiation between marine and terrestrially derived organic matter. *Limnol. Oceanogr.* 46, 2087–2093. doi: 10.4319/lo.2001.46.8.2087.

Stedmon, C. A., Markager, S., and Bro, R. (2003). Tracing dissolved organic matter in aquatic environments using a new approach to fluorescence spectroscopy. *Mar. Chem.* 82, 239–254. doi: 10.1016/S0304-4203(03)00072-0.

Stedmon, C. A., Markager, S., Tranvik, L., Kronberg, L., Slätis, T., and Martinsen, W. (2007a). Photochemical production of ammonium and transformation of dissolved organic matter in the Baltic Sea. *Mar. Chem.* 104, 227–240. doi: 10.1016/j.marchem.2006.11.005.

Stedmon, C. A., and Nelson, N. B. (2015). "The Optical Properties of DOM in the Ocean," in *Biogeochemistry of Marine Dissolved Organic Matter* (Elsevier), 481–508. doi: 10.1016/B978-0-12-405940-5.00010-8.

Stedmon, C. A., Thomas, D. N., Granskog, M., Kaartokallio, H., Papadimitriou, S., and Kuosa, H. (2007b). Characteristics of Dissolved Organic Matter in Baltic Coastal Sea Ice: Allochthonous or Autochthonous Origins? *Environ. Sci. Technol.* 41, 7273–7279. doi: 10.1021/es071210f.

Stenson, A. C., Marshall, A. G., and Cooper, W. T. (2003). Exact Masses and Chemical Formulas of Individual Suwannee River Fulvic Acids from Ultrahigh Resolution Electrospray Ionization Fourier Transform Ion Cyclotron Resonance Mass Spectra. *Anal. Chem.* 75, 1275–1284. doi: 10.1021/ac026106p.

Stramska, M. (2009). Particulate organic carbon in the global ocean derived from SeaWiFS ocean color. *Deep Sea Res. Part I Oceanogr. Res. Pap.* 56, 1459–1470. doi: 10.1016/j.dsr.2009.04.009.

Strom, S. L., Benner, R., Ziegler, S., and Dagg, M. J. (1997). Planktonic grazers are a potentially important source of marine dissolved organic carbon. *Limnol. Oceanogr.* 42, 1364–1374. doi: 10.4319/lo.1997.42.6.1364.

Stubbins, A., Hood, E., Raymond, P. A., Aiken, G. R., Sleighter, R. L., Hernes, P. J., et al. (2012). Anthropogenic aerosols as a source of ancient dissolved organic matter in glaciers. *Nat. Geosci.* 5, 198–201. doi: 10.1038/ngeo1403.

Stubbins, A., Hubbard, V., Uher, G., Law, C. S., Upstill-Goddard, R. C., Aiken, G. R., et al. (2008). Relating Carbon Monoxide Photoproduction to Dissolved Organic Matter Functionality. *Environ. Sci. Technol.* 42, 3271–3276. doi: 10.1021/es703014q.

Stubbins, A., Lapierre, J.-F., Berggren, M., Prairie, Y. T., Dittmar, T., and del Giorgio, P. A. (2014). What's in an EEM? Molecular Signatures Associated with Dissolved Organic Fluorescence in Boreal Canada. *Environ. Sci. Technol.* 48, 10598–10606. doi: 10.1021/es502086e.

Stuermer, D. H., and Harvey, G. R. (1974). Humic substances from seawater. *Nature* 250, 480–481. doi: 10.1038/250480a0.

Sulzberger, B., and Durisch-Kaiser, E. (2009). Chemical characterization of dissolved organic matter (DOM): A prerequisite for understanding UV-induced changes of DOM absorption properties and bioavailability. *Aquat. Sci.* 71, 104–126. doi: 10.1007/s00027-008-8082-5.

Swan, B. K., Martinez-Garcia, M., Preston, C. M., Sczyrba, A., Woyke, T., Lamy, D.,

et al. (2011). Potential for Chemolithoautotrophy Among Ubiquitous Bacteria Lineages in the Dark Ocean. *Science.* 333, 1296–1300. doi: 10.1126/science.1203690.

Swenson, M. M., Oyler, A. R., and Minor, E. C. (2014). Rapid solid phase extraction of dissolved organic matter. *Limnol. Oceanogr. Methods* 12, 713–728. doi: 10.4319/lom.2014.12.713.

Tang, K., Page, J. S., and Smith, R. D. (2004). Charge competition and the linear dynamic range of detection in electrospray ionization mass spectrometry. *J. Am. Soc. Mass Spectrom.* 15, 1416–1423. doi: 10.1016/j.jasms.2004.04.034.

Tarnocai, C., Canadell, J. G., Schuur, E. A. G., Kuhry, P., Mazhitova, G., and Zimov, S. (2009). Soil organic carbon pools in the northern circumpolar permafrost region. *Global Biogeochem. Cycles* 23, GB2023. doi: 10.1029/2008GB003327.

Tartaglia, A., Locatelli, M., Kabir, A., Furton, K. G., Macerola, D., Sperandio, E., et al. (2019). Comparison between Exhaustive and Equilibrium Extraction Using Different SPE Sorbents and Sol-Gel Carbowax 20M Coated FPSE Media. *Molecules* 24, 382. doi: 10.3390/molecules24030382.

Tfaily, M. M., Hodgkins, S., Podgorski, D. C., Chanton, J. P., and Cooper, W. T. (2012). Comparison of dialysis and solid-phase extraction for isolation and concentration of dissolved organic matter prior to Fourier transform ion cyclotron resonance mass spectrometry. *Anal. Bioanal. Chem.* 404, 447–457. doi: 10.1007/s00216-012-6120-6.

Thomas, D. N., Papadimitriou, S., and Christine, M. (2010). "Biogeochemistry of sea ice," in *Sea ice 2*, 425–467. doi: 10.1007/978-90-481-2642-2_639.

Timko, S. A., Maydanov, A., Pittelli, S. L., Conte, M. H., Cooper, W. J., Koch, B. P., et al. (2015). Depth-dependent photodegradation of marine dissolved organic matter. *Front. Mar. Sci.* 2, 66. doi: 10.3389/fmars.2015.00066.

Tranvik, L. J., and Sieburth, J. M. (1989). Effects of flocculated humic matter on free and attached pelagic microorganisms. *Limnol. Oceanogr.* 34, 688–699. doi: 10.4319/lo.1989.34.4.0688.

Verdugo, P. (2012). Marine Microgels. *Ann. Rev. Mar. Sci.* 4, 375–400. doi: 10.1146/annurev-marine-120709-142759.

Verdugo, P., Alldredge, A. L., Azam, F., Kirchman, D. L., Passow, U., and Santschi, P.

H. (2004). The oceanic gel phase: a bridge in the DOM–POM continuum. *Mar. Chem.* 92, 67–85. doi: 10.1016/j.marchem.2004.06.017.

Verdugo, P., and Santschi, P. H. (2010). Polymer dynamics of DOC networks and gel formation in seawater. *Deep Sea Res. Part II Top. Stud. Oceanogr.* 57, 1486–1493. doi: 10.1016/j.dsr2.2010.03.002.

Volk, T.T., Hoffert, M.I.M.I., 1985. Ocean carbon pumps: analysis of relative strengths and efficiencies in ocean-driven atmospheric CO2 changes. In: Sundquist, E.T.E.T., Broecker, W.S.W.S. (Eds.), The Carbon Cycle and Atmospheric CO2: Natural Variations Archean to Present. Geophys. Monogr. Ser. vol. 32. AGU, Washington, DC, pp. 99–110.

von Wachenfeldt, E., Bastviken, D., and Tranvika, L. J. (2009). Microbially induced flocculation of allochthonous dissolved organic carbon in lakes. *Limnol. Oceanogr.* 54, 1811–1818. doi: 10.4319/lo.2009.54.5.1811.

von Wachenfeldt, E., Sobek, S., Bastviken, D., and Tranvik, L. J. (2008). Linking allochthonous dissolved organic matter and boreal lake sediment carbon sequestration: The role of light-mediated flocculation. *Limnol. Oceanogr.* 53, 2416–2426. doi: 10.4319/lo.2008.53.6.2416.

Wagner, S., Jaffé, R., Cawley, K., Dittmar, T., and Stubbins, A. (2015). Associations Between the Molecular and Optical Properties of Dissolved Organic Matter in the Florida Everglades, a Model Coastal Wetland System. *Front. Chem.* 3, 66. doi: 10.3389/fchem.2015.00066.

Wakeham, S. G., Pease, T. K., and Benner, R. (2003). Hydroxy fatty acids in marine dissolved organic matter as indicators of bacterial membrane material. *Org. Geochem.* 34, 857–868. doi: 10.1016/S0146-6380(02)00189-4.

Walker, S. A., Amon, R. M. W., and Stedmon, C. A. (2013). Variations in high-latitude riverine fluorescent dissolved organic matter: A comparison of large Arctic rivers. *J. Geophys. Res. Biogeosciences* 118, 1689–1702. doi: 10.1002/2013JG002320.

Wang, W., He, C., Gao, Y., Zhang, Y., and Shi, Q. (2019). Isolation and characterization of hydrophilic dissolved organic matter in waters by ion exchange solid phase extraction followed by high resolution mass spectrometry. *Environ. Chem. Lett.* 17, 1857–1866. doi: 10.1007/s10311-019-00898-6.

Watanabe, E., and Hasumi, H. (2009). Pacific Water Transport in the Western Arctic Ocean Simulated by an Eddy-Resolving Coupled Sea Ice–Ocean Model. *J. Phys. Oceanogr.* 39, 2194–2211. doi: 10.1175/2009JPO4010.1.

Weishaar, J. L., Aiken, G. R., Bergamaschi, B. A., Fram, M. S., Fujii, R., and Mopper, K. (2003). Evaluation of Specific Ultraviolet Absorbance as an Indicator of the Chemical Composition and Reactivity of Dissolved Organic Carbon. *Environ. Sci. Technol.* 37, 4702–4708. doi: 10.1021/es030360x.

Wetzel, R. G. (1984). Detrital dissolved and particulate organic carbon functions in aquatic ecosystems. *Bull. Mar. Sci.* 35, 503–509.

Williams, P. M., and Druffel, E. R. M. (1987). Radiocarbon in dissolved organic matter in the central North Pacific Ocean. *Nature* 330, 246–248. doi: 10.1038/330246a0.

Williamson, C. E., Stemberger, R. S., Morris, D. P., Frost, T. M., and Paulsen, S. G. (1996). Ultraviolet radiation in North American lakes: Attenuation estimates from DOC measurements and implications for plankton communities. *Limnol. Oceanogr.* 41, 1024–1034. doi: 10.4319/lo.1996.41.5.1024.

Woosley, R. J., and Millero, F. J. (2020). Freshening of the western Arctic negates anthropogenic carbon uptake potential. *Limnol. Oceanogr.* 65, 1834–1846. doi: 10.1002/lno.11421.

Wünsch, U. J., Acar, E., Koch, B. P., Murphy, K. R., Schmitt-Kopplin, P., and Stedmon, C. A. (2018a). The Molecular Fingerprint of Fluorescent Natural Organic Matter Offers Insight into Biogeochemical Sources and Diagenetic State. *Anal. Chem.* 90, 14188–14197. doi: 10.1021/acs.analchem.8b02863.

Wünsch, U. J., Geuer, J. K., Lechtenfeld, O. J., Koch, B. P., Murphy, K. R., and Stedmon, C. A. (2018b). Quantifying the impact of solid-phase extraction on chromophoric dissolved organic matter composition. *Mar. Chem.* 207, 33–41. doi: 10.1016/j.marchem.2018.08.010.

Xu, H., Guan, D., Zou, L., Lin, H., and Guo, L. (2018). Contrasting effects of photochemical and microbial degradation on Cu(II) binding with fluorescent DOM from different origins. *Environ. Pollut.* 239, 205–214. doi: 10.1016/j.envpol.2018.03.108.

Xu, H., and Guo, L. (2018). Intriguing changes in molecular size and composition of

dissolved organic matter induced by microbial degradation and self-assembly. *Water Res.* 135, 187–194. doi: 10.1016/j.watres.2018.02.016.

Yamamoto-Kawai, M., McLaughlin, F. A., Carmack, E. C., Nishino, S., and Shimada, K. (2008). Freshwater budget of the Canada Basin, Arctic Ocean, from salinity, δ 18 O, and nutrients. *J. Geophys. Res.* 113, C01007. doi: 10.1029/2006JC003858.

Yamamoto-Kawai, M., Tanaka, N., and Pivovarov, S. (2005). Freshwater and brine behaviors in the Arctic Ocean deduced from historical data of δ18O and alkalinity (1929–2002 A.D.). *J. Geophys. Res.* 110, C10003. doi: 10.1029/2004JC002793.

Yamashita, Y., Hashihama, F., Saito, H., Fukuda, H., and Ogawa, H. (2017). Factors controlling the geographical distribution of fluorescent dissolved organic matter in the surface waters of the Pacific Ocean. *Limnol. Oceanogr.* 62, 2360–2374. doi: 10.1002/lno.10570.

Yamashita, Y., and Jaff , R. (2008). Characterizing the Interactions between Trace Metals and Dissolved Organic Matter Using Excitation−Emission Matrix and Parallel Factor Analysis. *Environ. Sci. Technol.* 42, 7374–7379. doi: 10.1021/es801357h.

Yamashita, Y., Nosaka, Y., Suzuki, K., Ogawa, H., Takahashi, K., and Saito, H. (2013). Photobleaching as a factor controlling spectral characteristics of chromophoric dissolved organic matter in open ocean. *Biogeosciences* 10, 7207–7217. doi: 10.5194/bg-10-7207-2013.

Zabłocka, M., Kowalczuk, P., Meler, J., Peeken, I., Dragańska-Deja, K., and Winogradow, A. (2020). Compositional differences of fluorescent dissolved organic matter in Arctic Ocean spring sea ice and surface waters north of Svalbard. *Mar. Chem.* 227, 103893. doi: 10.1016/j.marchem.2020.103893.

Zark, M., and Dittmar, T. (2018). Universal molecular structures in natural dissolved organic matter. *Nat. Commun.* 9, 3178. doi: 10.1038/s41467-018-05665-9.

Zhang, J., Kattner, G., and Koch, B. P. (2019). Interactions of trace elements and organic ligands in seawater and implications for quantifying biogeochemical dynamics: A review. *Earth-Science Rev.* 192, 631–649. doi: 10.1016/j.earscirev.2019.03.007.

Zherebker, A., Shirshin, E., Rubekina, A., Kharybin, O., Kononikhin, A., Kulikova, N.

A., et al. (2020). Optical Properties of Soil Dissolved Organic Matter Are Related to Acidic Functions of Its Components as Revealed by Fractionation, Selective Deuteromethylation, and Ultrahigh Resolution Mass Spectrometry. *Environ. Sci. Technol.* 54, 2667–2677. doi: 10.1021/acs.est.9b05298.

Zhou, Y., He, D., He, C., Li, P., Fan, D., Wang, A., et al. (2021). Spatial changes in molecular composition of dissolved organic matter in the Yangtze River Estuary: Implications for the seaward transport of estuarine DOM. *Sci. Total Environ.* 759, 143531. doi: 10.1016/j.scitotenv.2020.143531.

Zielinski, O., Rüssmeier, N., Ferdinand, O., Miranda, M., and Wollschläger, J. (2018). Assessing Fluorescent Organic Matter in Natural Waters: Towards In Situ Excitation–Emission Matrix Spectroscopy. *Appl. Sci.* 8, 2685. doi: 10.3390/app8122685.